THE SEA IS GONE PEOPLE ARE NOT

UN Multi-Partner Human Security Trust Fund for the Aral Sea Region in Uzbekistan

Ministry of Ecology, Environmental Protection and Climate Change of the Republic of Uzbekistan

COUNCIL OF MINISTERS OF THE REPUBLIC OF KARAKALPAKSTAN

UNDP

Funded by the United Nations Multi-Partner Trust Fund for Human Security for the Aral Sea region in Uzbekistan (MPTFHS).

Government of the Republic of Uzbekistan | Government of Norway | European Union | Suomi Finland | Government of the Republic of Korea | Alwaleed Philanthropies | Government of the Federal Republic of Germany

DUST MIGRATION MODEL FOR THE SOUTHERN ARAL SEA REGION

This material has been prepared within the framework of the joint UNDP and FAO programme “Strengthening Community Knowledge and Skills in the Aral Sea Region Countries to Address Environmental Challenges through Innovative Approaches to Managing Air, Land and Water Resources”, with the financial support of the United Nations Multi-Partner Trust Fund in the Aral Sea Region in Uzbekistan (MPHTSF), its donors and development partners.

The research and data collection methodology were prepared by UNDP expert, Doctor of Physical and Mathematical Sciences, Ms. B. S. Tleumuratova. The views and opinions expressed in this document do not necessarily reflect the views of the Fund’s donors and development partners.

The Country Development Programme at a Glance (UNDP) is the leading UN organization fighting injustice caused by poverty, climate change and poverty. Working with a broad network of experts and partners in 170 countries and territories, we help create comprehensive, long-term solutions for people and the planet.

CONTENTS

INTRODUCTION

Research on the long-term dynamics of natural processes is necessary to identify their stable trends and dependence on various factors. The results of such studies are in demand for forecasting these processes and developing corresponding response measures through anthropogenic impact on their factors. Such research is especially relevant for regions with dynamic transformations of the natural environment, such as the Southern Aral Sea region (SASR)—the epicenter of the Aral Sea crisis.

However, despite the high frequency and intensity of dust storms in the region, no emergency warning system currently exists to alert the population to hazardous dust concentrations. This gap underscores the urgent need for improved forecasting and response measures.

Among the environmental problems of the SASR, one of the most important is the issue of dust migration, caused by the presence of vast desert surfaces in this region: the Kyzylkum, Karakum, Ustyurt, and Aralkum Deserts. At the plenary session on dust storm problems during the 21st session of the Committee to Combat Desertification under the United Nations (CRIC-21 UNCCD), the Minister of Ecology, Environment and Climate Change of the Republic of Uzbekistan Aziz Abdukhakimov emphasized that "for Uzbekistan, the problem of sand and dust storms, which are becoming more frequent and intense, is more relevant than ever." The demand for this project is also driven by the Decree of the President of the Republic of Uzbekistan No. PP-338 dated September 24, 2024, "On Priority Measures to Combat Dust Storms and Improve Atmospheric Air Quality."

An analysis of global literature on dust migration and atmospheric dust load studies, presented in Chapter 1 of the Report, indicates the understudied nature of this problem in the SASR due to the lack of ground-based monitoring that meets modern information requirements. Individual expeditionary studies of dust migration factors cannot provide representative data due to the vastness of the desert territories and significant spatiotemporal variability in their characteristics, which result from the unstable ecosystem of the SASR under crisis conditions. Thus, the task of building a dust migration model in the SASR based on ground-based monitoring can only be solved with an automated, extensive monitoring network that continuously registers indicators such as wind speed and direction, humidity, the mechanical composition of the underlying surface, air temperature, and humidity across the entire region.

In this study, long-term dust migration is determined by the activity of the wind regime, precipitation dynamics, vegetation cover (VC), and characteristics of desert surfaces, i.e., a combination of meteorological and ecological factors, the values of which can be obtained from electronic databases, literary sources, or Earth remote sensing (ERS) methods. When using these data in the long-term dust migration model, preliminary quantitative statistical analysis of the long-term dynamics of these factors is necessary, including correlation and regression analyses, distribution function calculations, approximation of actual data series, etc.

This project develops a dust migration model using a classical Gaussian model as the base, with the author's modification involving problem formulation, boundary conditions, algorithm construction, and a system of accepted conditions and simplifications. To quantitatively assess dust migration in the SASR from natural sources (Aralkum, Kyzylkum, Karakum, Ustyurt), two models were developed. The first model, the Long-Term Impact Model (LTI), is used to compute dust concentration fields over a specific period (month). This model is used at the analysis stage. The second model is designed to determine the long-term dynamics of atmospheric dust load (MYDD) at the synthesis stage. Descriptions of these models and calculation results are provided in Chapter 1 of the Report. Additionally, this chapter includes a detailed literature review and a constructive section discussing measures to mitigate dust migration.

The second chapter of the Report is devoted to the quantitative assessment of ecosystem services of vegetation as protection against salt dust emissions from the Desiccated Aral Seabed (DASB). For the first time, the degree of reduction in salt emissions (million tons/year) due to afforestation on the DASB is presented in concrete numbers, depending on their total projective coverage and the dynamics of the total area of plantations. For calculations, a computer model was developed in the MS Access environment.

The work uses the results of numerical modeling, regression equations, and empirical formulas obtained in the studies of scientific consultant B.S. Tleumuratova and employees of the Laboratory for Modeling Ecological Processes at the Karakalpak Branch of the Academy of Sciences of the Republic of Uzbekistan, E.P. Urazimbetova and Zh.Zh. Kublanov.

CHAPTER 1. DUST MIGRATION MODEL FOR THE SOUTHERN ARAL SEA REGION. MAPPED SPATIOTEMPORAL DYNAMICS OF AIR DUSTINESS IN THE LOWER AMU DARYA OASIS UNDER THE COMBINED INFLUENCE OF NATURAL SOURCES (DESERT SURFACES OF ARALKUM, USTYURT, KYZYLKUM, KARAKUM)

1.1 Relevance and Demand for the Topic

Atmospheric dust load (AD) is an important part of the global problem of environmental pollution. A significant portion of pollutants consist of dust, both industrial and natural in origin. Natural sources of atmospheric dust (desert territories) compared to industrial ones have much larger spatial scales of influence, are less manageable, and have a number of understudied aspects. AD is relevant for many countries worldwide, especially those located in desert zones, including Uzbekistan, vast territories of which are occupied by the Kyzylkum, Ustyurt, Aralkum, and partially Karakum deserts.

According to data from meteorological stations (MS), Earth Observation remote sensing (ERS), and modeling results, the total mass of dust entering the Earth's atmosphere is estimated at several hundred to several thousand million tons per year (Nickovic et al., 2001; Prospero et al., 2002). In addition to soil particles, dust contains heavy metals, pesticides, and microbes.

Excessive atmospheric dust load increases population morbidity and affects the regional environment and climate, altering biogeochemical cycles, exerting radiative effects on the atmosphere (Lemaître et al., 2010), suppressing cyclone activity (Dunion and Velden, 2004), and influencing cloud microphysics and the hydrological cycle (Dipu et al., 2013). Singh et al. (2008) found that dust deposition over the Arabian Sea can affect chlorophyll blooms, influence phytoplankton, and cool the ocean surface.

Other possible negative consequences of dust storms include:

- Reduced visibility, affecting air and road transport;
- Decreased sunlight reaching the Earth's surface;
- A "Blanket" thermal effect;
- The "Voeikov effect" with an air temperature increase of 6-7°K;
- Suppression of vegetation cover.

The growing AD worldwide affects radiative and thermal balances by absorbing and scattering solar radiation (Kondratyev, 1991; Wu et al., 2018; Tleumuratova, 2018), as well as precipitation formation processes and the cryosphere (Creamean et al., 2013; Karydis et al., 2011; Pan et al., 2019; Twohy et al., 2009; Tleumuratova, 2018), and has become a significant climate-forming factor.

Along with the well-known Albrecht, Voeikov, and Twomey effects, the dust influences cyclonic activity, manifesting in enhanced frontogenesis in the lower atmosphere (Chen et al., 1995), weakening of tropical cyclones (Dunion and Velden, 2004; Chen et al., 2010), and the intensity of the African Easterly Jet (Lavaysse et al., 2011; Tao et al., 2018). The effect of dust particle radiation scattering on surface wind has been studied in Australia (Alizadeh Choobari et al., 2013) and Iran (Alizadeh Choobari et al., 2012; Chen et al., 2023; Gautam et al., 2010), revealing a significant influence of dust aerosols on mid-tropospheric warming over the Indo-Gangetic Plains and Hindu Kush and reduced glacier albedo due to dust deposition. A similar influence of dust from the Middle East and Southwest Asia on accelerating glacier melting in the western Himalayas was studied by Prasad et al. (2009).

Protecting and strengthening public health is a primary state task aimed at sustainable socio-economic development of the country. Accordingly, numerous studies have been conducted on the impact of environmental pollution on population morbidity and mortality. Diseases related to atmospheric dust load arise from inhaling dust particles along with microbes, heavy metals, pesticides, and other pollutants contained in the soil (Bozlaker et al., 2013; Chen et al., 2004; Erel et al., 2006; Kaiser, 2005; Poulsen et al., 1995; Sanchez de la Campa et al., 2013; Schulz et al., 2012). Due to their micro- and nano-sizes, particles easily enter the lungs and penetrate the bloodstream. According to expert estimates in 2014, exposure to dust particles caused about 400,000 premature deaths in Europe from cardiopulmonary diseases in the population over 30 years old. Dust storms contribute to diseases such as asthma, tracheitis, pneumonia, allergic rhinitis, and silicosis (Wu et al., 2021). In addition to these well-known respiratory diseases (Bartzokas et al., 2004; Nastos et al., 2011; Middleton, 2020; Al-Hemoud et al., 2018; Kang et al., 2012; Wang et al., 2014), mineral dust is considered one of the most important risk factors for allergies and meningitis in Iran (Miri et al., 2007) and cardiovascular diseases in West Africa (Martiny and Chiapello, 2013), as well as psychological and cognitive (Ghaisas et al., 2016; Gordeev et al., 2013) and neurodegenerative diseases. (Aleya and Uddin, 2020; Chin-Chan et al., 2015; Galán-Madruga et al., 2020; Galán-Madruga and García Cambero, 2022; Shafiee et al., 2021) Currently, atmospheric dust load is the biggest public health problem in the Aral Sea region, as dust from the exposed Aral Seabed, containing toxic sulfates, is doubly dangerous (UNDP, 2012; Savchenko and Kozhakhmetov, 2017). In the Aral region, low birth rates, high mortality rates, low population health indices, unfavorable ecological conditions, and socially significant diseases reduce life expectancy

(Mukasheva, 2015). Research results in the Kyzylorda region of Kazakhstan indicate the adverse effects of atmospheric dust load on somatic and gynecological morbidity rates, as well as the etiology and structure of miscarriages. At the same time, the low health index of women is reflected in the health of their children (Abitaev et al., 2014; Mazhitova, Seisebaeva, and Umbetova, 2005).

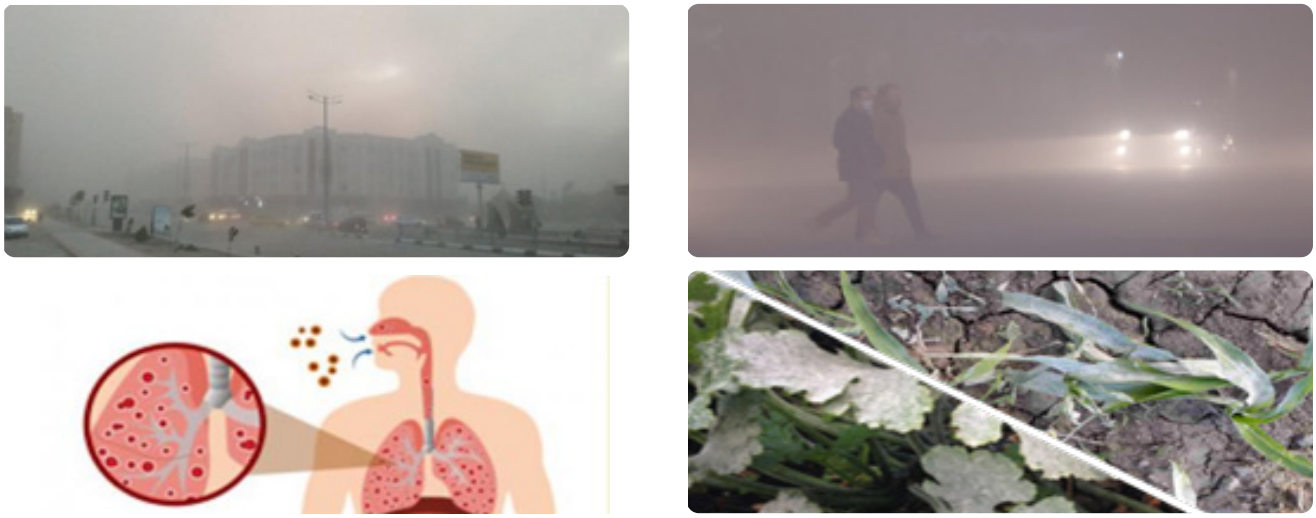

Fig.1.1. Consequences of Dust Storms

The most significant diseases related to dust are circulatory system disorders, malignant neoplasms, and tuberculosis. Solving these problems is especially urgent for the SASR, where most of the population lives in the central oasis, surrounded on all sides by the Kyzylkum, Karakum, Ustyurt, and Aralkum deserts, which are sources of large-scale atmospheric pollution during dust storms (Fig.1.1).

Studying desert dust cycles (from emission to long-distance transport and deposition) is crucial for addressing issues related to climate change, weather, ecosystems, air quality, and human health.

Most studies on atmospheric dust load focus on diagnosing dust concentrations during dust storms, the significance of which lies in their short-term, acute impact on the environment. However, as is known, long-term exposure to pollutants, even in much lower concentrations, is more dangerous, as it can lead to chronic poisoning. This aspect, in relation to the atmospheric dust load from deserts, is the least studied. In the Lower Amu Darya oasis, where most of the population of the SASR lives, including all of Khorezm, the Republic of Karakalpakstan, and the Kunyaurgench and Tashauz regions of Turkmenistan, atmospheric dust load is entirely unstudied (except for salt emissions from the exposed Aral Seabed). Along with studying the long-term dynamics of atmospheric dust load, which allows identifying process trends for forecasting purposes, it is also important to study its seasonal dynamics as a component. This provides scientifically based information on where and when in the Lower Amu Darya oasis region, the maximum permissible concentration (MPC) of dust is typically exceeded.

Moreover, the results of zoning atmospheric dust load can be used to determine zones of enhanced monitoring for healthcare and environmental protection agencies. Overall, the patterns, especially trends in atmospheric dust loads, can also be used in climatology, as atmospheric dust is a significant factor in climatic changes.

The relevance of the work is evidenced by its alignment with the tasks of environmental protection and rational use of natural resources, as defined in government documents such as the Decree of the President of the Republic of Uzbekistan No. PP-338 dated September 24, 2024, "On Priority Measures to Combat Dust Storms and Improve Atmospheric Air Quality," the Decree of the President of the Republic of Uzbekistan No. UP-158 dated September 11, 2023, "On the 'Uzbekistan-2030' Strategy," the Decree of the President of the Republic of Uzbekistan No. PP-76 dated December 30, 2021, "On Measures to Protect the Environment and Organize the Activities of State Bodies in the Field of Environmental Control," the Decree of the President of the Republic of Uzbekistan No. PP-4850 dated November 6, 2020, "On Approval of the Concept for the Development of the Forestry System of the Republic of Uzbekistan Until 2030," the Decree of the President of the Republic of Uzbekistan No. UP-5863 dated October 30, 2019, "On Approval of the Environmental Protection Concept of the Republic of Uzbekistan Until 2030," the Resolution of the Cabinet of Ministers of the Republic of Uzbekistan No. 41 dated January 25, 2022, "On Additional Measures to Transform the Aral Sea Region into a Zone of Ecological Innovations and Technologies," the Resolution of the Cabinet of Ministers No. 31 dated January 18, 2022, "On Additional Measures to Create a 'Green Cover'—Protective Forests on the Exposed Bed of the Aral Sea and the Aral Sea Region," and other regulatory legal documents adopted in this sphere.

1.2 Analysis of Dust Migration Factors and Data Used

The territory of the SASR generally represents the Lower Amu Darya oasis (LADO), surrounded by desert surfaces of Kyzylkum, Karakum, Ustyurt, and Aralkum—powerful sources of dust (Fig. 1.2). The uniqueness of this territory lies not only in its geographical aspect but also in the fact that the SASR is at the epicenter of the Aral Sea crisis with all its negative consequences. The flat topography, active wind regime (Fig. 1.3), scarcity of precipitation cleanses the atmosphere, and the presence of vast desert territories create maximally favorable conditions for dust emission from the underlying surface and its spread over long distances.

Fig. 1.2. Lower Amu Darya Oasis Surrounded by Deserts

The study used meteorological (wind regime, precipitation) and ecological data (desert area, vegetation cover, mechanical composition of desert surfaces).

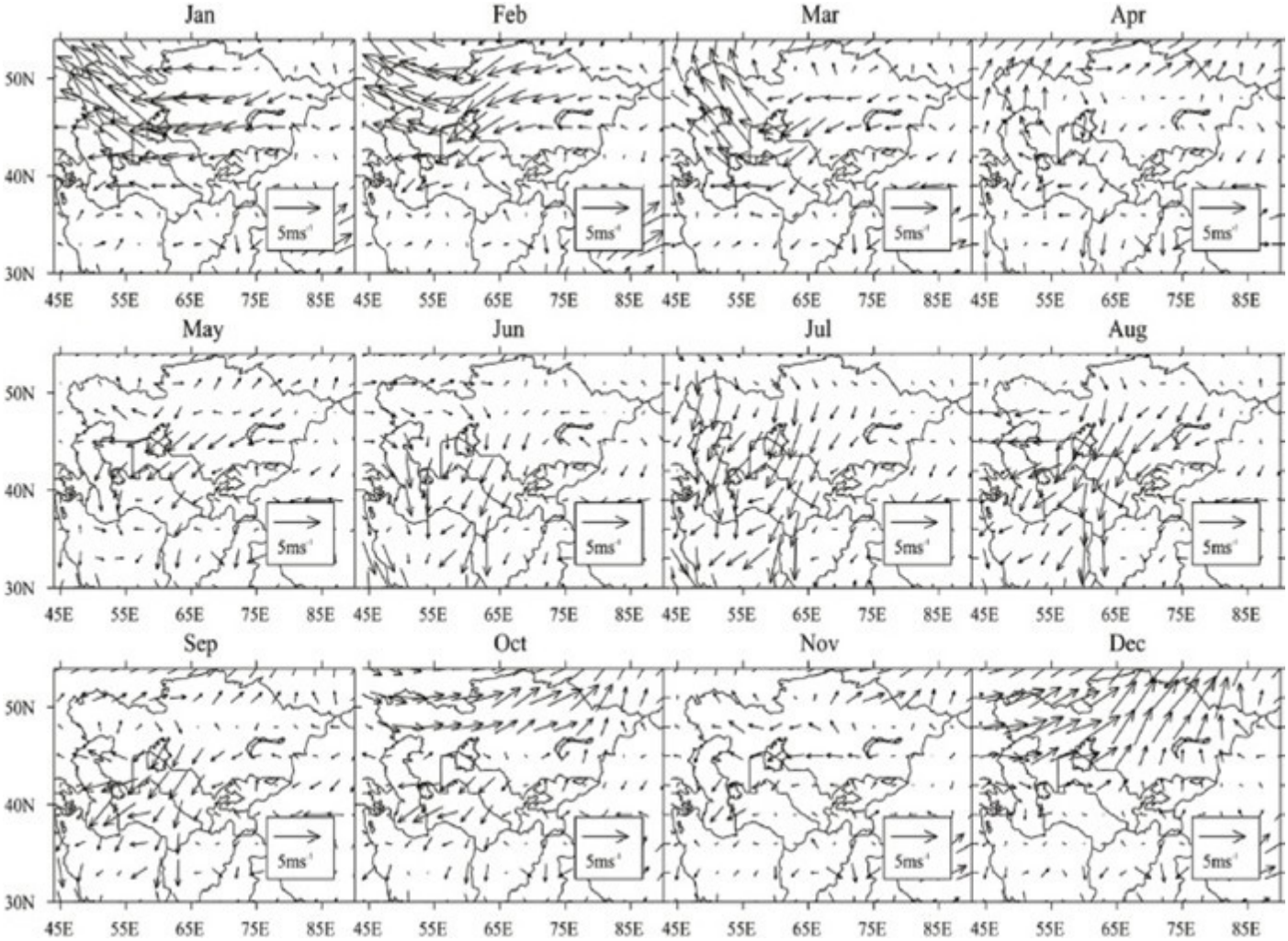

Fig. 1.3. Annual Wind Field at 1000 hPa (averaged from 1980 to 2018 using ECMWF datasets).

Below are graphs (Figs. 1.4-1.6) of the annual precipitation, wind speed, and direction in Muynak according to Weather Spark data (https://ru.weatherspark.com). The data is based on the MERRA-2 model. This data describes typical weather in Muynak, based on statistical analysis of historical hourly weather reports and model reconstructions from January 1, 1980, to December 31, 2016.

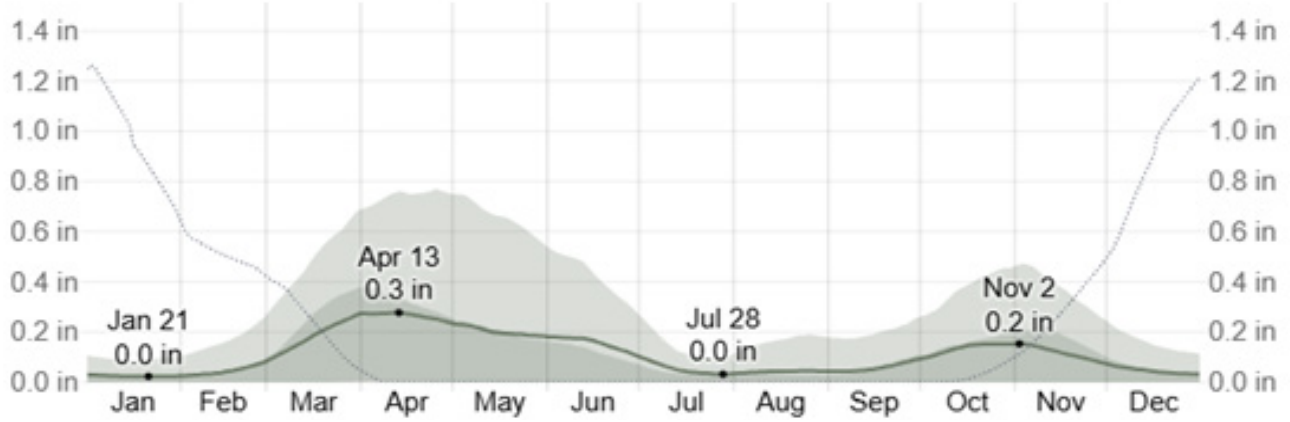

Fig. 1.4. Average Rainfall (solid line) Accumulated Over a 31-Day Period Centered on the Day in Question, with 25-75 and 10-90 Percentile Ranges. The Thin Dotted Line Represents the Corresponding Average Snowfall (https://ru.weatherspark.com).

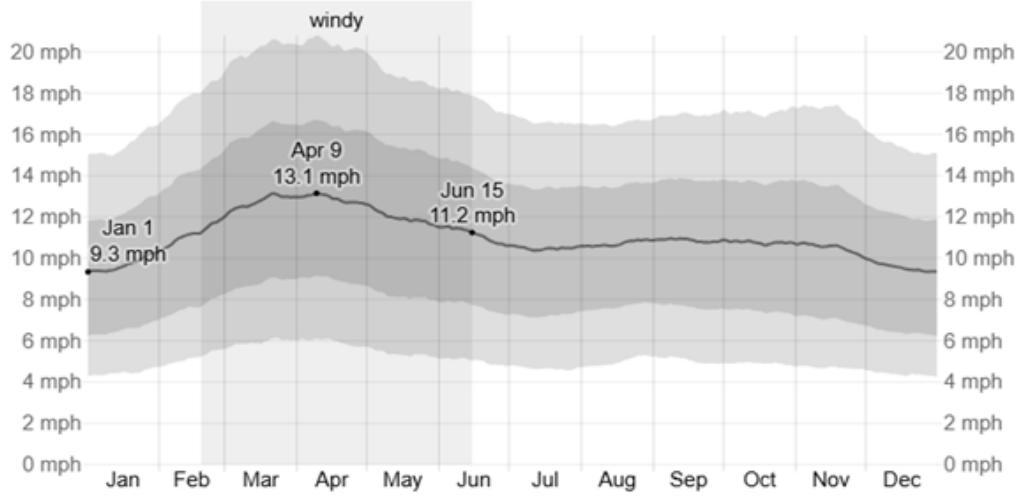

Fig. 1.5. Average Hourly Wind Speed (dark gray line) with 25-75 and 10-90 Percentile Ranges (https://ru.weatherspark.com).

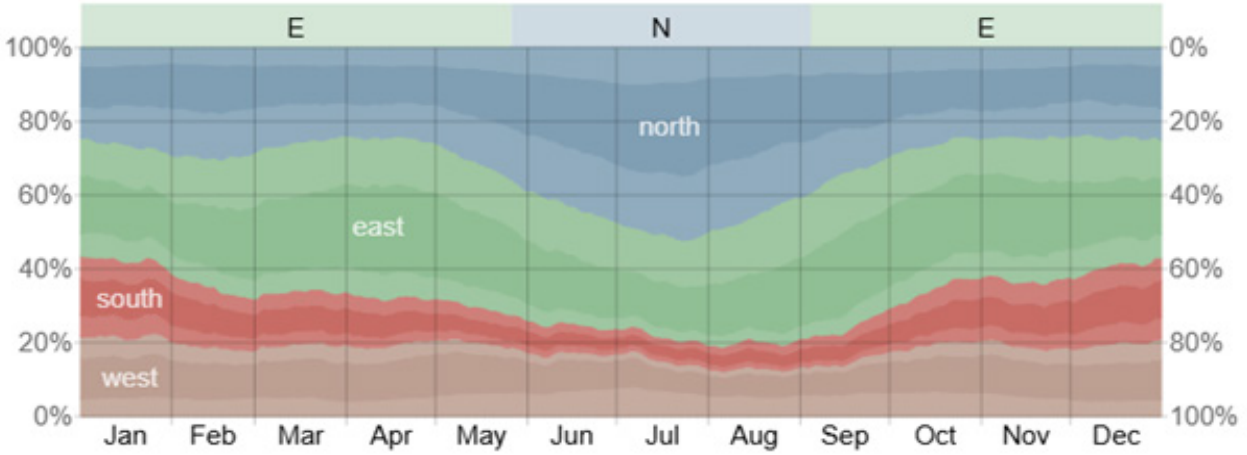

Fig. 1.6. Percentage of Hours During Which the Average Wind Direction Corresponds to Each of the Four Primary Wind Directions, Excluding Hours with Average Wind Speeds Less Than 1.6 km/h (https://ru.weatherspark.com).

The wind rose (Fig. 1.7) for the territories of the mentioned deserts, constructed using data (Scientific and Applied Climate Reference of the USSR; http://www.pogodaiklimat.ru), exhibits significant spatiotemporal dynamics.

An analysis of the wind roses for the deserts surrounding the LADO shows a growing trend in both wind intensification and an increase in the frequency of wind directions toward the LADO.

MC	1961	1990	2020
Muynak (Aralkum)	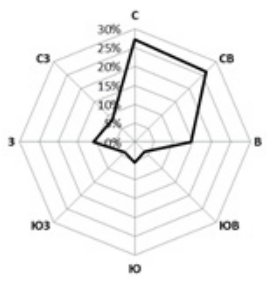	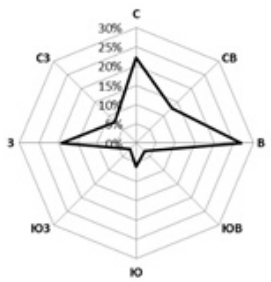	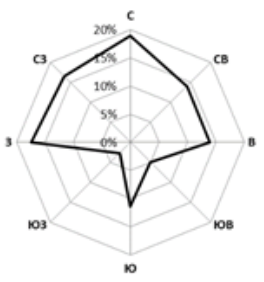
Jasliq (Ustyurt)	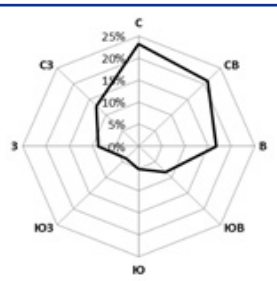	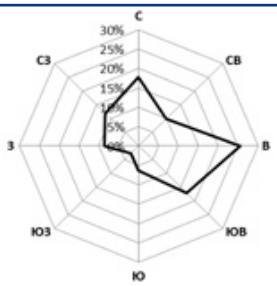	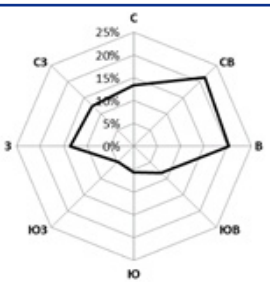

Takhtakupir (Kyzylkum)	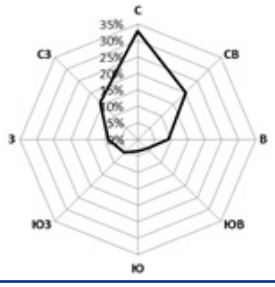	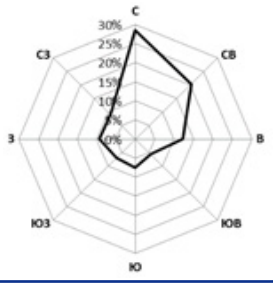	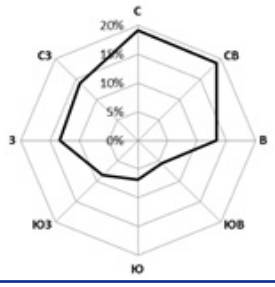	
Shakhsanem (Karakum)	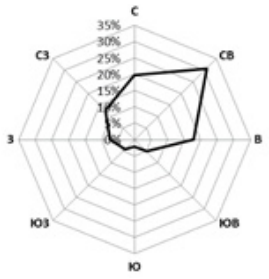	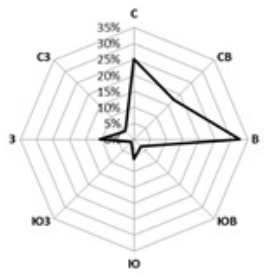	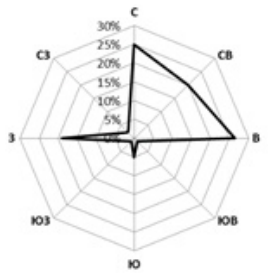	

Fig. 1.7. Spatiotemporal Dynamics of Annual Wind Roses by Meteorological Stations

Overall, trends in meteorological data indicate an increase in the dust migration-enhancing factor—wind patterns—and a decrease in the mitigating factor—precipitation. This results in a nonlinear progression of dust migration from desert territories in the SASR.

In developing the migration model, additional data were used, such as the physiographic characteristics of the Southern Aral Sea deserts, which vary both temporally and spatially, as presented in Table 1.1 for the last decade.

Table 1.1

Physiographic Characteristics of the Southern Aral Sea Deserts

	Aralkum	Ustyurt	Kyzylkum	Karakum
Area (km²)	62,1	212	> 300	> 350
Mean Total protective (TPC) (%)	10	27	19	15
Wind Regime (%)	C (24)	B (26)	C (25)	B (30)
Precipitation (mm)	52,6	53,1	39,3	29,1
Soil Composition	Solonchaks, sands, loams	Gypsum, solonchaks, sandy-rocky	Sandy, gypsum, solonchak	Sandy, gray-brown, takyr-like

The areas of the Kyzylkum and Karakum deserts are expanding due to sand migration at a rate of 2.5 m/year. The Aralkum's area is increasing due to the desiccation of the Aral Sea. The Ustyurt's area, bounded by the Caspian Sea on one side and a cliff (chink) on the other, remains relatively stable. Overall, the expansion of deserts—i.e., dust sources—is clearly a factor intensifying dust migration.

Vegetation cover in the SASR shows a consistent decline. In natural deserts (Ustyurt, Kyzylkum, Karakum), this trend is driven by the Aral Sea crisis, climate warming, and, in part, salt emissions. In the Aralkum, the trend is due to increasing soil salinity and salt emissions.

The migration of dust, in terms of erodibility and health hazards, depends on soil composition. The most hazardous dust migration comes from the Aralkum, where 50–60% of the dust consists of easily erodible and toxic sulfates (Wikipedia contributors, n.d.).

The mechanical composition of Ustyurt's soils, which experience the highest wind activity, is shifting toward increased salinity due to the predominant westward and southwestward transport of salts from the Aralkum. Thus, dust from the Ustyurt contains not only gypsum but also salts of Aral origin.

The predominantly sandy composition of the Kyzylkum and Karakum deserts results in the lowest ecological hazard from dust migration in these areas.

1.3 Methods for Studying Dust Migration

Various methods are used in dust storm monitoring, implementing ground-based observations, satellite remote sensing, and integrated approaches using mathematical modeling. The combination of different monitoring methods allows for comprehensive and repeatedly verified information about the state of the environment (Tleumuratova, 2004).

Field monitoring (instrumental measurements, chemical analysis of air samples) of atmospheric air conditions in most studies serves to identify and quantitatively assess situations that may lead to atmospheric pollution and pose a threat to the life and health of citizens. Ground-based monitoring remains in demand to this day as the most realistic source of information on atmospheric pollution. Furthermore, ground-based monitoring data are widely used to adjust remote sensing of the Earth (ERS) data and validate model calculations. Therefore, the ground-based monitoring system is constantly being improved and currently represents automated and computerized technologies with continuous recording and storage of information on near-surface air and underlying surface conditions.

The most challenging task in atmospheric pollution monitoring is the quantitative assessment of the 3D distribution of dust in the atmosphere, which can be best approached through mathematicall modeling. Numerous models have been developed for both stationary and acute atmospheric pollution (Wu et al., 2020; Tleumuratova, 2004, 2018; Shao et al., 2011; Akhlaq et al., 2012; Sorek-Hamer et al., 2013).

The development of dust models requires an understanding of factors influencing dust emission: wind speed, soil structure, mechanical and mineral composition, moisture content, electrostatic forces, and others (Webb & Strong, 2011; Zobeck, 1991; Belnap & Gillette, 1997; Cornelis & Gabriels, 2003; Hagen, 2004; Nickovic et al., 2012; Journet et al., 2014; Perlwitz et al., 2015; Pérez García-Pando et al., 2016; Pi et al., 2017). Collectively, these factors determine the weight, drag, and cohesion between soil aggregate particles, as well as the critical friction velocity u_*, which is the most important parameter governing dust migration intensity.

Although dust model development has advanced significantly over the past 30 years, simulation results remain fraught with uncertainties. Dust models developed for specific regions require careful calibration when applied to other regions (Chen, Meng et al., 2022).

The primary issue with ERS methods is cloud cover, which impedes the accurate representation of aerosol conditions and underlying surface state. The sensitivity of the aerosol index (AI) to dust aerosols strongly depends on aerosol layer height; aerosols below ~500 m are scarcely detected (Hsu et al., 1999). Therefore, critical information on dust levels in the human activity layer (0–3 m) can only be obtained through ground-based contact measurements and modeling. The inadequate state of ground-based monitoring in the SASR makes mathematical modeling the sole viable method for determining air quality in this area.

Since existing models (Darmenova & Sokolik, 2007; Shao, 2000; Benedetti et al., 2019, among others) do not fully align with the objectives of this study, the development of specialized models addressing the requirements of the posed problem was necessary. Model development, in the broadest sense, involves not only constructing the mathematical model itself but also setting boundary conditions, designing calculation algorithms, and establishing a system of accepted assumptions and simplifications (Tleumuratova, 2018).

In this work, two models for the quantitative assessment of dust migration in the SASR from natural sources (Aralkum, Kyzylkum, Karakum, Ustyurt) were developed. The first model, the Long-Term Impact Model (LTI), calculates dust concentration fields over a specified time interval (monthly). This model is used during the analysis stage. The second model, the Multi-Year Dust Dynamics Model (MYDD), is employed during the synthesis stage to determine long-term dust dynamics.

The problem of atmospheric dust migration in the SASR is addressed in stages. At the first stage, input data for each of the four desert sources (monthly wind roses, precipitation amounts, total projective cover (TPC), and soil mechanical and granulometric composition) are statistically processed.

At the second stage, monthly average dust concentration fields from each source are computed individually. At the third stage, the calculated monthly average concentration fields are combined coordinate-wise, thereby determining the cumulative impact of all sources on atmospheric pollution.

The modeling period—1961–2020—is divided into decades (1961–1970, 1971–1980, etc.), as these intervals reflect significant natural transformations and align with traditional temporal divisions in ecological-geographical studies of the Aral Sea crisis evolution (Tleumuratova, 2018; Kublanov, 2023; Urazimbetova, 2024a). Additionally, this quanti-

zation mitigates substantial interannual variability in ecological conditions caused by external geophysical factors (e.g., droughts, low-water years, shifts in circulation epochs). Decades are numbered chronologically: N=1 for 1961-1970, N=2 for 1971–1980, and so forth.

The modeling domain encompasses the SASR and a significant portion of Aralkum to account for aerosol transport. The study area boundaries are approximately 45°53'N latitude to the north, 40°16'N latitude to the south, 57°07'E longitude to the west, and 62°23'E longitude to the east (Fig. 1.8).

Aggregately, the SASR comprises five areas: the Lower Amu Darya Oasis (LADO), Kyzylkum, Karakum, Ustyurt, and Aralkum. Since the majority of Karakalpakstan's population resides in the LADO, the quantitative assessment of atmospheric pollution in this area is of particular relevance and forms the focus of this study.

The global computational domain is a two-dimensional array of elementary cells sized 25×25 km (Fig. 1.8). During calculations, subarrays are formed: MKZ (Kyzylkum), MAK (Aralkum), MUS (Ustyurt), MKR (Karakum), and MV (Lower Amu Darya Oasis) (Urazimbetova & Tleumuratova, 2024).

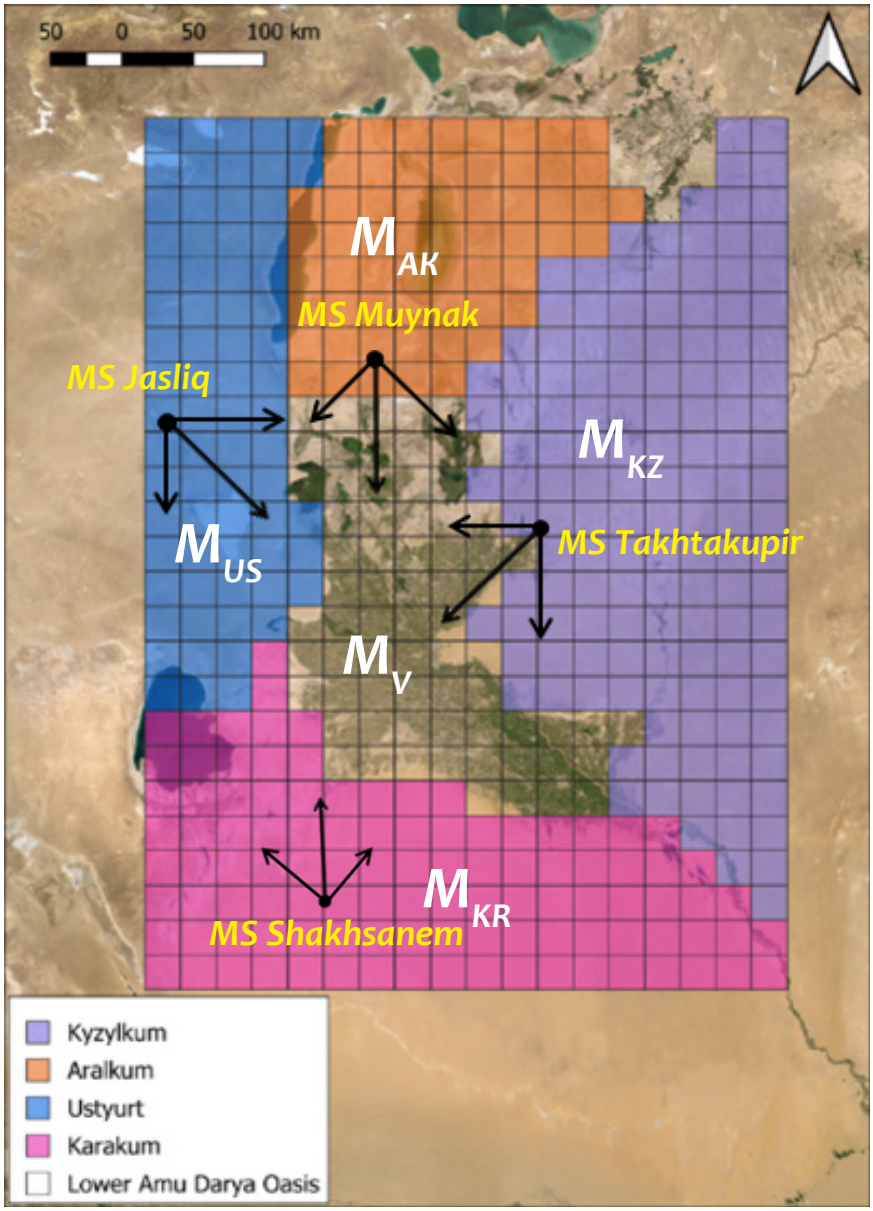

Fig. 1.8. Calculation domain

The base model chosen was a statistical Gaussian model based on Ermak's approximation, accounting for the dry deposition rate, the dominant mechanism in arid regions (Ermak, 1977):

$$C(x,y,z)=\frac{Q}{2\pi\sigma_y\sigma_z u}\exp\left\{-\frac{y^2}{2\sigma_y^2}\right\}\exp\left\{\frac{-V_g(z-h)}{2K}-\frac{V_g^2\sigma_z^2}{8K^2}\right\}\times\left[\exp\left\{-\frac{(z-h)^2}{2\sigma_z^2}\right\}+\right.$$
$$\left.+\exp\left\{-\frac{(z+h)^2}{2\sigma_z^2}\right\}-\sqrt{2\pi}\frac{V_1\sigma_z}{K}\exp\left\{\frac{V_1(z+h)}{K}+\frac{V_g^2\sigma_z^2}{2K^2}\right\}erfc\left\{\frac{V_1\sigma_z}{\sqrt{2}K}+\frac{z+h}{\sqrt{2}\sigma_z}\right\}\right] \quad (1.1)$$

where $C(x,y,z)$ – dust concentration (μg/m³), Q – emission flux (μg/m·s) (Lu & Shao, 2001), u – wind speed (m/s), σ_y – horizontal dispersion coefficient (m), σ_x vertical dispersion coefficient (m), V_d – dry deposition velocity of particles (m/s), V_g – gravitational settling velocity of particles (m/s), K – turbulent diffusion coefficient (m²/s) (Meister et al., 2000; Droppo, 2006; Venkatram, 1980).

To calculate the horizontal and vertical dispersion coefficients σ_y and σ_z, the empirical formulas proposed by Pasquill (1979) were used:

$$\sigma_y=\exp\left(l_y+J_y\ln(x)+K_y(\ln(x))^2\right)$$
$$\sigma_z=\exp\left(l_z+J_z\ln(x)+K_z(\ln(x))^2\right)$$

These formulas account for the influence of meteorological conditions and atmospheric stability class on the dispersion of pollutants.

The parameter values $l_y, J_y, K_y, l_z, J_z, K_z$ required for the computation of the dispersion coefficients σ_y and σ_z are presented in Table 1.2. This table demonstrates their dependence on the atmospheric stability class (ranging from A — extremely unstable, to F — extremely stable). The values are based on experimental data and are widely used in atmospheric diffusion modeling.

Dependence of Dispersion Coefficients on Atmospheric Stability Table 1.2

Stability Class	l_y	J_y	K_y	l_z	J_z	K_z
A	-1,104	0,9878	-0,0076	4,679	-1,7172	0,277
B	-1,634	1,035	-0,0096	-1,999	0,8752	0,0136
C	-2,054	1,0231	-0,0076	-2,341	0,9477	-0,002
D	-2,555	1,0423	-0,0087	-3,186	1,1737	-0,0316
E	-2,754	1,0106	-0,0064	-3,783	1,301	-0,045
F	-3,143	1,0148	-0,007	-4,49	1,4024	-0,054

Particle density and diameter were assigned based on the most common aerosol microparticles found in the Aral Sea region (Table 1.3).

Characteristics of Desert Soil Composition Table 1.3

Code	Name	Mineral	Density (g/cm³)	Size (μm)
1	Quartz dust	Quartz	2,45	1
2	Quartz PM5	Quartz	2,45	5
3	Quartz PM10	Quartz	2,45	10
4	Feldspar dust	Feldspar	2,6	1
5	Feldspar PM5	Feldspar	2,6	5
6	Feldspar PM10	Feldspar	2,6	10
7	Halite dust	Halite	2,2	1
8	Halite PM5	Halite	2,2	5
9	Halite PM10	Halite	2,2	10

The key innovation of our model is that pollution fields are determined not from a single source (as is typical) but from a complex of sources (Aralkum, Kyzylkum, Karakum, Ustyurt), each with distinct underlying surface characteristics (vegetation cover, soil mechanical composition) and wind regimes.

Input Data

S The primary input for the model is wind speed and direction.

The assessment of the long-term (monthly average) impact of pollution sources on the environment typically involves calculating the average concentration of pollutants over a period T (Marchuk, 1982). Since the assumption of constant wind velocity $\vec{U}$ throughout such an extended period T is too rough and far from reality, the entire modeling period T is divided into several sufficiently small time intervals Δt_i, during which a specific type of atmospheric circulation can be considered stationary. As the transition between circulations occurs over a much shorter time than the duration of this type of motion, it can be assumed that the shift between motion types happens instantaneously (Marchuk, 1982). Thus, the average concentration of pollutants over the period T is expressed as a linear combination of solutions to the main task C_i for each time interval Δt_i (Tleumurátova, 2004):

$$C = \frac{1}{T}\sum_{i=1}^{n} C_i \Delta t_i \qquad (1.2)$$

Atmospheric circulation types are differentiated by three parameters: atmospheric stratification, wind velocity, and wind direction. By numbering all possible values of these parameters, we establish a one-to-one correspondence between the set of atmospheric circulation types characteristic of the period T, and the triplets of natural numbers (k,m,l), where m- the atmospheric stratification index, l- is the wind velocity index, and k- is the wind direction index. The choice of these three parameters is due to the fact that in the Gaussian model, wind velocity $\vec{U}$ and the turbulent diffusion coefficient K_z, are included as coefficients that determine the pollutant distribution. Since the concept of "atmospheric circulation type" is broader than the specified set of three meteorological parameters, it will be referred to as the meteorological situation (k,m,l).

We denote the frequency of occurrence of a given meteorological situation (k,m,l) by $f(k,m,l)=(\Delta t_i)/T$, where Δt_i is the time duration of the situation and T is the total modeling period. Let $C_{k,m,l}$ be the solution to the governing equation under the meteorological situation (k,m,l) over the period T. This method of presenting input information requires a significant number of statistical calculations on the frequency of meteorological situations (k,m,l) differentiated for each source and for each month of the modeling period. Statistical analysis is complicated by the fact that meteorological situations are three-parameter indicators.

Desert Aerosol Transport

The transport of desert aerosol is significantly influenced by the vegetation cover, which is known to reduce wind speed and, consequently, the volume of dust transport. To calculate the degree of wind attenuation by vegetation cover, the following formula is applied (Bykova, Dubov, 1974):

$$u_r = 0{,}83\delta_f c_{Hh}^{0,5} u_a + (1-\delta_f)\, u_a \qquad (1.3)$$

where $\boldsymbol{u^a}$- the background wind velocity, $\boldsymbol{c_{Hh}}$- is the heat exchange coefficient at the upper boundary of the vegetation layer, and, $\boldsymbol{\delta_f}$ - total projective cover (TPC) (Tleumurátova, Kublanov, 2022).

The consideration of the vegetation cover's dust transport mitigation effect is performed by substituting the value of $\boldsymbol{u_r}$ into the Gaussian model.

In addition, it is well known that even very slight precipitation (0.1 mm) reduces dust transport to zero. Therefore, to account for precipitation effects, the frequency of days with precipitation is subtracted. Accounting for the mitigating influence of vegetation cover and precipitation on atmospheric dust load is one of the novel aspects in the development of the long-term impact model (LTI).

The final result of implementing the LTI is the average dust concentration over the period T (month) $\boldsymbol{C_p\,(\bar{x}\,\bar{y}\,\bar{z})}$ – which is represented as a weighted sum (Tleumuratova, 2004):

$$C_{\partial}(\bar{x},\bar{y},\bar{z}) = \sum_{n}^{N}\sum_{k}^{K}\sum_{m}^{M}\sum_{l}^{L} S(x,y,z,n,k,m,l)\cdot\left[f(k,m,l) - f_{oc}\right] \qquad (1.4)$$

where p is the number of sources, $S(x,y,z,n,k,m,l)$- is the solution of the Gaussian model obtained for the p - th under the meteorological situation (k,m,l), $f(k,m,l)$- Frequency of the meteorological situation, f_{oc}- Decadal average frequency of precipitation during warm seasons.

Statistical approximation and decadal averaging are extensively applied during the synthesis phase. The long-term dust migration dynamics in the Southern Aral region are represented by the long-term dynamics of atmospheric dust load (MYDD), a statistical framework comprising regression equations derived from this study and prior work. These equations serve as empirical generalizations of natural processes.

Statistical analysis of the four factors influencing dust transport dynamics in the Aral Sea region over the period 1961–2020 has shown a pronounced trend toward an increase in the number of days with wind speeds exceeding 4 m/s, an expansion of desert areas, a decrease in precipitation, and a reduction in the overall projective vegetation cover. An important condition of the MYDD model is the pairwise independence of the factors, which allows their combined influence on atmospheric pollution to be represented as a superposition of singular effects.

When determining the multi-year dynamics of atmospheric pollution in Karakalpakstan, the MYDD (in contrast to the LTI) employs a relationship that expresses the ground-level concentration in terms of the total dust transport volume V from the deserts (Tleumuratova, 2018):

$$C_н = 3{,}3kV\exp(-0{,}015x - 0{,}6) \qquad (1.5)$$

where k - a scaling coefficient, $C_н$ - is the ground-level concentration of salts (Tleumurátova, 2018), and x - the distance from the boundary nodes of the source in the direction of the prevailing wind.

Preliminary statistical analysis showed that the discrepancy between the calculation results using relation (1.5) and the Gaussian model is insignificant, not exceeding 8%.

The methodology from (Tleumuratova, 2004, 2018; Kublanov, 2023) was employed to estimate V.

The emission of desert aerosol per unit area of a specific source V_0 over a specific period T is equal to the product of the source strength F and the duration of energy-active (exceeding 4 m/s) wind speeds T_e (hours/year), determined from meteorological reference books (Tleumuratova, 2002):

$$V_0\,(T,N)=F(T,N)\;T_э\,(T,N) \tag{1.6}$$

Then, evidently, the total desert aerosol emission from the entire source area is $V_p=V_0\,S_p$.

To determine the source strength F (impurity flux per unit area per unit time, μg/m²·s) the formula from (Tleumuratova, 2004, 2018; Kublanov, 2023) is used, based on Lu and Shao (2001):

$$F=\frac{0{,}12C_H g\rho_s}{p}Q, \qquad Q=\frac{c\rho u_*^3}{g}\left[1-\left(\frac{u_{*кр}}{u_*}\right)^2\right] \tag{1.7}$$

where: Q: impurity discharge rate, ρ: air density, ρ_s: particle density, p: deformation pressure exerted by the soil surface on moving aerosol particles, g: gravitational constant, u_*: friction velocity, $c=0{,}25+0{,}33\,w_g/u_*$: Owen's coefficient (Owen, 1964), d: particle diameter, u_{*cr}: critical friction velocity (Kondratyev & Grigoriev, 2000), C_S: near-surface aerosol concentration, determined by the salt content in the soil's surface layers (Tleumuratova, 2004).

To account for the influence of mitigating factors (vegetation cover [VC] and precipitation), the average annual dust emission N for decade V_0 is first computed without considering these factors using Formula (1.6).

By calculating $\Delta F=F(u_a)-F(u_r)$ using Formula (1.3), the reduction in dust emission strength of the underlying surface (μg/m²·s) is obtained (Tleumuratova, 2004, 2018; Kublanov, 2023). The average annual weakening effect of vegetation cover on salt emission in the N-th decade is computed as:

$$\Delta V_{РП}\,(N)=\Delta F(N)\;T_э\,(N)\;S_p\,(N) \tag{1.8}$$

where:

$T_e\,(N)$- annual duration of energy-active wind speeds in the N-th decade,

$S_p\,(N)$- source area (desert).

The weakening effect of precipitation on emission is calculated by:

$$\Delta V_{oc}=V_0 f_{oc} \tag{1.9}$$

Thus, the real average seasonal dust emission from the p-th desert, accounting for the influence of vegetation cover (VC) and precipitation, is:

$$V_p(N)=V_0(N)-\Delta V_{РП}(N)-\Delta V_{oc}(N) \tag{1.10}$$

Substituting the obtained value V_p into Formula (1.5), we determine the average seasonal dust concentration field in the N decade caused by wind-driven emission from the p-th desert.

Structure of the MYADLD Model

The Multi-Year Atmospheric Dust Load Dynamics (MYADLD) model consists of six computational blocks (Fig 1.9). Each block is directly linked to specific data and equations described earlier in the section:

1. **First Block**: Uses statistical data from four major dust sources (Aralkum, Ustyurt, Kyzylkum, Karakum) such as wind speed, precipitation, vegetation cover (VC), and soil texture. These data form the basis for regression equations that model the long-term dynamics of dust emission drivers.
2. **Second Block**: Estimates baseline dust emission V_0 under conditions of no vegetation cover and no precipitation. This is based on the occurrence of wind speeds exceeding 4 m/s and soil susceptibility to deflation, as described by equations (1.6) and (1.7).
3. **Third Block**: Calculates the reduction in emissions due to vegetation cover and precipitation. It applies weakening coefficients from equations (1.3), (1.8), and (1.9), using average VC and precipitation values for each desert region.
4. **Fourth Block**: Derives the actual seasonal dust emission V_p for each desert by applying the reduction factors from Block 3 to the baseline values from Block 2. This process is represented by equation (1.10).
5. **Fifth Block**: Produces seasonal dust concentration fields based on emissions from Block 4. It spatially distributes dust using the relationships defined in equation (1.5).
6. **Sixth Block**: Aggregates the seasonal fields from Block 5 across all sources and decades. This results in the cumulative dust concentration field for the modeled period, incorporating each desert's contribution independently.

This structure ensures that every input—meteorological, ecological, and geographic—is systematically processed and contributes logically to the final simulation output. A critical assumption of the model is the pairwise independence of factors, enabling the combined influence on atmospheric pollution to be represented as a superposition of source-specific effects.

The algorithm for calculating the multi-year dynamics of atmospheric dust load is two-cyclic:

- The outer cycle iterates over the number of deserts.
- The inner cycle iterates over the decades of the modeling period.

The MYADLD model's implementation software was written in the C++ programming language (Appendix 3).

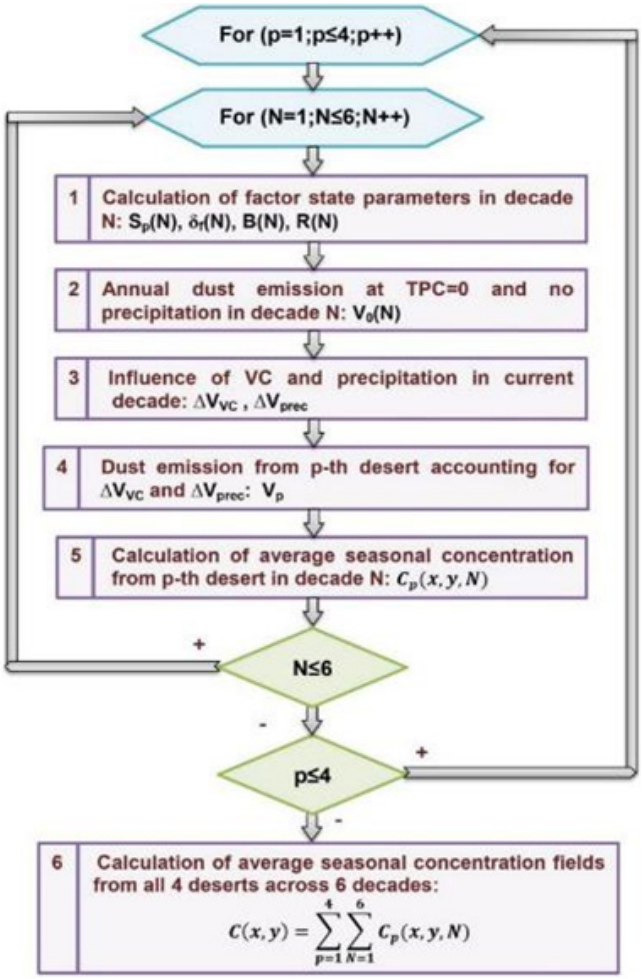

Fig. 1.9. Algorithm for Implementing the MYDD

The originality of the developed software is confirmed by Certificate No. DGU 37107: "Software Suite for Modeling the Impact of Soil Aerosol Wind Erosion from Desert Territories on Atmospheric Pollution in the Lower Amu Darya Oasis" and Certificate No. DGU 42031: "Software Suite for Modeling Vegetation Cover Mitigation of Soil Aerosol from Deserts" ("Cho'llardan tuproq aerozolini o'simlik qoplami bilan ushlab qolish modeli uchun dasturiy ta'minot to'plami").

1.4 Results of Dust Migration Research in the Southern Aral Sea Region

1.4.1 Statistical Analysis of Long-Term Dust Migration Factors

The emission of dust-sand aerosol into the atmosphere depends primarily on wind regimes, which are governed by atmospheric circulation processes. We conducted a statistical analysis to align time-series observational data (Subbotina & Chanysheva, 2006; http://www.pogodaiklimat.ru), integrate datasets, and derive statistical indicators. Key results are summarized below. First, we analyzed long-term wind regime data (days with wind speeds > 4 m/s) for the four dust emission sources (Fig. 1.10). The analysis revealed a consistent increase in the number of days with wind speeds exceeding 4 m/s across all four regions, indicating a growing potential for dust emissions over time.

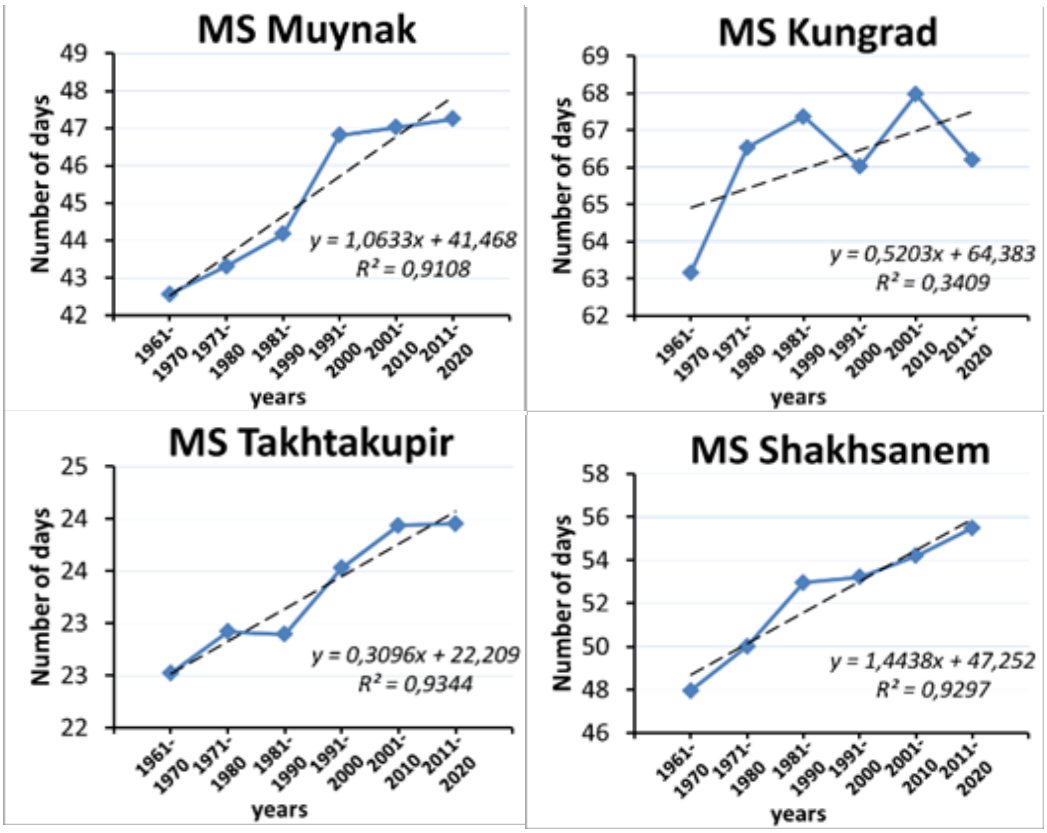

Fig. 1.10. Number of days with wind speeds exceeding 4 m/s.

Statistical analysis of warm-season precipitation data (Fig. 1.11) revealed a significant recent trend toward fewer rainy days, likely due to excessive atmospheric aerosol (condensation nuclei) concentrations. As shown in (Tleumuratova, 2018), aerosol concentrations exceeding a critical threshold (100–150 μg/m³) at condensation levels suppress precipitation formation. Additionally, reduced rainfall may be attributed to regional climate warming (2–3 K), causing cloud droplets to evaporate before reaching the surface.

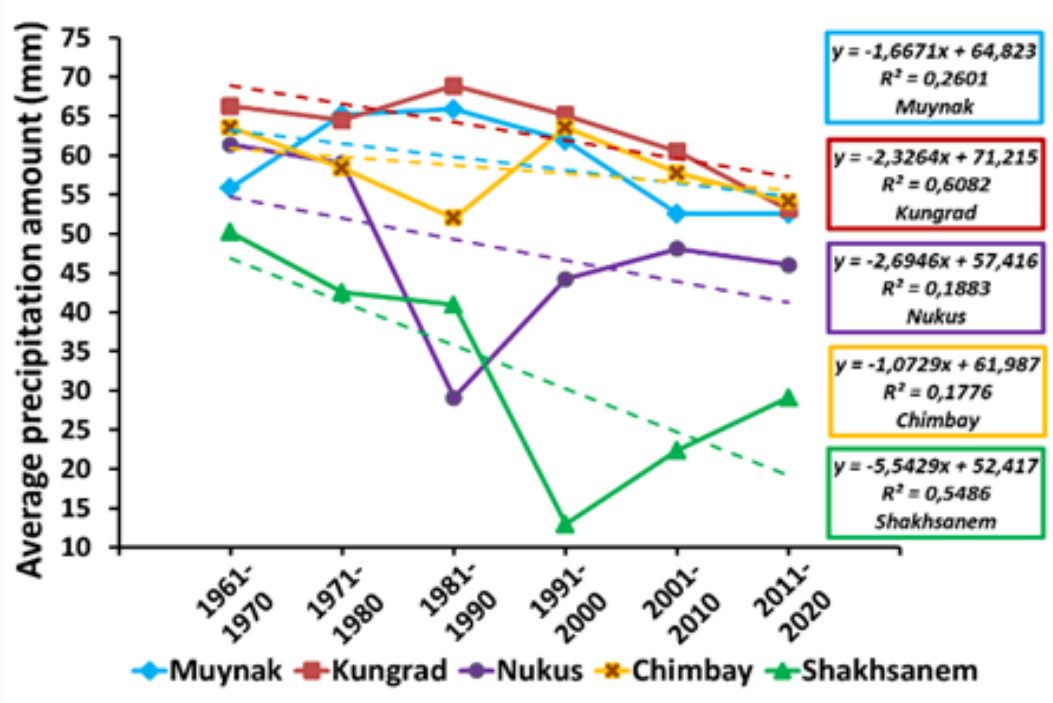

Fig. 1.11. Long-term precipitation dynamics (April–October) from meteorological stations.

The long-term dynamics of the third atmospheric dust loading (ADL) factor—desert source areas—are shown in Fig. 1.12. The Ustyurt Plateau's area remains stable due to natural boundaries (Caspian Sea to the west, cliffs to the east). The Aralkum Desert exhibits the most dynamic expansion, approaching its climatic attractor. In other words the desert is expanding in a steady, climate-driven direction. The Kyzylkum and Karakum deserts are expanding at an average rate of 0.75 m/year due to sand migration. Satellite imagery from Landsat 8 and Sentinel-2 corroborates these trends.

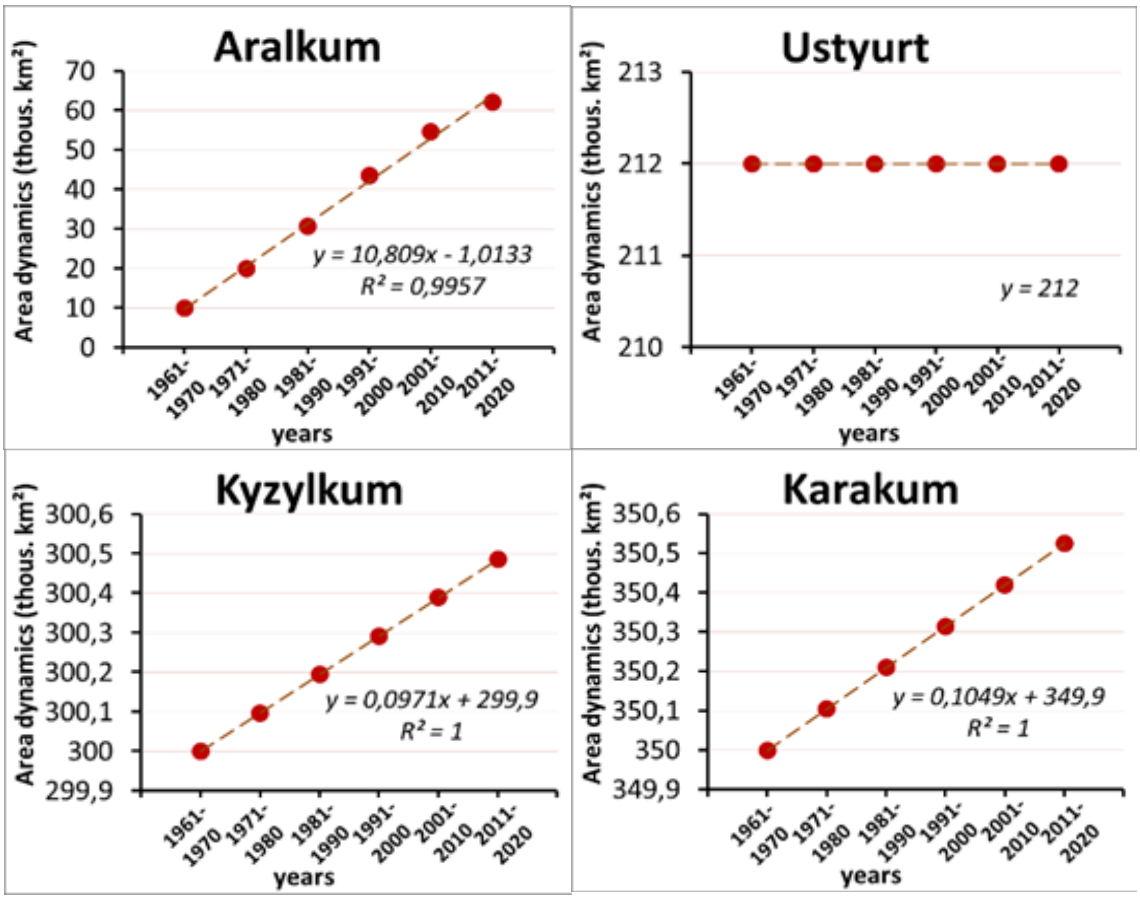

Fig. 1.12. Long-term dynamics of desert areas.

Determining the multi-year dynamics of vegetation cover (VC) in deserts is challenging due to the scarcity of continuous high-resolution data on total projective cover (TPC). To address this limitation, we complemented field data with remote sensing observations, including NDVI-based vegetation indices, where available, to support and validate the interpolated estimates of vegetation cover dynamics. In botanical studies of the past decade (Aimbetov et al., 2017; Aimuratov, 2020), whose field surveys collectively cover no more than **20%** of the SASR, the primary focus has been on plant species dynamics. Although the data from these expeditions is not representative, by applying **spatiotemporal interpolation** (based on distance-weighted averages between surveyed areas), **correlation analysis** (to quantify relationships between vegetation indicators and climatic variables), **and factor analysis** (to reduce dimensionality and identify dominant patterns), assuming TPC is directly proportional to plant biodiversity and precipitation amounts, we approximated the multi-year dynamics of vegetation cover in the deserts.

The factors driving changes in the Aral Sea flora include:

- Deterioration of the region's water-salt regime,
- Reduced air humidity,
- Increased temperatures during the growing season,
- Aeolian salt deposition from the Aral Sea's post-aquatic land (Tleumuratova, 2018).

Correlation analysis showed weak links between vegetation cover in the four deserts the Amu Darya River discharge. For example, the correlation coefficient for Ustyurt is **0.36**. In the study by Tleumuratova, Mustafaeva, and Ollambergenov (2020), empirical data yielded correlation coefficients between the number of plant species on the Ustyurt Plateau and air temperature **(-0.85)** and humidity **(0.86)**.

The relationship between TPC of vegetation cover and increasing soil salinity at SASR is strongest in Aralkum. For other emission sources—the Ustyurt, Kyzylkum, and Karakum Deserts—the soil salinity factor is significantly weaker. The soils of these deserts were non-saline in 1961 (0.12–0.2%), but had become locally weakly saline by 2020 due to salt emissions (SE) from the desiccated Aral Seabed (DAS). The Ustyurt is the most affected by this process.

In addition to worsening water regimes and climate, the transformation of vegetation cover is significantly impacted by SE from post-aquatic land (the Aralkum), which affects the above-root plant systems. The reduction in TPC due to SE is estimated in the study by Kublanov (2023) using the ratio:

$$\delta_f = \frac{C_w}{C_{\text{кр}}} \tag{1.8}$$

where:

$C_w = 0{,}7943e^{0{,}8858N,}$

C_{cr} - is the annual average MPC (maximum permissible concentration), approximated by analogy with known MPCs of other polluting aerosols as 1500 μg/m³ (Kublanov, 2023).

Since this study addresses the generalization of multi-year dynamics, the rates of vegetation cover transformation (changes in TPC) are **averaged by decades** (based on literature data for various landscapes). The generalized multi-year dynamics of vegetation cover TPC across dust emission areas, calculated considering degradation factors and aligned with limited empirical data, are shown in **Fig. 1.13.**

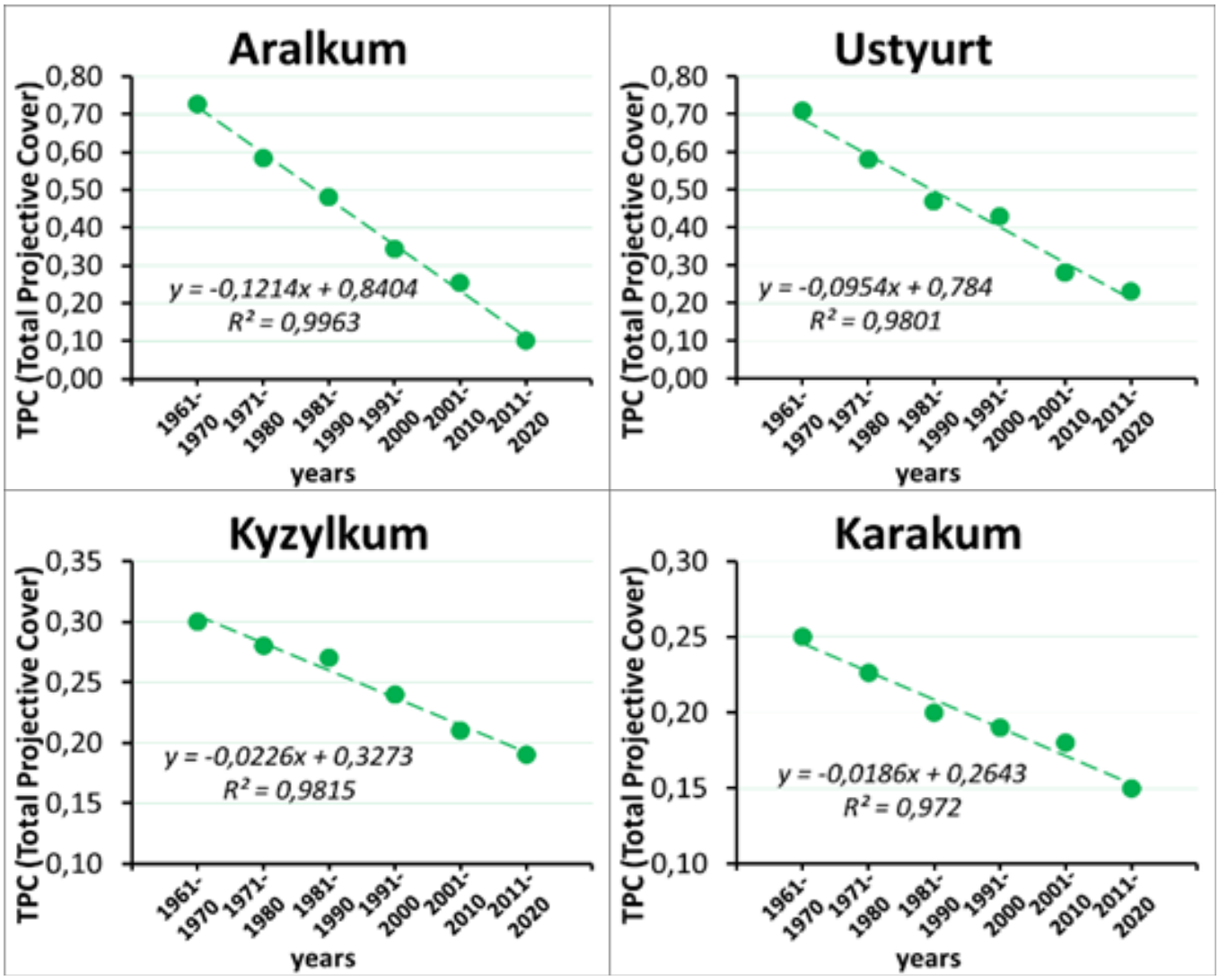

Fig. 1.13. Dynamics of the mean TPC of deserts.

In addition to long-term dynamics, desert vegetation cover exhibits significant seasonal variability (Fig. 1.14).

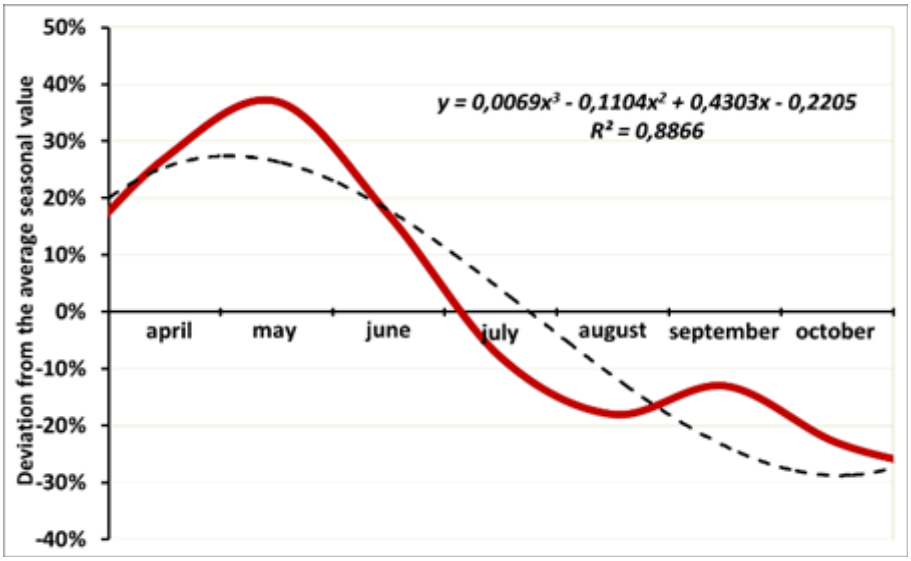

Fig. 1.14. Seasonal variation of TPC (deviations from average seasonal values), averaged across the four desert regions. The red line shows the observed deviations; the black dotted line is the polynomial trend fit.

Biomass peaks in May, after which vegetation begins to wither, partially recovering with autumn rains. Thus, the model incorporates seasonal TPC dynamics (as approximated in Fig. 1.15) to account for vegetation's role in suppressing dust emissions.

A decrease in TPC across all deserts, primarily due to climate change, indicates widespread degradation of desert vegetation in the SASR.

Table 1.4 summarizes the long-term dynamics of the four atmospheric dust loading factors described above. These are the primary inputs for the models. Overall, long-term trends in atmospheric dust load include increased wind activity, desert expansion, reduced precipitation, and declining desert vegetation.

Multi-Year Atmospheric Dust Load Dynamics (MYADLD) **Table 1.4**

	Area $(S_p(N))$	TPC $(\delta_f(N))$	*Wind regime* $(B(N))$	Precipitation $(R(N))$
A	10,809N–1,0133	–0,1214N+0,8404	1,0633N+41,468	–1,6671N+64,823
U	212	–0,0954N+0,784	0,5203N+64,383	–2,3264N+71,215
Kz	0,0971N–299,9	–0,0226N+0,3273	0,3096N+22,209	–1,0729N+61,987
Kr	0,1049N+349,9	–0,0186N+0,2643	1,4438N+47,252	–5,5429N+52,417

Notes:

- Area is measured in thousand km², TPC as fractions of unity, Wind Regime as the number of days per warm season with wind speeds >4 m/s, Precipitation in mm/year.
- N: Decade number; A: Aralkum; U: Ustyurt; Kz: Kyzylkum; Kr: Karakum.
- Enhancing factors: Area, Wind Regime; Mitigating factors: TPC, Precipitation (Fig. 1.15).

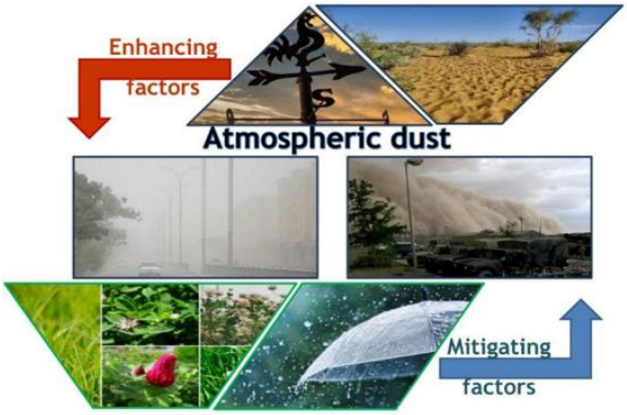

Fig. 1.15. Atmospheric dust load factors.

1.4.2 Results of Dust Migration Calculations from an Individual Desert

Results from the first two research stages are illustrated using ground-level monthly average dust concentrations from Kyzylkum in April (Fig. 1.16).

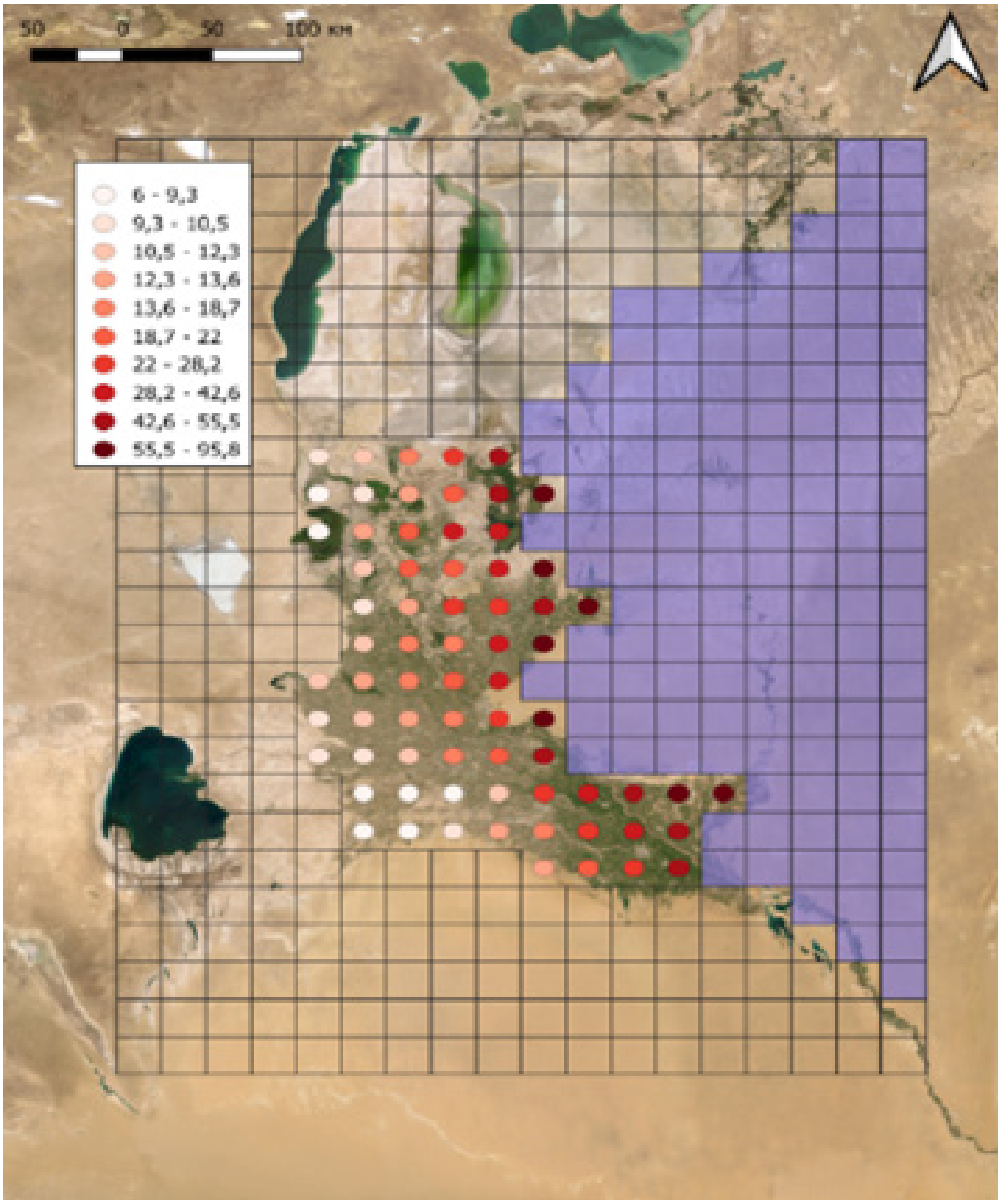

Fig. 1.16. Monthly average concentration (μg/m³) of dust from Kyzylkum in April 2023 in the oasis zone.

The mean TPC for Kyzylkum in April is 43% (Bekhzod A. et al., 2016). Given Kyzylkum's location relative to the Lower Amu Darya Oasis (LADO), dominant dust-transporting winds are easterly, northeasterly, and southeasterly. Days with precipitation and the subsequent 24 hours (12 days total) were excluded from statistical analysis. Data from the Takhtakupyr Meteorological Station show easterly (32%) and northeasterly (19%) winds prevailed in April. Dust concentrations in the eastern LADO ranged from 5.6 to 88.9 μg/m³, while the northeastern LADO saw 0.4–6.9 μg/m³, against a monthly average MPC of 100 μg/m³ (SanPiN RUz No. 0293-11). The southern LADO experiences higher dust levels than the north due to predominant easterly/northeasterly winds, with the highest dustiness in the east and lowest in the west (Urazimbetova, 2024b).

Dust from Kyzylkum blankets the entire LADO. The single-impact zone (for given wind speed/direction) depends strongly on wind speed (Fig. 1.17).

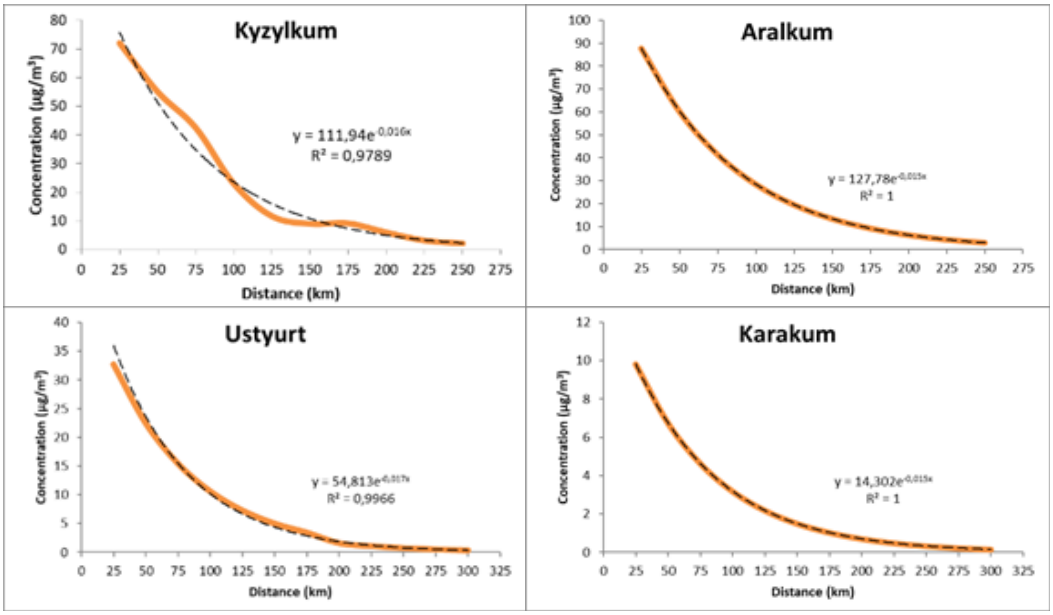

Fig. 1.17. Regression curves illustrating the exponential decrease in dust concentration (y) with distance (x) from the desert boundary, evaluated at a wind speed of 10 m/s.

The trend equation represents the results of regression analysis for the dependence of the influence zone extent of Kyzylkum at a wind speed of 10 m/s:

$$y=111,94e^{(-0,016x)}$$

Similar regression equations were derived for Aralkum, Ustyurt, and Karakum (respectively: $y=127,78e^{(-0,015x)}$, $y=154,81e^{(-0,008x)}$, $y=14,3e^{(-0,015x)}$, where x - is the distance from the desert boundary (Urazymbietova, 2024a).

1.4.3 Atmospheric dust load from the Combined Deserts of the Southern Aral Sea Region

At the third stage, the computed monthly average concentration fields were combined coordinate-wise to determine the cumulative impact of all sources on atmospheric pollution. The superposition of monthly average dust concentrations from all sources (Kyzylkum, Aralkum, Ustyurt, Karakum) across months is shown in Fig. 1.18.

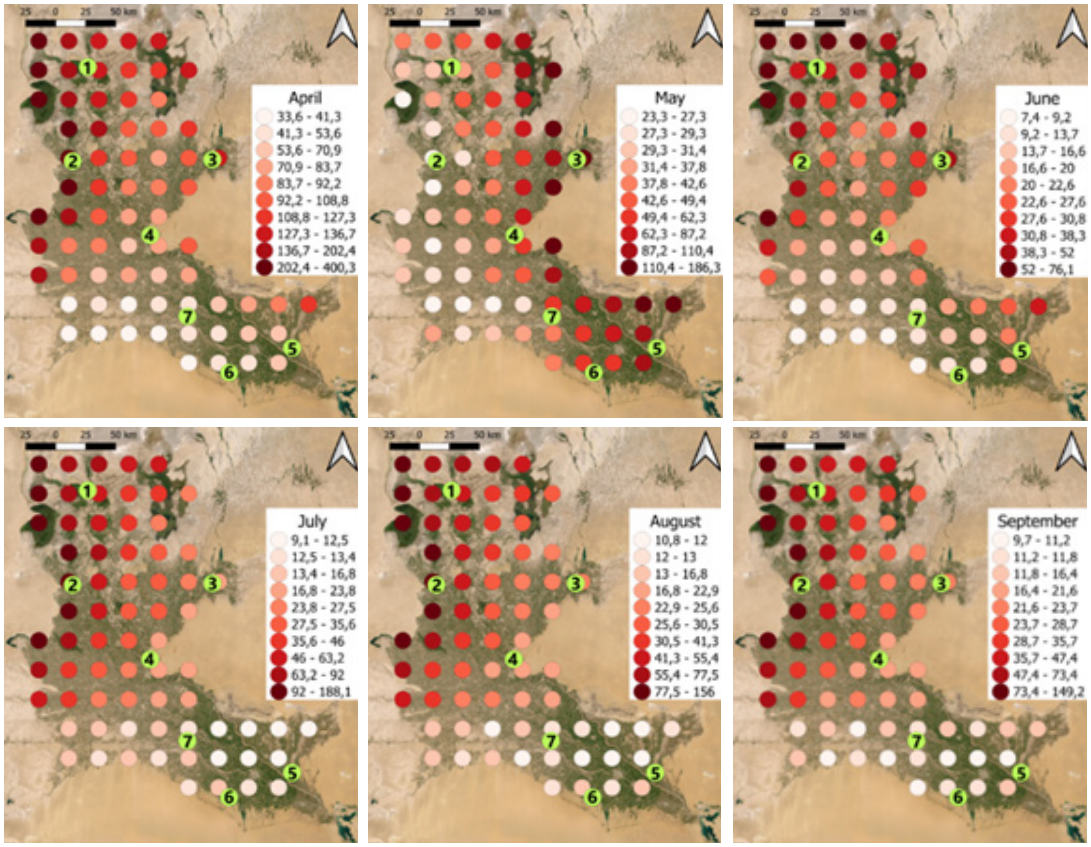

Fig. 1.18. Monthly average concentration (µg/m³) of dust from all sources (1: Muynak, 2: Kungrad, 3: Takhtakupyr, 4: Nukus, 5: Turtkul, 6: Khiva, 7: Dashoguz).

As seen in Fig. 1.18, the greatest contribution to atmospheric dust load (AD) comes from Ustyurt, which has a more active wind regime. In descending order, contributions include salt-dust flows from Aralkum, dust-sand flows from Kyzylkum, and Karakum. The minimal contribution from Karakum is due to the rarity of southerly winds (7%) in the SASR. Consequently, the most dust-polluted areas are the northwestern regions of the Lower Amu Darya Oasis (LADO), where the monthly average MPC (100 μg/m³, SanPiN RUz No. 0293-11, 2011) is exceeded in April, July, and September. In the eastern LADO, the MPC is exceeded only in May.

Migration activity is a key feature of soil aerosols, defining their unique spatial distribution. As shown in Table 1.5, dust concentrations also exhibit significant spatiotemporal dynamics.

Table 1.5

Annual Trend (April–November) of Atmospheric Pollution in Different Regions of Karakalpakstan (μg/m³)

District	Months Years							Annual average
	IV	V	VI	VII	VIII	IX	X	
Amudarya	65,6	75,3	17,1	7,0	8,9	6,5	10,4	27,3
Beruniy	61,5	85,5	16,9	5,4	7,3	6,2	8,9	27,4
Bozatau	93,3	49,3	19,5	13,9	16,1	8,9	17,8	31,3
Kanlikol	126,4	31,8	20,4	20,7	22,8	11,7	25,8	37,1
Karauzyak	106,3	115,8	29,4	11,0	14,7	10,2	16,8	43,5
Kegeyli	90,9	71,5	21,3	11,5	14,1	8,7	15,9	33,4
Kungrad	263,4	26,1	35,2	44,0	47,6	23,4	55,3	70,7
Moynaq	142,8	36,3	30,8	27,0	30,3	14,7	30,4	44,6
Nukus	75,3	63,2	17,9	9,6	11,6	7,3	13,1	28,3
Nukus district	83,6	42,3	16,5	12,6	14,4	8,0	16,1	27,6
Taqiatash	72,1	58,4	16,8	9,4	11,3	7,1	12,7	26,8
Takhtakupir	133,7	179,7	39,4	10,2	15,4	12,5	18,9	58,5
Tortkul	68,6	99,8	18,9	6,2	8,2	7,1	10,0	31,3
Khodjeyli	67,4	31,5	13,0	10,8	12,1	6,6	13,3	22,1
Chimbay	85,8	61,5	19,9	11,6	13,9	8,2	15,4	30,9
Shomanay	156,9	31,1	23,1	25,8	28,1	14,3	32,3	44,5
Ellikqala	76,7	118,1	22,8	5,1	7,8	7,4	10,2	35,4

The table shows that the atmosphere is most polluted in the Shumanay, Takhtakupyr, and Kanlykul districts, located near Kyzylkum, as well as in the Kungrad and Muynak districts, closest to Aralkum, where salt-dust flows pose significant health risks.

Assessment of Desert Dust Contribution to Air Pollution in the Lower Amu Darya Oasis

The contribution of desert dust to atmospheric pollution was evaluated by comparing model results with ground-based measurements from POST-5 and POST-7 recorders (Comde-Derenda GmbH, Germany) in Nukus (Fig. 1.19) and field measurements (Fig. 1.20) in Ustyurt, Kyzylkum, and Muynak.

Fig. 1.19. Automatic Recorders

Fig. 1.20. Field Measurements and Aerosol Counter

The contribution of desert dust in rural areas averaged 67% across the region, while in urban areas it was 32% (Table 1.6). This difference is attributed to higher vehicular traffic and reduced vegetation cover in cities. However, urban infrastructure such as paved surfaces and buildings tends to trap or suppress surface dust emissions, leading to relatively lower contributions from desert dust in urban areas.

Table 1.6

Automatic Recorder Data and Model Results (Nukus City)

Month	April	May	June	July	August	September	October
Station Data (μg/m³)	102,27	82,07	75,61	79,01	79,58	66,68	97,97
Model Results (μg/m³)	75,3	63,2	17,9	9,6	11,6	7,3	13,1
Discrepancy (μg/m³)	26,97	18,87	57,71	69,41	67,98	59,38	84,87
Contribution (%)	73%	77%	23%	12%	15%	11%	13%

Overall, the LTI model (Table 1.6) accurately reflects the bimodal seasonal trend of atmospheric dust load (AD), with a significant peak in April and a smaller peak in October, linked to autumn wind intensification and vegetation degradation (Urazimbetova, 2024a). This discrepancy may be explained by the fact that station measurements in autumn are more influenced by local anthropogenic factors such as agricultural activity (e.g. harvesting and plowing), which are not fully accounted for in the model. In contrast, spring peaks are primarily driven by broader meteorological factors like wind intensity and vegetation cover loss, which the model captures more effectively.

1.4.4 Results of the MYDD Model Implementation

Modeled seasonal average dust concentration fields at 2 m height for the 1st (1960s) and 6th (2010s) decades are compared in Fig. 1.21. The figure shows increased AD across the entire study area, particularly in the northeastern and northwestern regions of the Lower Amu Darya Oasis (LADO).

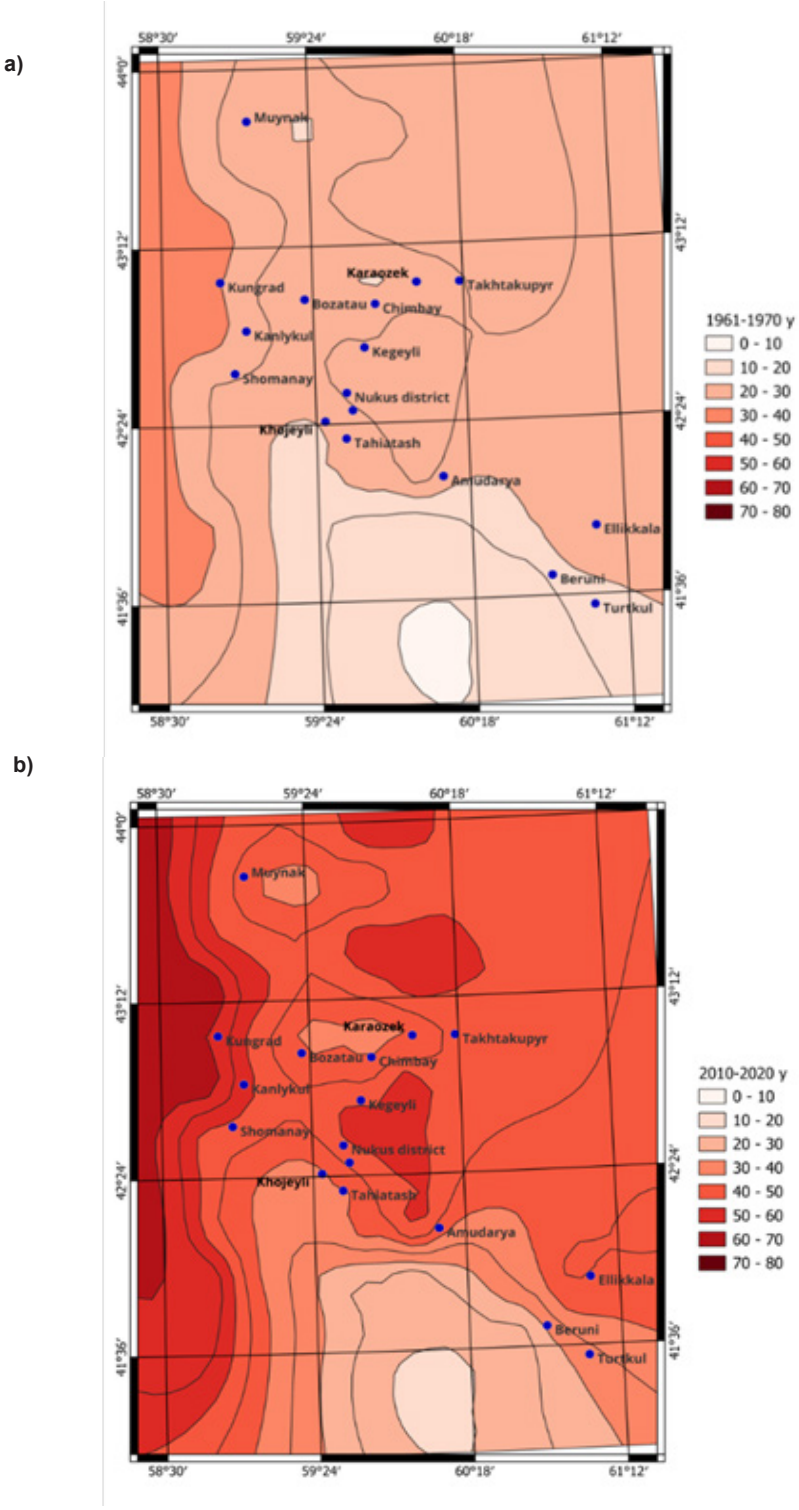

Fig. 1.21. Dynamics of Monthly Average Dust Concentration (μg/m³) from All Sources (a) 1961-1970, (b) last decade.

Long-term AD dynamics are clearly depicted in the graph (Fig. 1.22). Seasonal average dust concentrations are highest in the Kungrad and Takhtakupyr districts. Notably, seasonal averages approaching the MPC (100 μg/m³) indicate frequent daily exceedances.

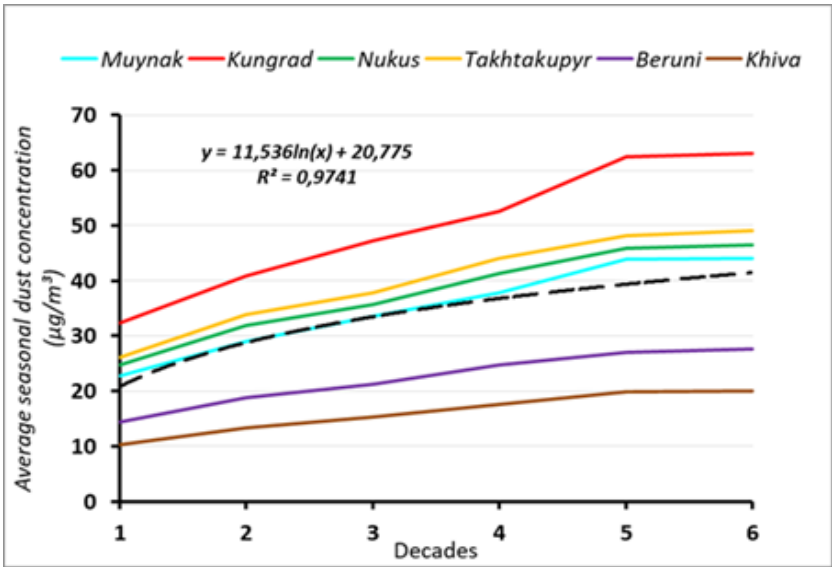

Fig. 1.22. Dynamics of Seasonal Average Dust and Sand Concentrations from the Desert Complex in Various Zones of the Lower Amu Darya Oasis

The regional long-term trend is expressed by the equation:

$$C(x,y,N)=11,536\ ln(N)+20,775 \quad (1.9)$$

Since long-term AD dynamics are based on approximations of factor trends, we conducted a correlation analysis to assess the functional reliability of the derived regression equations.

Correlation Analysis of Atmospheric dust load and Wind Activity

The analysis revealed a very strong correlation between atmospheric dust load and wind activity (Table 1.7), confirming wind regime (specifically, the number of days with wind speeds >4 m/s) as the primary driver of AD.

Table 1.7

Correlation of Dust Concentration (μg/m³) with Wind Regime

Years	Nukus City		Moynaq		Takhtakupyr		Khiva	
	Dust Conc. (μg/m3)	Days with wind over 4 m/s	Dust Conc. (μg/m3)	Days with wind over 4 m/s	Dust Conc. (μg/m3)	Days with wind over 4 m/s	Dust Conc. (μg/m3	Days with wind over 4 m/s
1961-1970	24,7	22,52	22,8	42,57	26,1	22,52	10,2	47,95
1971-1980	31,8	22,92	29,1	43,31	33,8	22,92	13,3	50,01
1981-1990	35,7	22,90	33,5	44,17	37,7	22,90	15,4	52,96
1991-2000	41,4	23,53	37,9	46,82	44,0	23,53	17,5	53,21
2001-2010	45,8	23,94	43,9	47,02	48,2	23,94	19,8	54,20
2011-2020	46,5	23,95	44,0	47,25	49,0	23,95	20,0	55,50
Corr	0,97		0,96		0,97		1	

Additional statistical analysis of dust storm frequency revealed periodic decreases/increases (Fig. 1.23). The lack of correlation with AD trends is due to the rarity of dust storms (no more than 5–6 per season).

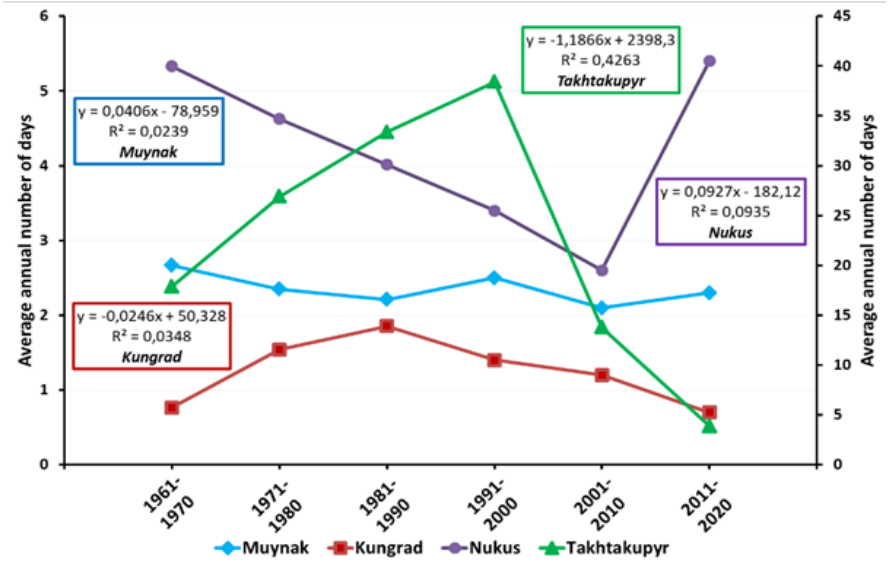

Fig. 1.23. Dynamics of Dust Storm Frequency in Karakalpakstan.

This disproves claims by many authors that salt emission (SE) from the Desiccated Aral Seabed (DASB) is decreasing, based solely on dust storm counts. Instead, annual dust emissions must be determined by the statistical frequency of all wind events exceeding **4 m/s.**

Correlation analysis of the relationship between atmospheric pollution and precipitation revealed an average correlation coefficient of **-0.8** (Table 1.8), indicating a **very strong inverse relationship**. However, the relative contribution of this factor to atmospheric dust load (ADL) is much lower than wind activity due to the low precipitation amounts during the warm season.

Correlation of Dust Concentration (μg/m³) with Precipitation **Table 1.8**

Years	Nukus City		Moynaq		Takhtakupyr		Khiva	
	Dust Conc. (μg/m3)	Days with Precip.	Dust Conc. (μg/m3)	Days with Precip.	Dust Conc. (μg/m3)	Days with Precip.	Dust Conc. (μg/m3	Days with Precip.
1961-1970	24,7	0,10	22,8	0,09	26,1	0,08	10,2	0,07
1971-1980	31,8	0,10	29,1	0,09	33,8	0,07	13,3	0,08
1981-1990	35,7	0,08	33,5	0,08	37,7	0,07	15,4	0,07
1991-2000	41,4	0,08	37,9	0,09	44,0	0,07	17,5	0,06
2001-2010	45,8	0,08	43,9	0,08	48,2	0,07	19,8	0,07
2011-2020	46,5	0,08	44,0	0,09	49,0	0,07	20,0	0,06
Corr	-0,9		-0,61		-0,9		-0,8	

Functional Dependence of Dust Migration on Desert Area and TPC

Table 1.9 demonstrates very high correlation between dust concentration, desert area, and vegetation cover.

Table 1.9

Correlation of Dust Concentration (μg/m³) with Total Desert Area and Mean TPC

Years	Nukus city	Moynaq	Takhtakupyr	Khiva
1961-1970	24,7	22,8	26,1	10,2
1971-1980	31,8	29,1	33,8	13,3
1981-1990	35,7	33,5	37,7	15,4

1991-2000	41,4	37,9	44,0	17,5
2001-2010	45,8	43,9	48,2	19,8
2011-2020	46,5	44,0	49,0	20,0
Corr.with area	0,99	0,99	0,99	0,99
Corr.with VC	-0,98	-0,99	-0,98	-0,98

Thus, the high correlation coefficients between dust concentration and all four factors suggest a very strong relationship between dust migration and these factors.

The error of the statistical MYADLD model, primarily arising from the approximation of multi-year factor dynamics, does not exceed **10%**. Here, we assumed wind regime and precipitation data to be reliable. The model's error is mainly due to the **non-representative spatial and temporal data** on TPC of desert vegetation. Nevertheless, the model's accuracy is constrained by several factors, including the limited spatial and temporal resolution of vegetation and precipitation datasets, potential underestimation of anthropogenic impacts, and simplification of multi-factor interactions in desert environments.

Overall, the rate of dust migration is slowing due to limitations in wind activity, which cannot increase indefinitely. The expansion of Aralkum—responsible for the highest ADL growth rates in in the first four decades (1960-1999)—is also constrained. Nevertheless, dust migration continues to progress due to the persistent decline in vegetation cover (VC) and precipitation (Urazimbetova, 2024a). The identified trends and patterns are formalized through regression equations with reliability estimates of **0.7–0.95.**

1.5. Forecasting Atmospheric Pollution Mitigation Measures

Projections Using the MYDD Model:

We calculated projections using the MYDD model based on increasing **Total Projective Cover (TPC)** from **0.3 to 0.5** and warm-season precipitation from **19 to 23 mm** (Fig. 1.24) show reduced desert impacts on atmospheric pollution in the **Southern Aral Sea Region.**

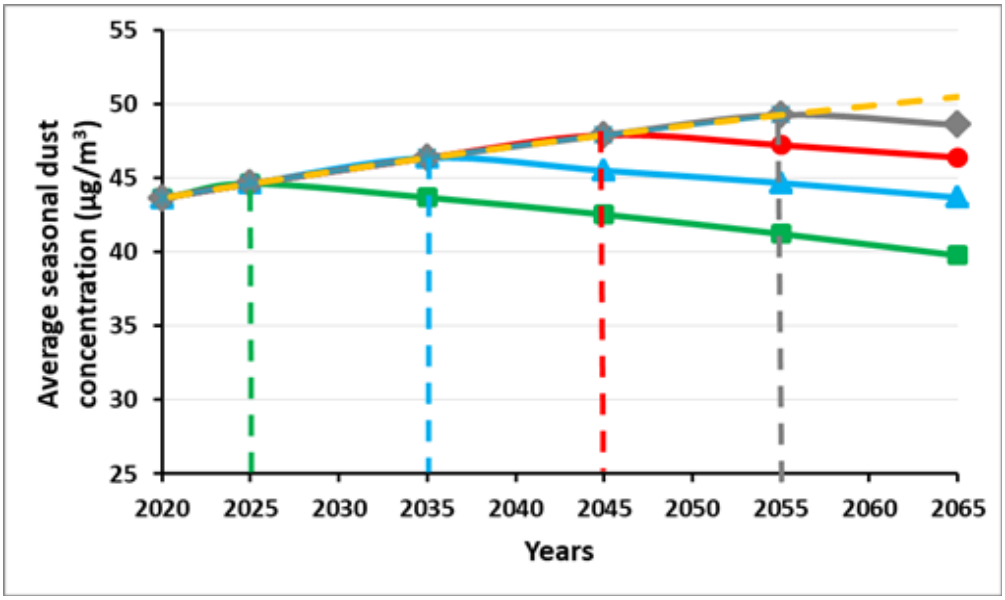

Fig. 1.24. Forecasting the dynamics of dust content in the Lower Amudarya oasis with an increase in the total projective cover from 0.3 to 0.5.

The earlier the mitigation measures are implemented, the more effective they are.

As shown in Fig. 1.24, initiating mitigation in 2025 (green line) can already reduce average seasonal dust concentration by approximately 1 µg/m³ by 2035 and by 5 µg/m³ by 2065.

Later interventions – beginning in 2035 (blue), 2045 (red), or 2055 (gray) – demonstrate progressively smaller impacts. The yellow dashed line represents the baseline scenario without any mitigation, showing the highest projected dust levels.

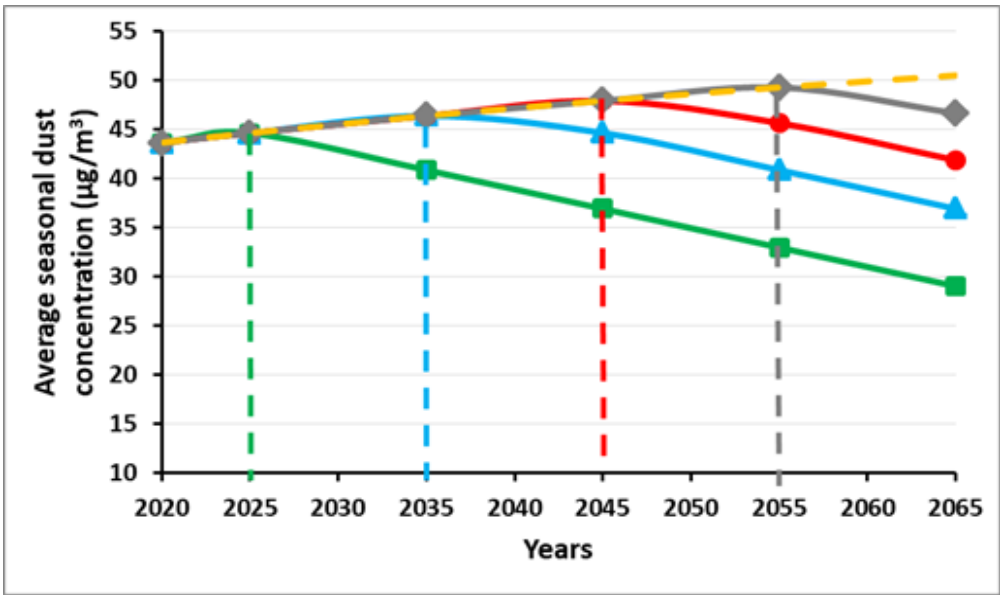

Fig. 1.25. Forecasting dust concentration in the Lower Amudarya oasis with an increase in the seasonal number of days with precipitation from 19 to 23 mm.

As shown in the graphs (Fig. 1.24–1.25), earlier application of measures to reduce atmospheric dust load (AD) — particularly during **critical intervention stages** — results in greater efficacy (Urazimbetova, 2024). Therefore, the effectiveness of mitigation measures depends on the **timeliness of their implementation**, which is particularly critical for progressing negative processes.

Below we describe options for combating desert dust, including chemical stabilization, artificial precipitation, afforestation, and water body creation, which demonstrates **the real potential for successful regulation of atmospheric dust load** and improvement of ecological conditions. Further in-depth research on these interventions is also required.

The model indicates that the conditions for dust emission are:

- Wind speed ≥4 m/s.
- Air temperature >0°C
- Suitable underlying surface conditions (weak vegetation cover, soil volumetric moisture ≤ 5%, fine-dispersed soil mechanical composition.

These conditions are nearly permanent in deserts during warm seasons. Mitigating dust emissions requires neutralizing at least one condition. Since wind/temperature regimes and soil composition are beyond human control, viable measures are:

a) Increasing soil moisture.
b) Increasing Total Projective Cover (TPC).
c) Creating protective surface coatings.

The most effective approach is a **combination** of these measures.

Dust emission mitigation measures can be categorized into four types:

1. **Chemical protection** of the underlying surface against weathering.
2. **Artificial precipitation** to moisten the surface.
3. **Phytoremediation** (greening).
4. **Creating water reservoirs.**

Below, we evaluate the efficacy and environmental safety of these measures.

1. **Chemical Protection Against Weathering**

This involves treating soils with various chemical compositions. Researchers from the Institute of Chemistry and Physics of Polymers and the Institute of General and Inorganic Chemistry of the Academy of Sciences of Uzbekistan have developed several such technologies. High efficacy in stabilizing sands has been demonstrated by:

- **Nerozin** (a polymer-based compound).
- Mixtures of **SSB (sulfite-alcohol stillage) and PVA (polyvinyl acetate emulsion)** (Cao et al., 2024; Wang et al., 2022).
- **Acetone-formaldehyde (ACF)** resin-based compositions (Kholmuminov et al., 2003).
- **Liming method**: Soil treatment with **highly dispersed ash** (fly ash from **GRES electrostatic filters**) followed by a binder and surfactant solution, utilizing **industrial waste** (Goméz et al., 2019; Jaramillo et al., 2023).

Advantages:
- Economically viable due to industrial waste reuse.

Risks:
- Environmental safety requires **at least 5 years** of field testing to confirm the durability of protective crusts.
- Degradation or crumbling of crusts risks releasing toxic sulfates and organic compounds into the atmosphere.
- Applicable only to highly saline, non-rehabilitable areas of the Desiccated Aral Seabed (DASB).

Limitation: Quantitative estimates of annual dust/salt emission reduction via chemical stabilization are unavailable.

2. **Creation of Water Reservoirs**

Initiated in the **1990s** to improve ecological conditions on the DASB. **Benefits** include:
- Enhanced vegetation (herbaceous and woody tugai).
- Increased summer air humidity (Kurbaniyazov, 2017).
- Habitat restoration for fish, birds, muskrats, and ungulates.

Challenges:
- Frequent breaches, siltation, and overgrowth require regular maintenance.

Quantitative Impact:
- Artificial reservoirs and the Central Aral reduced salt emission by **4.56 million tons/year** (2019) versus total DASB emissions of **128.8 million tons/year** (Kublanov, 2024).

3. Artificial Precipitation

Key Principle: Soil moisture >5% reduces wind-driven salt/dust emission probability to near-zero. Post-rain pro tective crusts further inhibit dust storms.

Methods:
- **Cloud Seeding**: Airplane dispersal of silver iodide or salts (developed by General Electric, 1940s).
- **Drone-Dispersed Negative Ions** (Dubai, 2021): Forces water molecules to coalesce into raindrops.

Limitations:3
- Requires pre-existing low-level clouds.
- Poor controllability.

Application: 1 mm rainfall prior to high-wind events (>10 m/s) effectively prevents emissions. Artificial precipitation also combats drought, enhances vegetation, reduces atmospheric dust, and mitigates climate warming.

4. **Afforestation** (Phytoremediation)

Global examples:
- **USA (1930s)**: The "Dust Bowl" prompted the **Protective Belt of the Great Plains**, planting 200 million trees to reduce Texas dust storms.
- **China**: The "Great Green Wall" halted Gobi Desert expansion (**3,600 km²/year**) via billions of trees.
- **Africa**: The "Great Green Wall" mitigates Sahara dust storms (Goffner, Sinare & Gordon, 2019; Mbow, 2017).

Uzbekistan:
- Large-scale planting only on the **DASB periphery.**
- **Neglected deserts** (Kyzylkum, Ustyurt) could benefit from reduced desertification, dust, and livestock fodder shortages.

Challenges:
- Declining efficacy due to rising salt emissions and poor sapling survival on saline DASB areas (**2015–2021**).
- **Hyper-saline DASB zones** (2009–2024):
  - o **Phytoremediation impossible** due to extreme salinity.
  - o **Water reservoirs unfeasible** due to water source remoteness.Only chemical protection and artificial precipitation are viable.

CHAPTER 2
Quantitative Assessment of the Ecological Efficiency of Ecosystem Services provided by Vegetation Cover as Protection against Salt Emission from Aralkum

2.1 Relevance and Research Status of Salt Dust Migration from Aralkum

Researchers of the Aral Sea crisis identify wind-driven salt transfer (WDST) from the desiccated Aral Sea bed (DASB) to adjacent territories as one of its most dangerous consequences due to its severe impacts on human health and the environment (Micklin, 2007; Glazovsky, 1995; UNECE, 2004). The global significance of WDST is underscored by the establishment of international organizations, funds, and programs such as the International Fund for Saving the Aral Sea, the Comprehensive Program for Mitigating the Consequences of the Aral Catastrophe and Developing the Aral Sea Region, and the Multi-Partner Trust Fund for Human Security in the Aral Sea Region.

Over the half-century since the Aral crisis began, numerous studies have addressed salt-dust transport from the DASB (Rubanov, 1987; Rafikov, 1982; Chub, 2000; Galaeva, 1988; Semenov, 1991; Razakov & Kosnazarov, 1987; Wang et al., 2022; Indoitu et al., 2015; Groll et al., 2013; Tleumuratova, 2004, 2018; Banks et al., 2022; Micklin, 2007; Ge et al., 2022, among others). These works typically focused on isolated aspects of WDST over short timeframes. Differences in methodologies have led to significant variability and uncertainty in quantitative estimates of salt transfer parameters. While these qualitative studies provide foundational empirical data, their limited temporal coverage and spatial non-representativeness complicates their application for strategic planning and long-term mitigation of WDST. While many of the aforementioned studies (Rubanov, 1987; Rafikov, 1982; Chub, 2000; etc.) have addressed various aspects of salt and dust transport from the desiccated Aral Sea bed — including meteorological influences, spatial distribution, and health impacts — long-term research specifically focusing on the unique atmospheric dynamics of salt aerosols has been conducted solely by B.S. Tleumuratova (2004, 2018).

For decades, the Aral Sea acted as a sink for suspended and dissolved substances carried by the Amu Darya and Syr Darya rivers. These include geogenic mineral loads, untreated wastewater with heavy metals (e.g., lead and cadmium; Wiggs et al., 2003), radioactive materials (uranium and radon) from mining industries in upstream Tajikistan and Kyrgyzstan (Kulmatov & Khojamberdiev, 2010), urban and industrial effluents from a population growing from 14 million in 1960 to nearly 50 million in 2011 (Dukhovny & de Schutter, 2011), and highly concentrated agrochemicals, pesticides, and salts used to combat widespread soil salinization (Micklin, 1988, 2007; O'Hara et al., 2000). Gas field development since 2011 on the southwestern DASB has introduced risks of heavy metal soil contamination and subsequent atmospheric dispersion (Zhollybekov et al., 2023).

The total salt mass on the Aral Seabed is estimated at 6 billion tons, forming a uniform layer of at least 0.5 m thickness across the Aralkum (Létolle et al., 2005). The salt reserve in the soil aeration zone reaches 2,200 tons/ha (Orlovsky, 2001).

Possible mitigation approaches include:

1. Shading: Reducing soil evaporation and salt ascent.
2. Salt Absorption: Direct uptake of salts from soil.
3. Barrier Effect: Blocking dry salt aerosol deposition and mineralized precipitation.
4. Wind Speed Reduction: Weakening near-surface wind speeds by multiple times near salt emission sources.

The degree of soil salinization mitigation is directly proportional to vegetation projective cover (VPC) (Tleumuratova, 2018).

Strategic decision-making for critical environmental issues requires reliable, scientifically validated, and quantitatively verified data. Thus, theoretical and applied research into the patterns of salt transport and its quantitative environmental impact is essential to build a robust scientific foundation for projects aimed at reducing WDST.

This study quantitatively evaluates the dynamics of vegetation-induced wind speed reduction and its impact on WDST from the DASB over the period 1961–2020.

2.2 Data Used

The study primarily relied on published data from authoritative sources, as field investigations to obtain new more comprehensive data would require multi-year efforts.

Salinity of Post-Aquatic Lands.

Current data on the ionic-salt composition of the Aral Sea's residual waters allowed for a mass balance assessment of the total salt mass and mineral composition deposited on the seabed during desiccation (Kurbaniyazov, 2017). **Astrakhanite** (Na2SO4·MgSO4·4H2O) accounts for **51.75%** of the total rock weight. The mineral composition of salts (Kurbaniyazov, 2017) is as follows (in billions of tons and percentages):

Calcium carbonate ($CaCO_3$): 0.07 (2%)
Magnesium carbonate ($MgCO_3$): 0.1 (2%)
Gypsum ($CaSO_4 \cdot 2H_2O$): 2.3 (49%)
Mirabilite ($Na_2SO_4 > 10H_2O$): 1.9 (40%)
Halite (NaCl): 0.4 (8%)

The upper layer of bottom sediments in the deep-sea zone consists almost entirely (>97%) of fine mirabilite crystals (Kurbaniyazov, 2017). The same study estimates the average rate of salt accumulation on the desiccated Aral seabed

at 0.1 billion tons per year (or ~3 kg/m²/year).

Sources of Salt emissions

The primary sources of salt emissions in the Aral region are crusty and crusty-puffy solonchaks (salt flats), as well as thenardite powder, which are highly erodible and transportable over long distances. Erodibility varies depending on salt reserves:

- **Crusty solonchaks**: 60–620 t/km²
- **Puffy solonchaks**: 440–2,800 t/km² (Bogdanova & Kostyuchenko, 1979).

Spatial Distribution of Salt Emission Sources

The spatial distribution of salt emission hotspots remains highly uncertain due to dynamic landscape changes and constant redistribution of terrigenous material. Large-scale salt redistribution occurs during dust storms, which also re-salinize older dried seabed areas.

Contrasting Perspectives on Dust Sources

It was previously asserted that "old" dried seabed surfaces (pre-1990s) ceased to be active dust and salt sources in recent decades due to desalination and vegetation colonization (Dosbergenov & Asanbayev, 2002). For instance, Semenov (2011) claimed that only "newly" exposed seabed areas are active dust zones, while "old" desiccated zones lost their significance as dust sources. However, Indoitu, Kozhoridze et al. (2015) propose an alternative hypothesis: both "old" dried surfaces and newly exposed seabed remain active dust emission zones (Fig. 2.1).

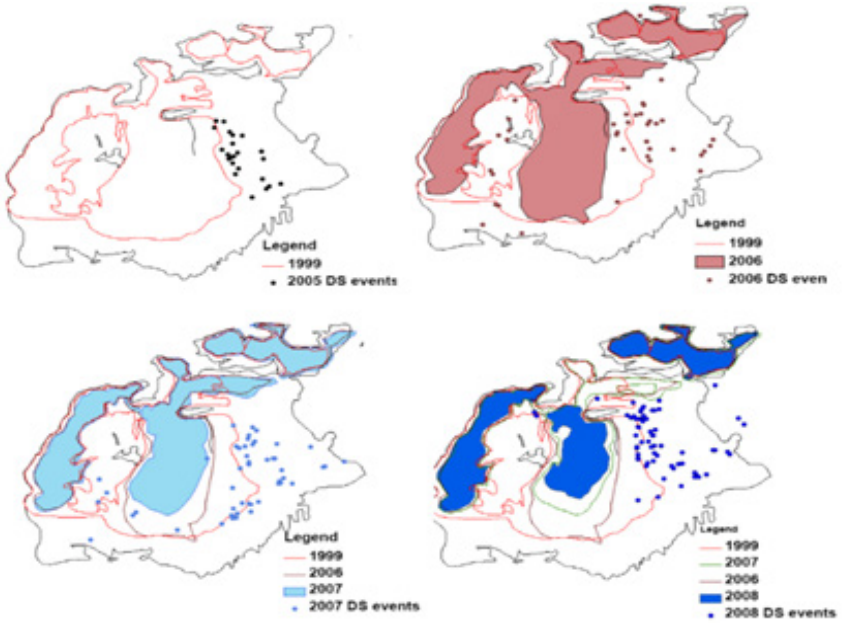

Figure 2.1. Dust Storm Hotspots on the Desiccated Aral Seabed 2005–2008 (Indoitu, Kozhoridze et al., 2015)

Currently (2021–2024), a trend toward the complete desiccation of the eastern basin has emerged (Fig. 2.2). This has sharply increased the total area of salt flats and heightened the urgency of developing measures to protect the Aral region from wind-driven salt transfer (WDST).

2019 year

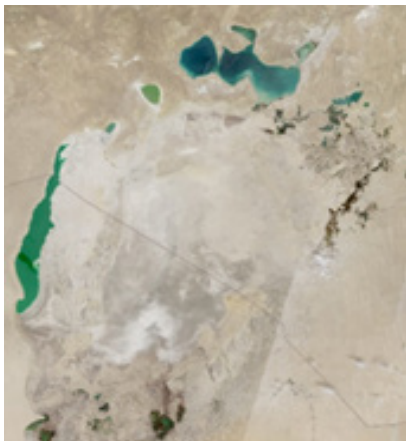

2020 year

2021 year

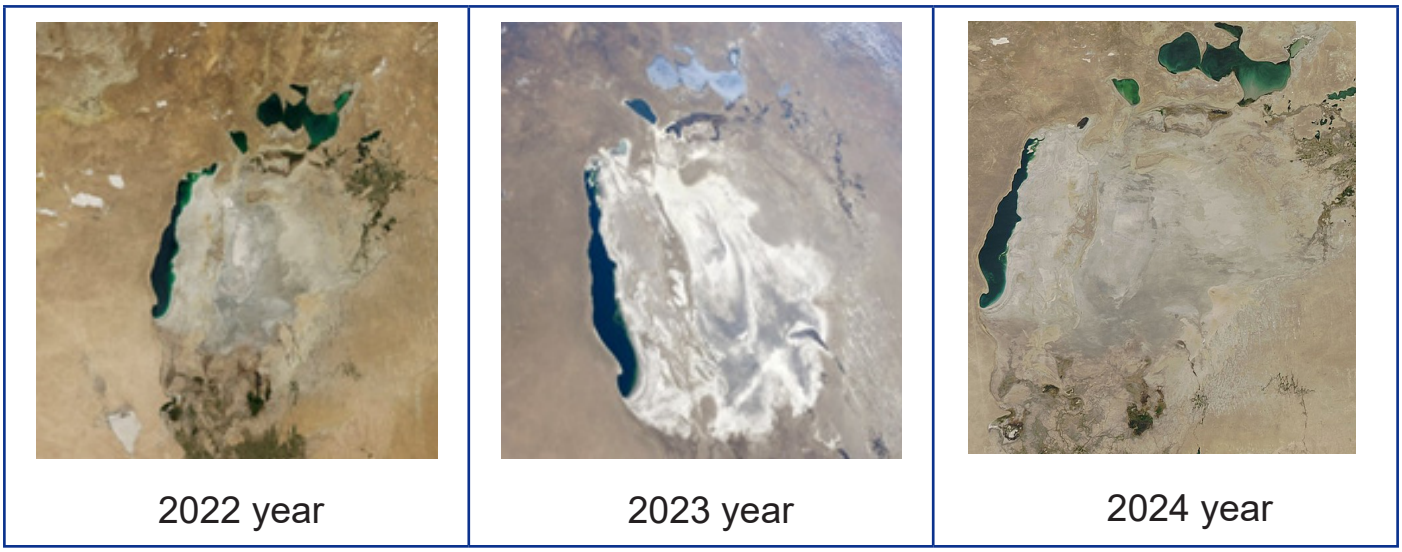

Figure 2.2. Desiccated Aral Seaed (2019–2024) with Salt Emission Sources
Source: USGS Earth Explorer (Landsat 8/9), https://earthexplorer.usgs.gov/.
Note: Minor differences in projection and scale are due to seasonal acquisition conditions.

Meteorological Parameters

Data averaged over the growing season reveal a trend of increasing wind speeds and decreasing precipitation during 2000–2020 (Wang et al., 2022), indicating meteorological conditions that exacerbate salt transfer. Wind direction over the Aralkum varies annually due to shifts in atmospheric circulation linked to global warming and changes in circulation epochs (Subbotina & Chanysheva, 2006). Overall, **70% of salt transfer occurs toward the west-south sector,** impacting Southern Priaralie.

Wind Dynamics and Atmospheric Transport

Wind characteristics and the pressure gradient between 850 hPa and 1000 hPa determine the direction and intensity of aerosol transport. Vertical wind shear between 1000 hPa and 850 hPa drives cold air intrusions from northern, northwestern, and northeastern directions (Orlovsky et al., 2005). Surface wind fields can be reliably represented using 1000 hPa wind vectors (Shi et al., 2020).

Historical Dust Storm Directions

- Grigoriev & Lipatov (1985) identified three primary dust plume directions using 1975–1981 satellite imagery:
  - Southwest: 60%
  - West: 25%
  - South/Southeast: 15%
- Recent studies (Indoitu, Kozhoridze et al., 2015; Wang et al., 2022) corroborate these patterns (Figs. 2.3–2.4).

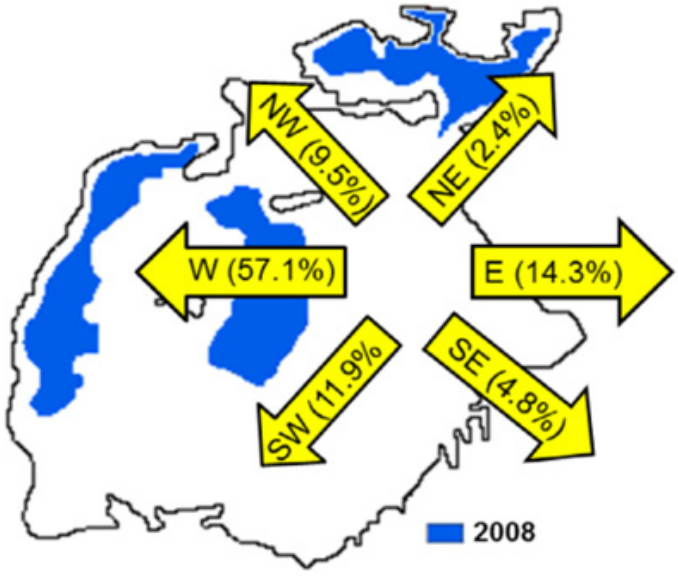

Figure 2.3. Dust Storm Plume Directions (2005–2008) (Indoitu, Kozhoridze et al., 2015).

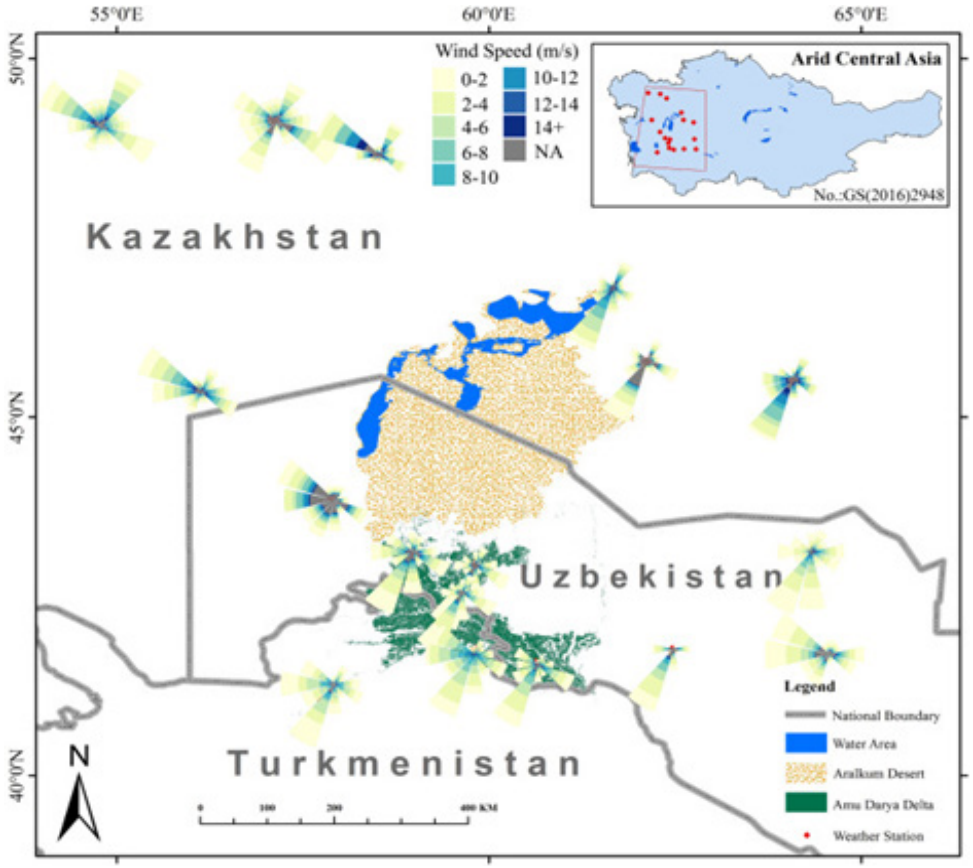

Figure 2.4. Adapted from Wang et al. (2022). Color scheme and symbol sizes are as presented in the original publication.

Regional Monitoring

A long-term dust deposition monitoring program (2003–2010) across 21 stations in Uzbekistan, Kazakhstan, and Turkmenistan revealed predominant southward dust transport (Groll et al., 2013) (Fig. 2.5).

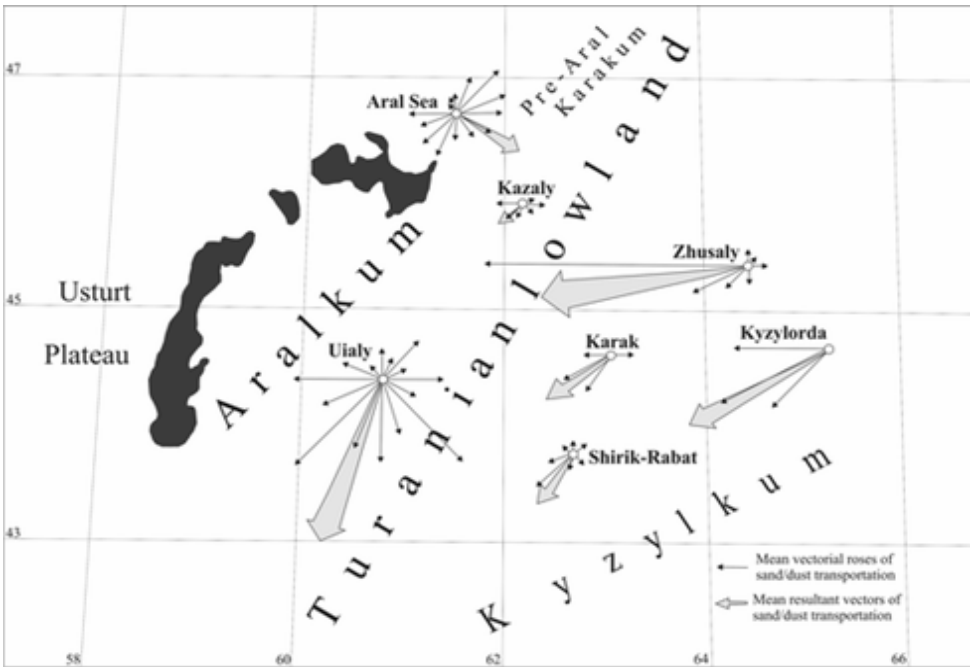

Figure 2.5. Sand and Dust Transport Directions in Priaralie (Groll et al., 2013)

A thorough statistical analysis of data from the Muynak Meteorological Station (Urazimbetova, 2025a), which formed the basis of our calculations, demonstrates a significant predominance of winds from the northern half of the compass throughout the modeling period.

Dust Storm Dynamics on the Desiccated Aral Seabed (DASB)

Monitoring of dust storm outbreaks on the DASB has revealed a significant increase in the temporal frequency of

these events. Analysis of multi-year remote sensing data from 1975 to 1982 documented 37 dust storms, while 33 dust storm events were recorded from 1985 to 1990 (Grigoriev & Zhogova, 1992). Between 1990 and 2002, measurements across nine meteorological stations in the Aral region registered 1,082 days with dust storms of varying intensity and duration (Shardakova & Usmanova, 2006).

For 2000–2009, Spivak et al. (2012) identified 134 dust storms across the entire Aral Sea basin using satellite imagery from the National Oceanic and Atmospheric Administration (NOAA). Analysis of NOAA AVHRR (Advanced Very-High-Resolution Radiometer) data by Indoitu et al. (2015) for 2005–2008 determined an annual frequency of 6–9 dust storms. Ge et al. (2016) further analyzed OMI Aerosol Index (AI) data, revealing a 50% increase in the annual mean AI over the Aral Sea region from 2005 to 2013, underscoring the Aralkum's growing role as a Central Asian dust source. Nobakht et al. (2021) utilized MODIS satellite data (2003–2012) to inventory dust emission sources, identifying the Aralkum—particularly its eastern and southern basins—as a major regional dust hotspot.

Contradicted Predictions and Recent Trends

Forecasts by Rubanov & Bogdanova (1987) of reduced salt emissions by the 2000s have proven inaccurate. Instead, dust storm intensity has intensified globally (Iwasaka, 2006; Goudie, 2014; Shi et al., 2020). At the Aral meteorological station (Aralsk, Kazakhstan), the number of dust storm days nearly doubled—from fewer than 40 days in previous decades to an average of 64 days annually during 1980–2000. Since 2000, an increase in dust storm activity has been recorded at nearly all meteorological stations in the study area. Future observations will clarify whether this trend persists. Such changes may be attributed to shifts in regional and global atmospheric circulation patterns (Darmenova & Sokolik, 2007).

Atmospheric Saturation and Aerosol Impacts

Remote sensing methods confirmed year-round saturation of the Aralkum atmosphere with mineral aerosols (2005–2008). While annual mean AI values remained consistently elevated throughout the year (National Plan, 2020), the spatial distribution of dust concentrations and emission sources expanded significantly. During outbreaks, the Aralkum merged with the Karakum and Kyzylkum deserts into a single massive dust plume, indicating stronger storms by the late 2000s (National Plan...2020). The western DASB now experiences the world's highest dust storm frequency (Goudie, 2018).

Environmental Consequences

- Precipitation mineralization in the Aral region increased 6–7-fold.
- Atmospheric aerosol concentrations reached 8×MPC (Maximum Permissible Concentration), peaking at 10–12×MPC during storms (Chub, 2000).
- The DASB continues to expand as a dominant salt/dust source (Galaeva & Idrisova, 2007; Wiggs et al., 2003).

Plant Community Evolution

Vegetation dynamics—the most studied aspect of salt transfer mitigation—have been explored through expeditions:

- Southern DASB: Extensively researched (Kabulov, 1990; Kurbaniyazov, 2017; Kuzmina & Treshkina, 2009).
- Northeastern DASB: Succession dynamics studied by Dimeeva (1997, 2007, 2011).
- Arkhangelsky Ridge: Investigated by Shomuradov et al. (2015, 2019) and Sherimbetov (2015).
- Eastern Basin (Post-2010): Devoid of vegetation due to hyper-salinity and inaccessibility (Novikova, 2019; Za vyalov et al., Russian Academy of Sciences).

Accelerated Succession and Challenges

Rapid plant community changes, driven by soil salinity dynamics, complicate generalization of long-term vegetation trends from fragmented field data.

Confirmed Predictions

- Rafikov (1982): Coastal clayey solonchaks ceased supporting halophytes (e.g., Tamarix) by the 2000s due to extreme salinity, becoming barren like the Akpetkinsky Archipelago salt flats.
- Gerasimov et al.: Predicted unstable initial colonization (1980–1990 desiccation zone) and lifeless solonchaks (1990–2000 zone), now validated.

Vegetation's Role in Mitigation

International studies (e.g., Indoitu et al., 2015) highlight vegetation's potential to curb salt transfer. However, quantitative links between vegetation cover (VPC) and salt transfer have been established only by Tleumuratova (2018) and Kubanov (2024), who developed methods to assess anthropogenic interventions (e.g., Kokaral Dam, afforestation).

Phytoremediation Assessment Methodology

To quantify afforestation's efficacy in reducing salt emissions (million tons/year), the following data are required:

1) T_e – Annual hours of energy-active wind speeds (>4 m/s) (sourced from meteorological databases);
2) S_{sal} – Total salt flat area (modeled);
3) S_{ALT} – Soil salinity (modeled);
4) $\delta_f t1$ – Pre-afforestation vegetation projective cover (modeled);
5) **VPC1** Post-afforestation VPC, averaged from field data (Kabulov, 1985; Sarybaev, 1987; Shomuradov et al., 2015; Kurbaniyazov, 2017; Kuzmina & Treshkin, 2006; Dimeeva, 1997) and set to 0.5 (Fig. 2.5).

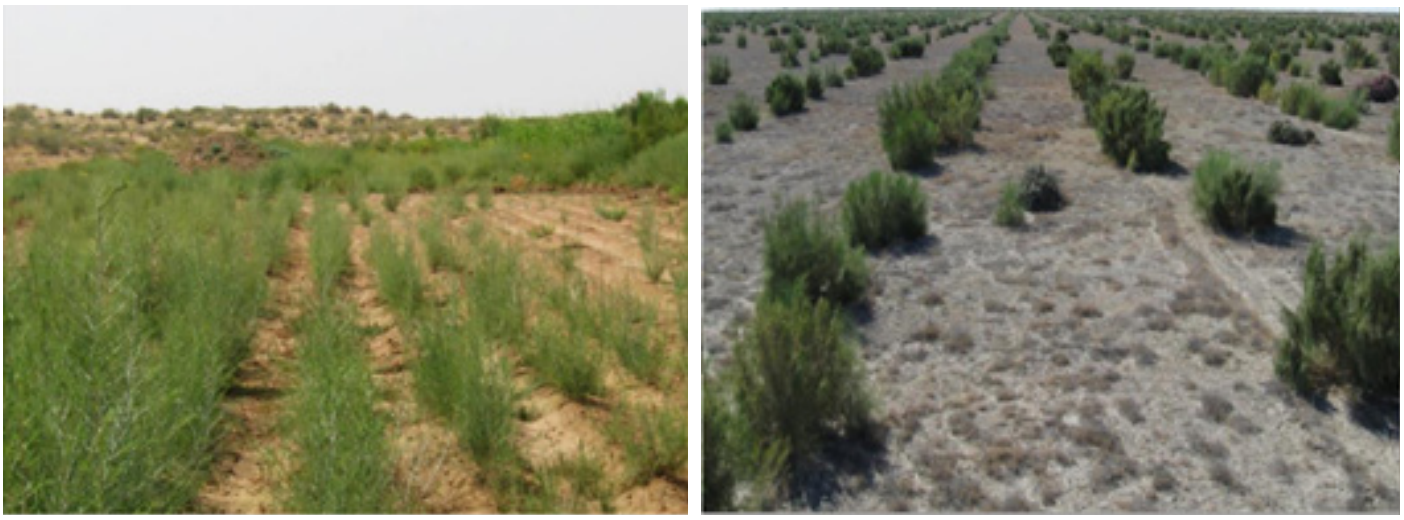

Fig. 2.5. Afforestation on the DASB (left: sandy soils; right: saline sandy loams)

Modeled data on DASB soil salinity and total vegetation projective cover (VPC) for 2020 are shown in Fig. 2.6 (Kubanov, 2023).

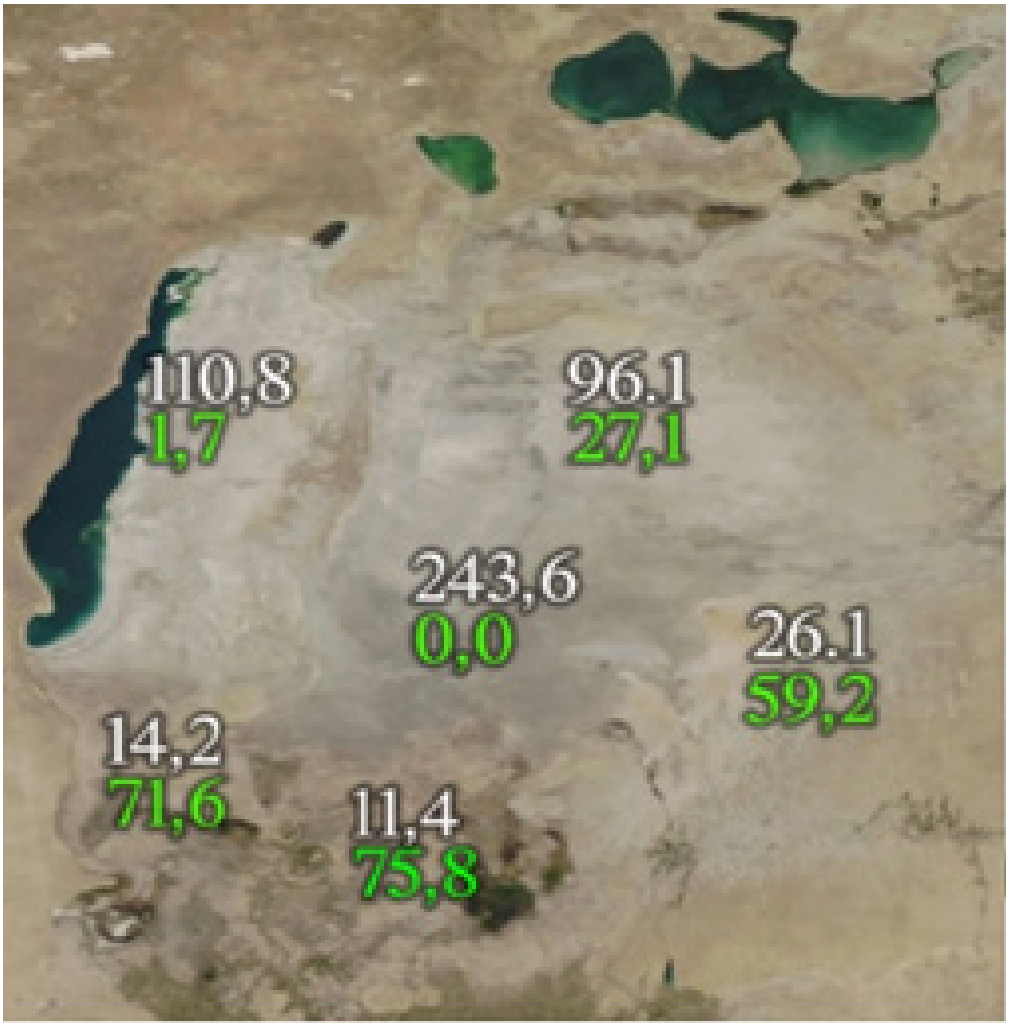

Fig. 2.6. Soil Salinity of the DASB

2.3 Research Methods

The method for assessing the effectiveness of phytoremediation on the Desiccated Aral Sea Bed (DASB) in mitigating salt transfer involves the following stages:

1. Modeling salt transfer dynamics based on the spatiotemporal variability of soil salinity and vegetation projective cover (VPC), which determines the degree of salt transfer reduction (Kubanov & Tleumuratova, 2023).
2. Determining, for each modeling period:
   - o Soil salinity.
   - o Total projective cover (TPC).
   - o Annual salt transfer volume (modeling results).
   - o Afforested area and corresponding VPC-adjusted annual salt transfer.
3. **Calculating the difference** between annual salt transfer (million tons/year) from afforested areas and hypothetical transfer from the same areas without vegetation (modeled data), yielding the quantitative efficacy of phytoremediation.

Vegetation's Impact on Salt Transfer

The effect of vegetation cover on salt transfer is determined by the reduction in the source strength of salts (ΔF), caused by the decrease in wind speed within the vegetation layer.

The reduction in salt transfer ΔV per unit area and time by a vegetation layer with TPC is calculated both for a single dust storm event and as an annual effect of salt transfer mitigation.

Phytoremediation signifies an increase in TPC by a certain value:

$$\Delta \delta_f = \delta_f(t_2) - \delta_f(t_1), \quad (2.1)$$

where $\delta_f(t_1)$ – is the TPC before phytoremediation, and $\delta_f(t_2)$ – is the TPC after phytoremediation. Thus, the effectiveness of phytoremediation, representing the reduction in salt transfer per unit area and time, is:

$$E_{un} = \Delta F((t2)) - \Delta F(\delta_f(t1)). \quad (2.2)$$

The **total annual effect of phytoremediation** (i.e., the reduction in salt transfer from the entire DASB per year) is:

$$E_{annual} = E_{un} \cdot T_e \cdot S_{salt}, \quad (2.3)$$

where:

- T_e – Annual hours of energy-active wind speeds (>4 m/s),
- S_{salt} – Total area of salt flats.

Modeling Period and Spatial Framework

- **Modeling period**: 1961–2024, divided into decades (1961–1970, 1971–1980, etc.), as this interval reflects significant natural transformations and aligns with the traditional chronological division of the Aral crisis evolution in ecological-geographical studies.
- **Decade numbering**: N=1 for 1961–1970, N=2 for 1971–1980, etc.
- **Temporal identification**: Time is also defined as the duration since the desiccation of a given DASB point (T=1,2,3...), i.e., the number of years since the point emerged above water, and as the time since the Aral Sea began drying (t), counted in years from 1961.

Spatial Scope

- **Horizontal**: The 1960 Aral Sea water area.
- **Vertical**: 3 m depth to 2000 m altitude.

Spatial-Temporal Complexity

The complexity of the geosystem's spatiotemporal dynamics over the extended period (1961–2017) necessitates a component-wise and segmented analysis differentiated by time intervals.

Spatial Quantization

- The modeling period is divided into decades, with the DASB partitioned into "desiccation strips" corresponding to each decade (1961–1970, 1971–1980, etc.).
- The diversity and scattered distribution of DASB landscape types preclude the use of Cartesian coordinates as arguments in formalization.
- Spatial localization is instead identified using desiccation strips from different decades.
- Division into decadal desiccation strips is also justified by the evolving rates and speeds of processes over time.

Assumptions

Salinization/desalination and vegetation colonization processes develop perpendicular to the shoreline of the corresponding year and are uniform along the entire length of the desiccation strip (Fig. 2.7).

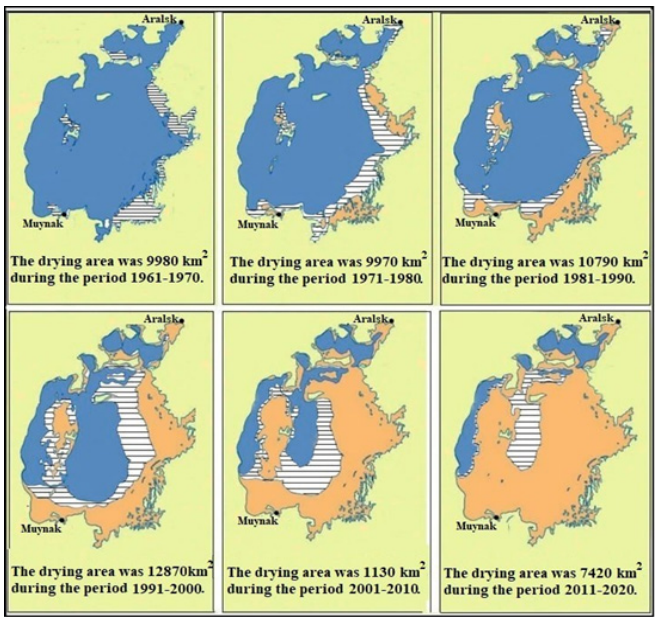

Fig. 2.7. Desiccation Strips for 1961–2020 (shaded areas)

2.4 Research Results

The results involve the generalization and formalization of the natural evolution of vegetation cover on the DASB, the retrospective calculation of the effect of natural vegetation cover (1961–2020), and the evaluation of phytoremediation effectiveness for 2011–2020.

Natural Evolution of Vegetation Cover on the DASB

To express vegetation dynamics as a function of soil salinity and salt transfer, the following regression equation was derived (Kubanov, 2023):

$$\delta_f(T,t) = -0{,}0002(S_{IIC})^3+0{,}0334(S_{IIC})^2-2{,}0651S_{IIC}+100-\Delta\delta_f \qquad (2.4)$$

Table 2.1

Dynamics of Vegetation Projective Cover (TPC, %) in Phytocenoses of the Western Escarpment Zone ("Chink") of the Desiccated Aral Sea Bed (DASB) Depending on Soil Salinity (g/kg) and Wind-Driven Salt Transfer

N	T=1		T=5		T=10		T=20	
	S_{salt}	$\delta_f(t)$	S_{salt}	$\delta_f(t)$	S_{salt}	$\delta_f(t)$	S_{salt}	$\delta_f(t)$
1	8,9	79,7	6,8	82,9	4,0	87,4	3,8	87,8
2	34,8	55,5	26,1	60,2	15,3	69,6	14,4	70,7
3	61,3	44,2	48,8	46,4	35,2	50,1	33,1	51,0
4	88,5	32,3	74,8	39,1	62,4	42,2	58,7	42,8
5	116,3	7,4	104,1	16,7	88,9	31,3	83,6	34,4
6	144,9	0,1	136,8	0,1	126,7	0,2	123,7	0,3

Table 2.2

Dynamics of Vegetation Projective Cover (TPC, %) in the Eastern Part of the DASB (by decade of desiccation) Depending on Soil Salinity (g/kg) and Wind-Driven Salt Transfer

N	T=1		T=5		T=10		T=20	
	$S_{salt}(N)$	$\delta_f(T,t)$	$S_{salt}(N)$	$\Delta\delta_f(T,t)$	$S_{salt}(N)$	$\Delta\delta_f(T,t)$	$S_{salt}(N)$	$\Delta\delta_f(T,t)$
1	15,6	71,7	14,7	72,7	9,6	79,2	8,1	81,5
2	43,8	51,5	37,6	53,4	19,3	64,5	14,6	69,2
3	75,4	42,8	70,8	44,3	58,5	47,2	44,6	50,0
4	126,6	1,8	110,3	8,6	91,5	31,5	85,0	36,1
5	237,1	0,0	203,5	0,0	154,5	0,0	135,4	0,1
6	370,7	0,0	325,7	0,0	251,8	0,0	244,2	0,0

Notes for Tables 2.1–2.2:

- T: Annual hours of energy-active wind speeds (>4 m/s)
- N: Decade number (1: 1961–1970, 2: 1971–1980, etc.).
- S_{salt}: Soil salinity (g/kg)
- ΔTPC: Change in vegetation projective cover (%) relative to baseline
- The first column indicates the decade number. Subsequent columns provide paired values of soil salinity (g/kg) in the T-th year of desiccation and the corresponding projective cover (%) for each decade
- Discrepancy: The average discrepancy (k) between modeled and field data (Kochkarova, 2020; Sarybaev, 1987; Shomuradov et al., 2015) is:
  - Causative part: k=−1.43k=−1.43.
  - Eastern part: k=5.53k=5.53.
- Limitation: Field data were obtained from limited, localized areas of the DASB with unique microclimatic conditions, soil salinity levels, groundwater tables, precipitation, and soil moisture. Therefore, modeled TPC values, derived from highly aggregated data for research purposes, may differ from field observations.

Impact of Vegetation Cover on Wind Speed Reduction **Table 2.3**

Wind Speed (m/s)	Projective Cover (TPC)										
	0	0,1	0,2	0,3	0,4	0,5	0,6	0,7	0,8	0,9	1
5	5	4,6	4,1	3,7	3,3	2,8	2,4	1,9	1,5	1,1	0,6
10	10	9,1	8,3	7,4	6,5	5,6	4,8	3,9	3,0	2,1	1,3
15	15	13,7	12,4	11,1	9,8	8,4	7,1	5,8	4,5	3,2	1,9
20	20	18,3	16,5	14,8	13,0	11,3	9,5	7,8	6,0	4,3	2,5
25	25	22,8	20,6	18,4	16,3	14,1	11,9	9,7	7,5	5,3	3,1
30	30	27,4	24,8	22,1	19,5	16,9	14,3	11,6	9,0	6,4	3,8

Explanation (Table 2.3):

- A surface with only 10% vegetation cover has minimal impact on wind speed, while full vegetation cover (TPC = 1.0) reduces wind speed by a factor of 10.

Equation: Reduction in Salt Transfer During a Dust Storm

The nonlinear reduction in salt transfer per unit area (V_b) by a vegetation layer with TPC during a dust storm is expressed as:

$$\Delta V_б = -1{,}8885\delta_f^2 + 4{,}9113\delta_f + 0{,}0127 \quad (2.5)$$

This equation was derived through regression analysis based on the modeling results of vegetation cover dynamics under varying wind intensities during dust storms (Fig. 2.8).

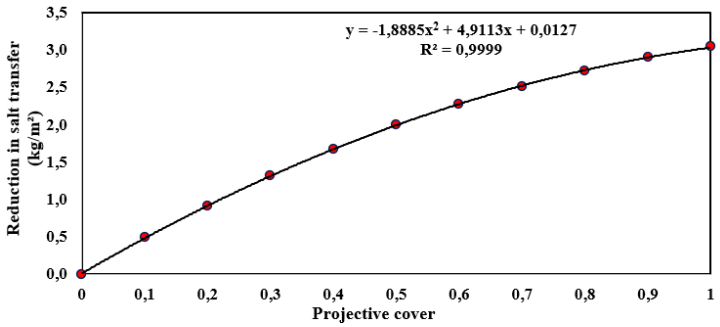

Fig. 2.8: Reduction in salt transfer by vegetation during a single salt-dust storm.

The reduction in salt transfer per unit area by the vegetation layer over decades is also nonlinear (Table 2.4). The table clearly illustrates how sharply the restraining effect of vegetation cover (VPC) on salt transfer weakens over time across desiccation strips from different decades, as the vegetation projective cover (TPC) decreases.

Decadal Reduction in Salt Transfer by Vegetation **Table 2.4**

Parameter	Unit	Decades					
		1	2	3	4	5	6
TPC (%)	%	82,2	63,1	51,1	0,6	0,1	0
Salt Transfer (no vegetation)	kg/m²	1,4	4,1	9,2	19,6	34,2	48,3
Salt Transfer (with vegetation)	kg/m²	0,4	1,7	4,2	17,1	33,4	48,3
Reduction (ΔV)	kg/m²	1,0	2,3	4,7	2,5	0,8	0
Reduction (%)	%	71	58	50	13	5	0

Explanation:

- The table demonstrates how the inhibitory effect of vegetation on salt transfer sharply diminishes over decades due to declining TPC and increasing soil salinity.

Equation: Annual Salt Transfer Reduction (Fig. 2.9)

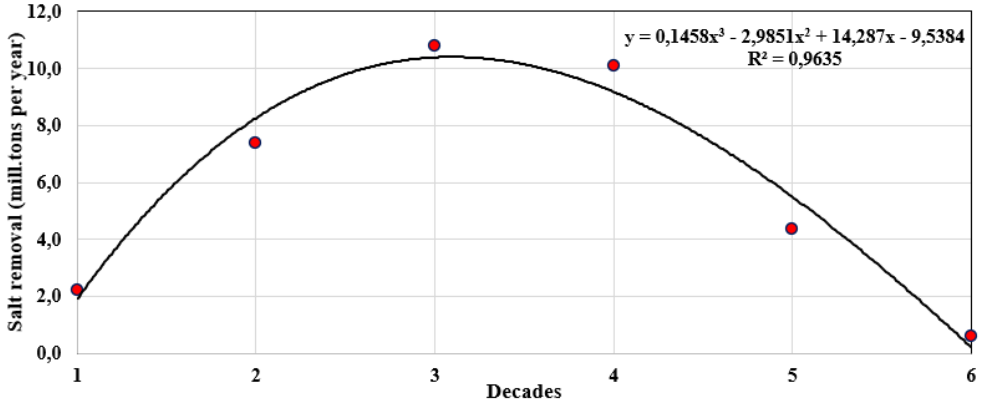

Fig. 2.9: Annual effect of vegetation on salt transfer reduction across decadal desiccation strips at Annual hours of energy-active wind speeds (>4 m/s) = 10

The annual effect of vegetation on salt transfer reduction (ΔVannual) is calculated as:

$$\Delta Vannual = 0{,}1458\ \delta_f 3 - 2{,}9851\ \delta_f 2 + 14{,}287\ \delta_f - 9{,}5384 \qquad (2.6)$$

Interpretation:

- The graph shows a decline in vegetation's mitigating effect over time due to decreasing TPC, driven by soil salinization outpacing vegetation colonization.
- The peak effect in the 3rd decade (1990s) occurred because salt transfer was already significant, but vegetation colonization was still sufficient to counteract it.

Implementation of the Phytoremediation Assessment Method

The aforementioned results were obtained by modeling the natural evolution of vegetation cover (VPC) on the Desiccated Aral Seabed (DASB), i.e., through the implementation of stages 1) and 2) of the method for evaluating the effectiveness of phytoremediation on the DASB in mitigating wind-driven salt transfer (WST). Below, we present the results of stage 3): calculating the difference between the annual volume of WST (million tons/year) from afforested areas and the hypothetical WST from the same areas without afforestation (modeled data), which quantifies the effectiveness of phytoremediation for 2011–2020 (Table 2.5).

Case Study:

Implementation of the developed method demonstrated that, for example, in 2019, when the afforested area totaled 483,000 hectares, the total salt transfer from these territories was reduced by 16.1 million tons/year (Table 2.5). Clearly, the effectiveness of afforestation increases with:

1. A greater difference in vegetation projective cover (VPC) before and after phytoremediation.
2. A larger afforested area.

Table 2.5

Areas and Effectiveness of Anthropogenic Interventions

Parameter	Unit	Years						
		2011	2015	2019	2021	2022	2023	2024
Modeled WST (no afforestation)	million tons/year	81,5	101,9	112,8	132,9	136,4	138,1	140,8
Afforested Area	thousand km2	2,85	3,31	4,83	4,94	5,14	5,34	5,56
Afforestation Effectiveness	million tons/year	9,4	11,0	16,1	16,4	17,1	17,7	18,4

Key Observations:

Despite the increase in afforested areas (Appendix 2), the percentage effectiveness of WST mitigation has declined due to:

1. Dominance of accelerating WST rates.
2. Partial reduction in sapling survival caused by increasing soil salinity.

Computational Method:

All calculations were performed using a custom-developed computer model (Appendix 4).

CONCLUSION

In this study, we investigated the seasonal and long-term dynamics of dust migration in the SASR using statistical and computer modeling methods. We identified and formalized patterns of spatiotemporal dynamics of dust migration and its driving factors. Enhancing factors of dust migration (desert area, wind regime) and mitigating factors (Vegetation Projective Cover (VPC), precipitation) were analyzed in detail using quantitative methods. The degree of influence of each factor on dust migration dynamics was quantitatively assessed.

In addition to diagnosing dust migration during the modeling period (1961–2020), the study constructively examined and forecasted measures to mitigate dust migration and their potential effects.

A key distinction of this work from numerous other studies on the Aral crisis lies in its extensive application of quantitative methods and systematic analysis over the entire Aral region? presentation of results through comprehensive maps, graphs, and quantitative summaries covering the entire Aral region.

Scientific Novelty:

- Development and implementation of models:
  - o LTI (Model of Long-Term Impact Model) to compute monthly average dust concentration fields in the SP for individual decades (1961–2020).
  - o MYDD (Model of Long-Term Dust Migration) to determine long-term dust migration dynamics in the region.
- First quantitative investigation of long-term dust migration dynamics in the DASB.
- First compilation of continuous digital datasets on the spatiotemporal dynamics (STD) of dust migration in the DASB.
- First formalized representations of STD patterns for dust migration and its drivers.
- Quantitative evaluation of the effectiveness of dust migration mitigation measures, such as phytoremediation and artificial precipitation.
- Quantitative assessment of the ecological efficiency of vegetation cover's ecosystem services in protecting against salt transfer from the Aralkum, using a custom-developed computer model.

CONCLUSIONS AND RECOMMENDATIONS

1. **Trends**: An overall increase in dust migration-enhancing factors (desert area, wind activity) and a decrease in mitigating factors (VPC, precipitation) are observed, leading to progressive atmospheric dust load in the SP, frequently exceeding WHO-established Maximum Permissible Concentrations (MPC). This correlates with rising local population morbidity and mortality rates.
2. **Health Research**: Epidemiological studies on the links between dust migration and regional morbidity are urgently needed.
3. **Monitoring Gaps**: The inadequate dust monitoring system in the SASR necessitates statistical modeling. The region's unique geographical and ecological position requires the development of a specialized model.
4. **Mitigation Measures**: Alongside phytoremediation, technologies for artificial precipitation (70% dust reduction efficacy vs. 15% for afforestation) must be prioritized.
5. **Natural vs. Industrial Sources**: Over 80% of atmospheric pollution in Karakalpakstan originates from natural desert dust sources (Aralkum, Ustyurt, Kyzylkum, Karakum). Industrial air pollution in Karakalpakstan has been shown to be spatially limited, typically affecting areas within 20–30 km of emission sources such as the Takhiatash TPP (Tleumuratova et al., 2020; 2021). In contrast, natural desert dust sources have a significantly broader zone.
6. **Source Ranking**: Statistical analysis identifies Aralkum as the dominant dust source, followed by Ustyurt, Kyzylkum, and Karakum.
7. **Forecasting and Monitoring**: The absence of emergency warnings for extreme dust concentrations due to flawed storm prediction methods underscores the need for:

o Enhanced research on dust event forecasting.
o A dense, technically advanced air quality monitoring network in the Lower Amu Darya Oasis.

8. **IT Infrastructure**: Air pollution monitoring systems must integrate computational tools, programming methods, and technical resources to optimize management efficiency and decision-making.
9. **Soil Salinization**: Toxic sulfate transfer from the DASB salinizes soils in the humid Southern Aral region, peaking in April–May, intensifyingpost-storm rainfall. Precipitation mineralization due to constant atmospheric salt presence exacerbates this.
10. **Phytoremediation Challenges**: With plant biomass and productivity reduced by 10–20% due to Aral-derived sulfates, expanding research on improving phytoremediation efficacy on the DASB is critical.
11. **Summer Dust Dynamics**: Convective uplift of soil microparticles under near-calm, arid conditions contributes to regional dustiness. Studies by Tleumuratova B.S. and Narymbetov B.Zh. show summer dust concentrations over deserts increase by 1.2 mg/m³. Further research on convective dust impacts is essential.
12. **Relational Database**: A structured relational database is needed to:

o Classify geosystem characteristics for efficient large-scale data storage.

- Formalize landscape descriptions of desert geosystems and link them to qualitative classifications.
- Enable rapid updates (e.g., vegetation cover density, DASB impact levels) without structural overhauls.
- Support sustainable resource strategies (e.g., pasture zoning, agricultural planning).

Final Note: Landscape-ecological classification is vital for regional ecological modeling. A relational database enhances data organization, enabling precise research and sustainable resource strategies. It serves both scientific and practical conservation purposes, particularly for the Kyzylkum Desert.

LIST OF REFERENCES

Abitaev D.S., Tatkeev T.A., Rakhimbekov M.S., Attshabarova S.S., Rahmetullaev B.B. Complex Influence of Environmental Factors on Public Health in the Aral Sea Region. Gigiena Truda i Meditsinskaya Ekologiya. 2014. No. 1. Pp. 13–18.

Aerosols and Climate / Ed. by K.Ya. Kondratyev. Leningrad: Gidrometeoizdat, 1991. 542 p.

Aghababaeian H. et al. Global health impacts of dust storms: a systematic review // Environmental health insights. – 2021. – T. 15. – C. 11786302211018390.

Aili A., Oanh N. T. K. Effects of dust storm on public health in desert fringe area: case study of northeast edge of Taklimakan Desert, China //Atmospheric Pollution Research. – 2015. – T. 6. – №. 5. – C. 805-814.

Aimbetov N.K. et al. Dynamics and Potential of the Natural Environment of the Southern Aral Sea Region: A Collective Monograph / Ed. by N.K. Aimbetov. Nukus: Ilim, 2017. 251 p.

Aimuratov R.P. Forage Plants of Ustyurt and Their Use in Improving Degraded Lands of the Aral Sea Region. Diss. ... Doctor of Philosophy (PhD) in Biological Sciences. Nukus, 2020. 116 p.

Akhlaq M., Sheltami T. R., Mouftah H. T. A review of techniques and technologies for sand and dust storm detection // Reviews in Environmental Science and Bio/Technology. – 2012. – T. 11. – C. 305-322.

Aleya L., Uddin M. S. Environmental pollutants and the risk of neurological disorders // Environmental Science and Pollution Research. – 2020. – T. 27. – №. 36. – C. 44657-44658.

Al-Hemoud A. et al. Health impact assessment associated with exposure to PM10 and dust storms in Kuwait // Atmosphere. – 2018. – T. 9. – №. 1. – C. 6.

Banks, J. R., Heinold, B., Schepanski, K. Impacts of the desiccation of the Aral Sea on the Central Asian dust life–cycle // Journal of Geophysical Research. Atmospheres, 2022. 127, e2022JD036618. https://doi.org/10.1029/2022JD036618.

Bartzokas A. et al. The effect of meteorological and pollution parameters on the frequency of hospital admissions for cardiovascular and respiratory problems in Athens // Indoor and Built Environment. – 2004. – T. 13. – №. 4. – C. 271-275.

Bekhzod A. et al. Present State of Pasture Types of the Central Kyzylkum //American Journal of Plant Sciences. – 2016. – T. 7. – №. 04. – C. 677.

Belnap J., Gillette D. A. Disturbance of biological soil crusts: impacts on potential wind erodibility of sandy desert soils in southeastern Utah // Land Degradation & Development. – 1997. – T. 8. – №. 4. – C. 355-362.

Benedetti A. et al. The value of satellite observations in the analysis and short-range prediction of Asian dust // Atmospheric Chemistry and Physics. – 2019. – T. 19. – №. 2. – C. 987-998.

Bogdanova N.M., Kostyuchenko V.P. Processes of Salt Accumulation on the Desiccated Aral Seabed and Their Relationship with Geomorphological and Lithological Conditions. Izvestiya Akademii Nauk SSSR. Seriya Geologicheskaya. 1977. No. 3. Pp. 29–31.

Bozlaker A. et al. Quantifying the contribution of long-range Saharan dust transport on particulate matter concentrations in Houston, Texas, using detailed elemental analysis // Environmental science & technology. – 2013. – T. 47. – №. 18. – C. 10179-10187.

Bykova D.P., Dubov A.S. Influence of Forest Belts on Dust Concentration Distribution During Dust Storms. Meteorologiya i Gidrologiya. 1974. No. 7. Pp. 23–36.

Cao, C., Cai, M., Zhao, L., & Li, G. (2024). Improving Water Stability of Soil Aggregates with Polyvinyl Alcohol as a Polymeric Binder. Polymers, 16(13), 1758.

Chen S. H., Wang S. H., Waylonis M. Modification of Saharan air layer and environmental shear over the eastern Atlantic Ocean by dust-radiation effects // Journal of Geophysical Research: Atmospheres. – 2010. – T. 115. – №. D21. – C. 1-22.

Chen S. J. et al. The effect of dust radiative heating on low-level frontogenesis // Journal of Atmospheric Sciences. – 1995. – T. 52. – №. 9. – C. 1414-1420.

Chen W. et al. Progress in dust modelling, global dust budgets, and soil organic carbon dynamics // Land. – 2022. – T. 11. – №. 2. – C. 176.

Chen Y. et al. Dust radiation effect on the weather and dust transport over the Taklimakan Desert, China // Atmospheric Research. – 2023. – T. 284. – C. 106600.

Chen Y. S. et al. Effects of Asian dust storm events on daily mortality in Taipei, Taiwan // Environmental research. – 2004. – T. 95. – №. 2. – C. 151-155.

Chin-Chan M., Navarro-Yepes J., Quintanilla-Vega B. Environmental pollutants as risk factors for neurodegenera-

tive disorders: Alzheimer and Parkinson diseases // Frontiers in cellular neuroscience. – 2015. – T. 9. – C. 124.

Choobari O. A., Zawar-Reza P., Sturman A. Feedback between windblown dust and planetary boundary-layer characteristics: sensitivity to boundary and surface layer parameterizations // Atmospheric environment. – 2012. – T. 61. – C. 294-304.

Choobari O.A, Zawar-Reza P., Sturman A. Low level jet intensification by mineral dust aerosols // Annales Geophysicae. – Göttingen, Germany : Copernicus Publications, 2013. – T. 31. – №. 4. – C. 625-632.

Chub V.E. Climate Change and Its Impact on the Natural Resource Potential of the Republic of Uzbekistan. Tashkent: SANIGMI, 2000. 252 p.

Cornelis W. M., Gabriels D. The effect of surface moisture on the entrainment of dune sand by wind: an evaluation of selected models // Sedimentology. – 2003. – T. 50. – №. 4. – C. 771-790.

Creamean J. M. et al. Dust and biological aerosols from the Sahara and Asia influence precipitation in the western US // science. – 2013. – T. 339. – №. 6127. – C. 1572-1578.

Darmenova K., Sokolik I. N. Assessing uncertainties in dust emission in the Aral Sea region caused by meteorological fields predicted with a mesoscale model // Global and Planetary Change. – 2007. – T. 56. – №. 3-4. – C. 297-310.

Decree of the President of the Republic of Uzbekistan No. UP-158 dated 11.09.2023 “On the ‘Uzbekistan – 2030’ Strategy.”

Decree of the President of the Republic of Uzbekistan No. UP-5863 dated 30.10.2019 “On Approval of the Environmental Protection Concept of the Republic of Uzbekistan until 2030.”

Dimeeva L.A. Classification of Vegetation in the Coastal Plains of the Aral and Caspian Seas. Vestnik Baltiiskogo Federalnogo Universiteta im. I. Kanta. 2011. Issue 7. Pp. 132–139.

Dimeeva L.A. Dynamics of Phytocoenosis Productivity on the Desiccated Aral Seabed. Izvestiya NAN Respubliki Kazakhstan. Seriya Biologicheskaya. 1997. No. 5. Pp. 17–24.

Dimeeva L.A. Patterns of Primary Successions on the Aral Coast. Aridnye Ekosistemy. 2007. Vol. 13. No. 33–34. Pp. 89–100.

Dipu S. et al. Impact of elevated aerosol layer on the cloud macrophysical properties prior to monsoon onset // Atmospheric Environment. – 2013. – T. 70. – C. 454-467.

Dosbergenov S.N., Asanbaev I.K. On Aeolian Salt Emission from the Desiccated Aral Seabed. Problemy Osvoeniya Pustyn. 2002. No. 2. Pp. 37–42.

Droppo J. G. Improved formulations for air-surface exchanges related to National Security Needs: dry deposition models. – Pacific Northwest National Lab.(PNNL), Richland, WA (United States), 2006. – №. PNNL-15876.

Dukhovny V.A., Stulina G.V., Ruziev I., Roshchenko E. Concept for Developing Phytoremediation Justification and Monitoring on the Desiccated Aral Seabed. *Central Asian International Scientific-Practical Conference Dedicated to the 15th Anniversary of the Interstate Commission for Water Coordination*. Almaty, Kazakhstan, 24–27 April 2007. Pp. 48–51.

Dunion J. P., Velden C. S. The impact of the Saharan air layer on Atlantic tropical cyclone activity // Bulletin of the American Meteorological Society. – 2004. – T. 85. – №. 3. – C. 353-366.

Erel Y. et al. Trans boundary transport of pollutants by atmospheric mineral dust //Environmental science & technology. – 2006. – T. 40. – №. 9. – C. 2996-3005.

Ermak D. L. An analytical model for air pollutant transport and deposition from a point source // Atmospheric Environment (1967). – 1977. – T. 11. – №. 3. – C. 231-237.

Eurasianet (2021) Film explores a dirty problem in Kyrgyzstan and Uzbekistan. https://eurasianet.org/film-explores-a-dirty-problem-in-kyrgyzstan-and-uzbekistan.

Galaeva O.S. On Monitoring the Emission of Sand-Salt Aerosols from the Desiccated Aral Seabed. Problemy Osvoeniya Pustyn. 1998. Vol. 3.4. Pp. 17–21.

Galaeva O.S., Idrisova V.P. Climatic Features of Dust Storms in the Aral Sea Region. Gidrometeorologiya i Ekologiya. 2007. No. 2. Pp. 27–40.

Galán-Madruga D. et al. Indoor and outdoor PM 10-bound PAHs in an urban environment. similarity of mixtures and source attribution // Bulletin of Environmental Contamination and Toxicology. – 2020. – T. 105. – C. 951-957.

Galán-Madruga D., García-Cambero J. P. An optimized approach for estimating benzene in ambient air within an air quality monitoring network // Journal of Environmental Sciences. – 2022. – T. 111. – C. 164-174.

Gautam R., Hsu N. C., Lau K. M. Premonsoon aerosol characterization and radiative effects over the Indo-Gangetic Plains: Implications for regional climate warming // Journal of Geophysical Research: Atmospheres. – 2010. – T. 115. – №. D17. – C. 1-15.

Ge Y, Wu, N, Abuduwaili J, Kulmatov R, Issanova G, Saparov G. Identifying Seasonal and Diurnal Variations and the Most Frequently Impacted Zone of Aerosols in the Aral Sea Region // Int. J. Environ. Res. Public Health 2022, 19, 14144. https://doi.org/10.3390/ijerph192114144.

Ge, Yongxiao, et al. "Temporal variability and potential diffusion characteristics of dust aerosol originating from the Aral Sea basin, central Asia." Water, Air, & Soil Pollution 227 (2016): 1-12.

Ghaisas S., Maher J., Kanthasamy A. Gut microbiome in health and disease: Linking the microbiome–gut–brain axis and environmental factors in the pathogenesis of systemic and neurodegenerative diseases // Pharmacology & therapeutics. – 2016. – T. 158. – C. 52-62.

Glazovsky, N. F. (1995). Environmental problems of the Aral region. Ambio, 24(6), 378–385.

Goffner D., Sinare H., Gordon L. J. The Great Green Wall for the Sahara and the Sahel Initiative as an opportunity to enhance resilience in Sahelian landscapes and livelihoods // Regional Environmental Change. – 2019. – T. 19. – C. 1417-1428.

Goméz, G. P., Martinez, J. G. B., & Cárdenas, J. C. R. (2019, October). Soil stabilization with lime and fly ash Estabilización de suelos con cal y ceniza volante. In 2019 Congreso Internacional de Innovación y Tendencias en Ingenieria (CONIITI) (pp. 1-6). IEEE.

Gordeev S. A. et al. Psychophysiological characteristics of panic disorder and generalized anxiety disorder // Zhurnal nevrologii i psikhiatrii imeni SS Korsakova. – 2013. – T. 113. – №. 5. – C. 11-14.

Goudie A. S. Desert dust and human health disorders //Environment international. – 2014. – T. 63. – C. 101-113.

Goudie, A. Dust storms and ephemeral lakes. Desert 2018, 23, 153–164.

Grigor'ev, Al. A. & Djogova, M. L. Strong dust blowouts in Aral region in 1985-1990. Proc. of the Russian Academy of Sciences, 325(3), pp. 672 675, 1992. (in Russian)

Grigoriev A.A., Lipatov V.B. Dust Storms Based on Space Research Data. Leningrad: Gidrometeoizdat, 1985. 31 p.

Groll M., Opp C., Aslanov I. Spatial and temporal distribution of the dust deposition in Central Asia–results from a long term monitoring program //Aeolian Research. – 2013. – T. 9. – C. 49-62.

Hagen L. J. Evaluation of the Wind Erosion Prediction System (WEPS) erosion submodel on cropland fields // Environmental Modelling & Software. – 2004. – T. 19. – №. 2. – C. 171-176.

Hsu N. C. et al. Comparisons of the TOMS aerosol index with Sun-photometer aerosol optical thickness: Results and applications // Journal of Geophysical Research: Atmospheres. – 1999. – T. 104. – №. D6. – C. 6269-6279.

http://www.pogodaiklimat.ru – Weather and Climate – Weather forecasts, weather news, climatic data.

https://apps.sentinel-hub.com/eo-browser – Access to raw satellite data, visualized imagery, statistical analysis, and other features.

https://earthexplorer.usgs.gov/ – Satellite imagery, aerial photography, and cartographic products via the U.S. Geological Survey.

https://eos.com/landviewer – Modern source of satellite data and analytics powered by artificial intelligence.

https://ru.weatherspark.com – Climate data with weather descriptions by month, day, and hour.

Indoitu R, Kozhoridze G, Batyrbaeva M, Vitkovskaya I, Orlovsky N, Blumberg D, Orlovskiy L. Dust emission and environment changes in the dried bottom of the Aral sea // Aeolian Research, 2015, PP.101-115.

Iwasaka, H. 2006: Impact of interannual variability of me teorological parameters on vegetation activity over Mongolia. J. Meteorol. Soc. Jpn., 84, 745-762, doi: 10.2151/jmsj.84.745.

Jaramillo, A., Cano, Y. P. G., Peláez, D. M. C., Montoya, G. I. H., Cano, C. A. M., & Alexander, F. (2023). Evaluation of the Effect of Binary Fly Ash-Lime Mixture on the Bearing Capacity of Natural Soils: A Comparison with Two Conventional Stabilizers Lime and Portland Cement. Materials, 16(3996), 1-17.

Journet E., Balkanski Y., Harrison S. P. A new data set of soil mineralogy for dust-cycle modeling // Atmospheric Chemistry and Physics. – 2014. – T. 14. – №. 8. – C. 3801-3816.

Kabulov S.K. Changes in Desert Phytocoenoses Under Aridization. Tashkent: Fan, 1990. 240 p.

Kabulov S.K. Hydrothermal Regime of the Aral Sea Region in the Context of the Aral Sea Problem. Izvestiya AN SSSR. Seriya Geograficheskaya. 1985. No. 2. Pp. 95–101.

Kaiser J. Mounting evidence indicts fine-particle pollution. – 2005. – T. 307. – №. 5717. – C. 1858-1861.

Kang J. H. et al. Asian dust storm events are associated with an acute increase in pneumonia hospitalization // Annals of epidemiology. – 2012. – T. 22. – №. 4. – C. 257-263.

Karydis V. A. et al. On the effect of dust particles on global cloud condensation nuclei and cloud droplet number // Journal of Geophysical Research: Atmospheres. – 2011. – T. 116. – №. D23. – C. 1-16.

Kholmuminov, A. A., Avazova, O. B., Mirkhaidarova, Y. N., Ruban, I. N., & Rashidova, S. S. (2003). Consolidation and melioration of salted sandy soils using a compound of acetone-formaldehyde resin with silk sericin. Russian journal of applied chemistry, 76, 775-777.

Kochkarova S.A., Mambetullaeva S.M. Study of Successional Processes of Vegetation Cover on the Dried Seabed of the Aral Sea // Journal Research on the Lepidoptera.– 2020.– Volume 51.– Issue 1. Pp.1245–1256.

Kondratyev K.Ya., Grigoriev A.A. Natural and Anthropogenic Ecological Disasters: Meteorological Disasters. Issledovanie Zemli iz Kosmosa. 2000. No. 4. Pp. 3–19.

Kubanov Zh.Zh. Quantitative Assessment of the Salt Parameter Dynamics on the Desiccated Aral Seabed. Diss. ... Doctor of Philosophy (PhD) in Biological Sciences. Nukus, 2023. 109 p.

Kubanov Zh.Zh., Tleumuratova B.S. Evaluating the Effectiveness of Anthropogenic Impacts on the Desiccated Aral Seabed in Reducing Salt Emission. Universum: Khimiya i Biologiya. 2023. No. 2(104). URL: https://7universum.com/ru/nature/archive/item/14961. Pp. 15–21.

Kulmatov R, Hojamberdiev M (2010) Distribution of heavy metals in atmospheric air of the arid zones in Central Asia. Air Qual Atmos Health 3:183–194

Kurbaniyazov A.K. Evolution of Landscapes on the Desiccated Aral Seabed. Moscow: Akademiya Estestvoznaniya, 2017. 148 p.

Kuzmina Zh.V., Treshkin S.E. Formation of Vegetation on Solonchaks of the Desiccated Aral Seabed Under Chang-

ing Climatic Conditions. Doklady Rossiiskoi Akademii Sel'skokhozyaistvennykh Nauk. 2009. No. 1. Pp. 32–35.

Kuzmina Zh.V., Treshkin S.E. Monitoring the Development of Black Saxaul (Haloxylon aphyllum) on Hydromorphic Solonchaks of the Desiccated Aral Seabed. Aridnye Ekosistemy. 2013. Vol. 19. No. 4(57). Pp. 40–48.

Lavaysse C., Chaboureau J. P., Flamant C. Dust impact on the West African heat low in summertime // Quarterly Journal of the Royal Meteorological Society. – 2011. – Т. 137. – №. 658. – С. 1227-1240.

Lemaître C. et al. Radiative heating rates profiles associated with a springtime case of Bodélé and Sudan dust transport over West Africa // Atmospheric Chemistry and Physics. – 2010. – Т. 10. – №. 17. – С. 8131-8150.

Létolle R. et al. The future chemical evolution of the Aral Sea from 2000 to the years 2050 //Mitigation and Adaptation Strategies for Global Change. – 2005. – Т. 10. – №. 1. – С. 51-70.

Lioubimtseva E. Environmental changes in arid Central Asia inferred from remote sensing data and ground observations // Аридные экосистемы. – 2005. – Т. 11. – №. 26-27. – С. 64-72.

Lu H., Shao Y. Toward quantitative prediction of dust storms: an integrated wind erosion modelling system and its applications // Environmental Modelling & Software. – 2001. – Т. 16. – №. 3. – С. 233-249.

Marchuk G.I. Mathematical Modeling in Environmental Problems. Moscow: Nauka, 1982. 320 p.

Martiny N., Chiapello I. Assessments for the impact of mineral dust on the meningitis incidence in West Africa // Atmospheric Environment. – 2013. – Т. 70. – С. 245-253.

Mazhitova Z.Kh., Seisebayeva R.Zh., Umbetova L.Zh. New Respiratory Diseases in Children Exposed to Air Pollution by Dust-Salt Particles. 2005.

Mbow C. The great green wall in the Sahel //Oxford Research Encyclopedia of Climate Science. – 2017.

Meister M. T. Air dispersion modeling of particulate matter from ground-level area sources : дис. – Texas A&M University, 2000.

Micklin P. Desiccation of the Aral Sea: a water management disaster in the Soviet Union. Science.1988. 241:1170–1176

Micklin, P. (2007). The Aral Sea disaster. Annual Review of Earth and Planetary Sciences, 35(1), 47–72. https://doi.org/10.1146/annurev.earth.35.031306.140120

Middleton N. Health in dust belt cities and beyond—an essay by Nick Middleton // bmj. – 2020. – Т. 371. – С. m3098.

Miri A. et al. Dust storms impacts on air pollution and public health under hot and dry climate // Int J Energy Environ. – 2007. – Т. 2. – №. 1. – С. 101-105.

Mkweather.com, 2021.

Mukasheva B.G. Climate Impact on Public Health in the Aral Sea Region. Gigiena Truda i Meditsinskaya Ekologiya. 2015. No. 4(49). Pp. 20–30.

Nastos P. T. et al. Environmental impacts on human health during a Saharan dust episode at Crete Island, Greece //Meteorologische Zeitschrift. – 2011. – Т. 20. – №. 5. – С. 517-529.

National Action Plan for Prevention and Mitigation of Sand and Dust Storm (SDS) Consequences in the Republic of Uzbekistan for 2021–2024.

Nickovic S. et al. A model for prediction of desert dust cycle in the atmosphere // Journal of Geophysical Research: Atmospheres. – 2001. – Т. 106. – №. D16. – С. 18113-18129.

Nickovic S. et al. High-resolution mineralogical database of dust-productive soils for atmospheric dust modeling // Atmospheric Chemistry and Physics. – 2012. – Т. 12. – №. 2. – С. 845-855.

Nobakht, M., Shahgedanova, M., &White, K. (2021). New inventory ofdust emission sources in Central Asiaand northwestern China derivedfrom MODIS imagery using dustenhancement technique. Journal ofGeophysical Research: Atmospheres,126, e2020JD033382

Novikova N.M. Ecological-Geographical Aspect of the Aral Crisis. Part 3. Research on the Dynamics of Natural Complexes in the Aral Sea Region. Ekosisytemy: Ekologiya i Dinamika. 2021. Vol. 5. No. 3. Pp. 60–65.

Novikova N.M. Ecological-Geographical Aspect of the Aral Crisis. Part 1. Development of the Aral Problem, Its Study, and Mitigation Measures. Ekosisytemy: Ekologiya i Dinamika. 2019. Vol. 3. No. 1. Pp. 5–66.

O'Hara S. L. et al. Exposure to airborne dust contaminated with pesticide in the Aral Sea region //The Lancet. – 2000. – Т. 355. – №. 9204. – С. 627-628.

Orlovsky L., Orlovsky N. White sand storms in Central Asia //Global Alarm: Dust and Sand Storms from the World's Drylands. United Nations. – 2001. – С. 169-201.

Orlovsky L., Orlovsky N., Durdyev A. Dust storms in Turkmenistan //Journal of Arid Environments. – 2005. – Т. 60. – №. 1. – С. 83-97.

Owen P. R. Saltation of uniform grains in air // Journal of Fluid Mechanics. – 1964. – Т. 20. – №. 2. – С. 225-242.

Pan H. et al. Seasonal and vertical distributions of aerosol type extinction coefficients with an emphasis on the impact of dust aerosol on the microphysical properties of cirrus over the Taklimakan Desert in Northwest China // Atmospheric Environment. – 2019. – Т. 203. – С. 216-227.

Pasquill F. Atmospheric dispersion modeling // Journal of the Air Pollution Control Association. – 1979. – Т. 29. – №. 2. – С. 117-119.

Pérez García-Pando C. et al. Predicting the mineral composition of dust aerosols: Insights from elemental composition measured at the Izaña Observatory // Geophysical Research Letters. – 2016. – Т. 43. – №. 19. – С. 520-529.

Perlwitz J. P., Pérez García-Pando C., Miller R. L. Predicting the mineral composition of dust aerosols–Part 1: Representing key processes // Atmospheric Chemistry and Physics. – 2015. – T. 15. – №. 20. – C. 11593-11627.

Pi H. et al. Evaluation of two empirical wind erosion models in arid and semi-arid regions of China and the USA // Environmental Modelling & Software. – 2017. – T. 91. – C. 28-46.

Poulsen O. M. et al. Sorting and recycling of domestic waste. Review of occupational health problems and their possible causes // Science of the total environment. – 1995. – T. 168. – №. 1. – C. 33-56.

Prasad A. K. et al. Melting of major Glaciers in the western Himalayas: evidence of climatic changes from long term MSU derived tropospheric temperature trend (1979–2008) // Annales Geophysicae. – Copernicus GmbH, 2009. – T. 27. – №. 12. – C. 4505-4519.

Prospero J. M. et al. Environmental characterization of global sources of atmospheric soil dust identified with the Nimbus 7 Total Ozone Mapping Spectrometer (TOMS) absorbing aerosol product // Reviews of geophysics. – 2002. – T. 40. – №. 1. – C. 1-31.

Rafikov A.A. Natural Conditions of the Desiccated Southern Coast of the Aral Sea. Tashkent: Fan, 1982. 147 p.

Rashki A. et al. Dust-storm dynamics over Sistan region, Iran: Seasonality, transport characteristics and affected areas // Aeolian Research. – 2015. – T. 16. – C. 35-48.

Razakov R.M., Kosnazarov K.A. Aeolian Emission and Environmental Protection Measures. Tashkent: Fan, 1987. 72 p.

Resolution of the Cabinet of Ministers of the Republic of Uzbekistan No. 41 dated 25.01.2022 “On Additional Measures to Transform the Aral Sea Region into a Zone of Ecological Innovations and Technologies.”

Resolution of the Cabinet of Ministers of the Republic of Uzbekistan No. 31 dated 18.01.2022 “On Additional Measures to Create a ‘Green Cover’ – Protective Forests on the Desiccated Aral Seabed and the Aral Sea Region.”

Resolution of the President of the Republic of Uzbekistan No. PP-338 dated 24.09.2024 “On Priority Measures to Combat Dust Storms and Improve Atmospheric Air Quality.”

Resolution of the President of the Republic of Uzbekistan No. PP-76 dated 30.12.2021 “On Measures for Environmental Protection and Organization of State Agencies in the Field of Environmental Control.”

Resolution of the President of the Republic of Uzbekistan No. PP-4850 dated 06.11.2020 “On Approval of the Concept for the Development of the Forestry System of the Republic of Uzbekistan until 2030.”

Rubanov I.V., Bogdanova N.M. Quantitative Assessment of Salt Deflation on the Desiccated Aral Seabed. Problemy Osvoeniya Pustyn. 1987. No. 3. Pp. 9–16.

Sanchez de la Campa A. et al. Chemical and microbiological characterization of atmospheric particulate matter during an intense African dust event in Southern Spain // Environmental science & technology. – 2013. – T. 47. – №. 8. – C. 3630-3638.

SanPiN 0293-11 dated 16.05.2011 “Hygienic Standards for Maximum Permissible Concentrations (MPC) of Pollutants in Ambient Air of Residential Areas in Uzbekistan.”

Sarybaev B. Flora and Vegetation of the Eastern Chink of Ustyurt. Tashkent: Fan, 1987. 88 p.

Savchenko, I. I., & Kozhakhmetov, A. A. (2017). Environmental pollution in the Aral region. KazNU Bulletin. Ecology Series, 2(54), 18–23.

Schulz M. et al. Atmospheric transport and deposition of mineral dust to the ocean: Implications for research needs // Environmental science & technology. – 2012. – T. 46. – №. 19. – C. 10390-10404.

Scientific-Applied Reference Book on the Climate of the USSR. Series 3. Long-Term Data. Parts 1–6. Issue 19. Uzbek SSR*. Leningrad: Gidrometeoizdat, 1989.

Semenov O.E., Tulina L.P., Chichasov G.N. On Climate Change and Ecological Conditions in the Aral Sea Region. In: Monitoring of the Natural Environment in the Aral Sea Basin (Development Challenges). St. Petersburg: Gidrometeoizdat, 1991. Pp. 150–176.

Shafiee M. et al. A readout system for microwave kinetic inductance detectors using software defined radios // Journal of Instrumentation. – 2021. – T. 16. – №. 7. – C. P07015.

Shao Y. et al. Dust cycle: An emerging core theme in Earth system science // Aeolian Research. – 2011. – T. 2. – №. 4. – C. 181-204.

Shao, Y. and C. H. Dong, 2006: A review on East Asian dust storm climate, modelling and monitoring. Glob al Planet. Change, 52, 1-22, doi: 10.1016/j.glopla cha.2006.02.011.

Shardakova L.Yu., Usmanova L.V. Analysis of Dust Storms in the Aral Sea Region. Problemy Osvoeniya Pustyn. 2006. No. 3. Pp. 30–34.

Sherimbetov S.G. Halophytic Vegetation of the Desiccated Aral Seabed and Its Role in Forming Biodiversity. Vestnik Gulistanskogo Gosudarstvennogo Universiteta. 2015. No. 3(58). Pp. 29–32.

Shi L. et al. Temporal variation of dust emissions in dust sources over Central Asia in recent decades and the climate linkages //Atmospheric Environment. – 2020. – T. 222. – C. 117176.

Shomurodov Kh.F., Adilov B.A. Current State of Vegetation on Vozrozhdeniya Island (Uzbekistan). Aridnye Ekosistemy. 2019. Vol. 25. No. 2(79). Pp. 27–34.

Shomurodov Kh.F., Saribaeva Sh.U., Akhmedov A. Distribution and Current Status of Rare Plant Species on the Ustyurt Plateau in Uzbekistan. Aridnye Ekosistemy. Otraslevye Problemy Osvoeniya Zasushlivykh Zemel. 2015. Vol.

21. No. 4(65). Pp. 75–83.

Singh R. P. et al. Enhancement of oceanic parameters associated with dust storms using satellite data //Journal of Geophysical Research: Oceans. – 2008. – T. 113. – №. C11, – C. 1-13.

Sorek-Hamer M. et al. Classification of dust days by satellite remotely sensed aerosol products //International journal of remote sensing. – 2013. – T. 34. – №. 8. – C. 2672-2688.

Spivak, L., Terechov, A., Vitkovskaya, I., Batyrbayera, M., & Orlovsky, L. (2012). Dynamics of dust transfer from the desiccated Aral Sea bottom analysed by remote sensing. In: Breckle, S.-W., Wucherer, W., Dimeyeva, L. A., & Ogar, N. P. (Eds.). Aralkum—a Man-Made Desert: The Desiccated Floor of the Aral Sea (Central Asia), Ecological Studies. Berlin: Springer, 218:97–106.

Subbotina O.I., Chanysheva S.G. Climate of the Aral Sea Region. Tashkent: NIGMI, 2006. 172 p.

Tao Z. et al. Microphysics and radiation effect of dust on Saharan air layer: An HS3 case study //Monthly Weather Review. – 2018. – T. 146. – №. 6. – C. 1813-1835.

Tleumuratova B.S. et al. Thermal Effect of Desertification in the Southern Aral Sea Region: A Collective Monograph / Ed. by B.S. Tleumuratova. Nukus, 2024. 244 p.

Tleumuratova B.S. Mathematical Modeling of Aerosol Transport in the Lower Atmosphere. Diss. ... Candidate of Physical-Mathematical Sciences. Tashkent, 2004. 138 p.

Tleumuratova B.S. Mathematical Modeling of Salt Emission from the Desiccated Aral Seabed During Dust Storms. Obedinennyi Nauchnyi Zhurnal. Moscow, 2002. No. 28(51). Pp. 40–42.

Tleumuratova B.S. Mathematical Modeling of the Impact of Ecosystem Transformations in the Southern Aral Sea Region on Soil-Climatic Conditions. Diss. ... Doctor of Physical-Mathematical Sciences. Tashkent, 2018. 209 p.

Tleumuratova B.S., Kubanov Zh.Zh. Modeling the Role of Vegetation in Reducing Wind-Driven Salt Emission on the Desiccated Aral Seabed. Proceedings of the III International Scientific-Practical Online Conference “Melioration as a Driver of Agricultural Modernization Under Climate Change”. Novocherkassk, 26–28 April 2022. Pp. 308–310.

Tleumuratova B.S., Mustafaeva R., Ollambergenov F.F. Synergetic Analysis of Biota Dynamics in the Southern Aral Sea Region. Vestnik KKO AN RU. 2020. No. 1. Pp. 10–16.

Tleumuratova, B. S., Erzhanova, L. K., Urumbaev, A. E., & Shermukhamedov, U. A. (2021). Kolichestvennaya otsenka zagryazneniya atmosfery promyshlennymi vybrosami Takhiatashskoy TETs [Quantitative assessment of air pollution from industrial emissions of the Takhiatash TPP]. Vestnik Karakalpakskogo otdeleniya AN RUz, (2), 94–98.

Tleumuratova, B. S., Shermukhamedov, U. A., & Utepbergenova, G. Kh. (2020). O monitoringe zagryazneniya atmosfery [On atmospheric pollution monitoring]. Vestnik Karakalpakskogo otdeleniya AN RUz, (3), 99–106.

Twohy C. H. et al. Saharan dust particles nucleate droplets in eastern Atlantic clouds // Geophysical Research Letters. – 2009. – T. 36. – №. 1. – C.1-6.

U.S. Geological Survey. (n.d.). Landsat 8 imagery via EarthExplorer [Satellite imagery]. U.S. Department of the Interior. https://earthexplorer.usgs.gov/

UNDP. (2012). The Aral Sea Crisis and Human Health. United Nations Development Programme.

United Nations Economic Commission for Europe (UNECE). (2004). Environmental Performance Reviews: Uzbekistan. United Nations Publications. https://unece.org/environmental-performance-review-uzbekistan-2004

Urazimbetova E.P. Modeling Atmospheric Dust Load in Karakalpakstan from the Kyzylkum Desert. Ekonomika i Sotsium. 2024. No. 4-1(119). Pp. 1126–1131. (b)

Urazimbetova E.P. Statistical Analysis of Long-Term Atmospheric Pollution Dynamics in Karakalpakstan. Diss. ... Doctor of Philosophy (PhD) in Technical Sciences. Nukus, 2024. 102 p. (a)

Urazimbetova E.P., Tleumuratova B.S. Quantitative Assessment of Atmospheric Dust Load in the Lower Amu Darya Oasis from Desert Surfaces. Doklady AN RUz. Tashkent, 2024. No. 4. Pp. 96–101.

Venkatram A. Estimating the Monin-Obukhov length in the stable boundary layer for dispersion calculations // Boundary-Layer Meteorology. – 1980. – T. 19. – №. 4. – C. 481-485.

Wang C. H., Chen C. S., Lin C. L. The threat of Asian dust storms on asthma patients: a population-based study in Taiwan // Global public health. – 2014. – T. 9. – №. 9. – C. 1040-1052.

Wang, W., Samat, A., Abuduwaili, J., Ge, Y., De Maeyer, P., & Van de Voorde, T. (2022). Temporal characterization of sand and dust storm activity and its climatic and terrestrial drivers in the Aral Sea region. Atmospheric Research, 275, 106242. https://doi.org/10.1016/j.atmosres.2022.106242

Wang, Y., Liu, J., Lin, C., Ma, X. F., Song, Z. Z., Chen, Z. H., ... & Qi, C. Q. (2022). Polyvinyl acetate-based soil stabilization for rock slope ecological restoration. Journal of Environmental Management, 324, 116209.

Webb N. P., Strong C. L. Soil erodibility dynamics and its representation for wind erosion and dust emission models // Aeolian Research. – 2011. – T. 3. – №. 2. – C. 165-179.

Wiggs GFS, O’Hara S, Wegerdt J, Van Der Meer J, Small I, Hubbard R (2003) The dynamics and characteristics of aeolian dust in dryland Central Asia: possible impacts on human exposure and respiratory health in the Aral Sea basin. Geogr J 169:142–157

Wikipedia contributors. (n.d.). Snizhenie urovnia Aral’skogo moria [Decrease in the Aral Sea level]. Wikipedia. Retrieved May 28, 2025, from https://ru.wikipedia.org/wiki/Снижение_уровня_Аральского_моря

Wu C., Lin Z., Liu X. The global dust cycle and uncertainty in CMIP5 (Coupled Model Intercomparison Project phase 5) models // Atmospheric Chemistry and Physics. – 2020. – T. 20. – №. 17. – C. 10401-10425.

Wu X. et al. Aerosol optical absorption coefficients at a rural site in Northwest China: The great contribution of dust particles // Atmospheric Environment. – 2018. – T. 189. – C. 145-152.

Wu Y. et al. Sand and dust storms in Asia: a call for global cooperation on climate change // The Lancet Planetary Health. – 2021. – T. 5. – №. 6. – C. e329-e330.

Yaping Shao. Physics and Modelling of Wind Erosion. Dordrecht, Hardbound: Kluwer Academic Publishers, 2000. – 408c.

Zhollybekov M.B., Tleumuratova B.S., Urazimbetova E.P. Changes in Soil Chemical Composition During Gas Field Development in the Southwestern Desiccated Aral Seabed. Vestnik KKO AN RUz. Nukus, 2023. No. 1. Pp. 68–71.

Zobeck T. M. Soil properties affecting wind erosion // Journal of Soil and water conservation. – 1991. – T. 46. – №. 2. – C. 112-118.

Appendix 1: List of abbreviations

AI	–	Aerosol Index
SE	–	Salt Emission from the Desiccated Aral Seabed (SEDAS)
WDST		Wind-Driven Salt Transport
ERS	–	Remote Sensing of the Earth
ADL	–	Atmospheric Dust Load
LTI	–	Long-Term Impact Model
MYADLD	–	Multi-Year Atmospheric Dust Load Dynamics
MS	–	Meteorological Station
LADO	–	Lower Amu Darya Oasis
DASB	–	Desiccated Aral Sea Bed
TPC	–	Total Projective Cover
MPC	–	Maximum Permissible Concentration
PAL	–	Post-Aquatic Land
DS		Dust Storm
VC	–	Vegetation Cover
SASR	–	Southern Aral Sea Region

Appendix 2. FOREST PLANTATION MAP

Scheme

Volumes of completed works "Fall 2019 - spring 2020"

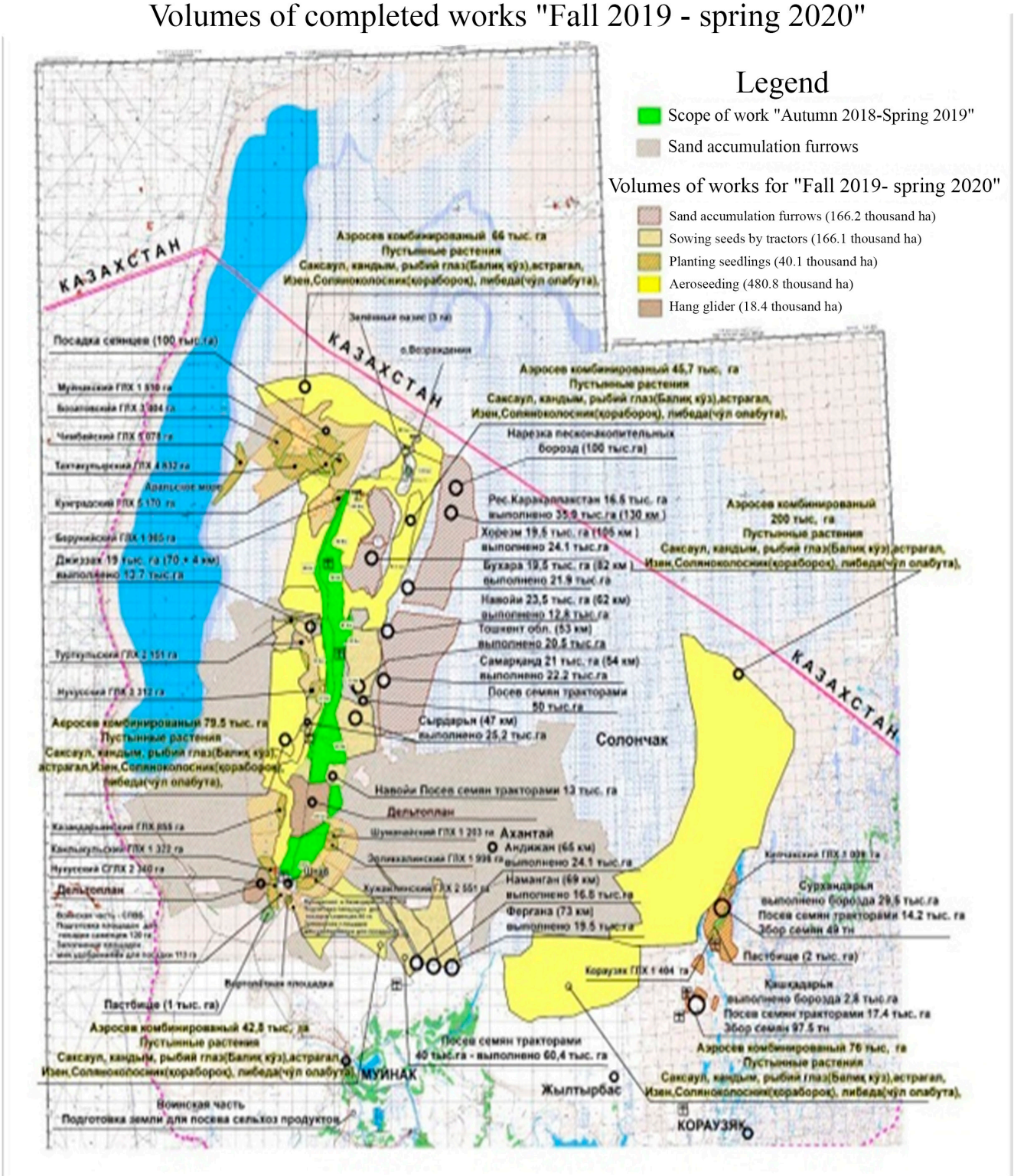

Appendix 3: MYADL Model Implementation Program

This appendix presents the source code for the implementation of the MYADL (Multi-Year Atmospheric Dust Load) model. The program calculates the annual dust load (ADL) based on long-term meteorological and environmental input data such as wind speed, surface salinity, and vegetation cover. The code is written in C++ and intended for research and educational purposes. Users should input the necessary parameters as prompted in the console interface to simulate ADL dynamics for specific years and regions.

```
#include <iostream>
#include <cmath>
#include<conio.h>
#include<iomanip>
using namespace std;
int main(int argc, char** argv) {
   setlocale(LC_ALL,"Russian");
   const int m=14,n=6;
 float OP=1;
 float d=10*pow(10,-6); //Диаметр частиц (мкм)
 float rod=2.65*pow(10,6); //Плотность частиц  (г/м3)
 float pd=2500000;     //Давление деформации(Н/м2)
 float calfa=5; //Коэффициент первого порядка
 float fd=0.2; // Общая объемная доля пыли в осадке (%)
 float pb=1000000; // отношение плотности частиц к воздуху (кг/м3)
 float CHh=0.023;
 float z=0.002;
 float AK_x[m];
 float AK_t[]={9.5349,15.4619,17.0357,16.3899,14.9933,13.7579}; //Температура воздуха (С)
  float AK_p[]={1015.8207,1014.5164,1016.0045,1017.3432,1018.0075,1018.7252}; //  Атмосферное давление (гПа)
 float AK_u[]={5.1867,4.2593,3.6419,3.5715,3.9083,4.4237}; //Скорость ветра (м/с)
  float AK_Te[]={12.559,16.571,9.624,7.675,10.625,12.219}; // продолжительность энергоактивных скоростей ветра
 float AK_Sp[]={9.9,19.9,30.7,43.6,54.7,62.1}; // Динамика площади пустынь
 float AK_OPP[]={0.7255,0.5795,0.4775,0.3285,0.0405,0.001}; //ОПП
  float AK_WR_1[]={2.5421,6.603,4.2861,5.0774,5.1525,4.1406}; // СВ
 float AK_WR_2[]={6.4878,4.415,4.5966,5.7846,7.079,7.5918}; // С
 float AK_WR_3[]={1.2512,2.1162,0.9916,1.0934,1.272,1.6642}; // СЗ
 float AK_Vp[n];// Вынос пустынного аэрозоля
 float AK_V_T[n];// вынос пустынного аэрозоля со всей площади
 float AK_dV[n]; //уменьшение выноса пустынного аэрозоля с единицы площади растительным слоем с ОПП
 float AK_dF[n];// уменьшения мощности пылеиспускания
 float AK_ur[n]; // степени ослабления ветра растительным покровом
 float AK_ro[n];     //плотность воздуха (г/м3)
 float AK_uua[n],AK_uur[n]; //скорость трения (м/с)
 float AK_wg[n]; //Скорость гравитационного осаждения примеси (м/с)
 float AK_ca[n],AK_cr[n];  //Коэффициент Оуэна
 float AK_ukr[n]; //Критическая скорость трения (м/с)
 float AK_Fua[n],AK_Fur[n]; //Мощность источника (г/м2с)
  float AK_Qa[n],AK_Qr[n]; //Расход примеси (г/м·с)
  float AK_koef=10*pow(10,-6); //коэффициент соразмерности
 float AK_Con[m][n],AK_Con1[m][n],AK_Con2[m][n],AK_Con3[m][n],AK_CH[n];
  float AK_myu[n]; //динамическая вязкость воздуха
 float AK_v[n];// кинематическая вязкость воздуха (м2/с)
 int i,j;
 cout<<endl;
 cout<<"                    Аралкум                    "<<endl;
 cout<<"  X  \t|  \t1  \t|  \t2 \t|  \tÇ \t|  \t4 \t|  \t5 \t|  \t6 \t|"<<endl;
AK_x[0]=0;AK_Con[0][0]=0;
for(i=0;i<m;i++)
{
    for(j=0;j<n;j++){
```

```
                AK_ro[j]=2900*AK_p[j]/(8.314*(273+AK_t[j]));
                AK_myu[j]=1717*pow(10,-5)*pow(((273+AK_t[j])/273),0.683);
                AK_v[j]=AK_myu[j]/AK_ro[j];
AK_wg[j]=2*9.8*d*d*(rod/AK_ro[j]-1)/(9*AK_v[j]);
AK_ukr[j]=sqrt(0.0123*(rod*9.8*d/AK_ro[j]+0.3/(AK_ro[j]*d)));
AK_ur[j]=0.83*OP*pow(CHh,(1./2))*AK_u[j]+(1-OP)*AK_u[j];
AK_uua[j]=0.04*(AK_u[j]-10)+AK_ukr[j];
AK_uur[j]=0.04*(AK_ur[j]-10)+AK_ukr[j];
AK_ca[j]=0.25+0.33*AK_wg[j]/AK_uua[j];
AK_cr[j]=0.25+0.33*AK_wg[j]/AK_uur[j];
AK_Qa[j]=AK_ca[j]*AK_ro[j]*pow(AK_uua[j],3)*abs(1-pow((AK_ukr[j]/AK_uua[j]),2))/9.8;
AK_Qr[j]=AK_cr[j]*AK_ro[j]*pow(AK_uur[j],3)*abs(1-pow((AK_ukr[j]/AK_uur[j]),2))/9.8;
AK_Fua[j]=0.12*9.8*calfa*fd*pb*AK_Qa[j]/pd;
AK_Fur[j]=0.12*9.8*calfa*fd*pb*AK_Qr[j]/pd;
AK_dF[j]=abs(AK_Fua[j]-AK_Fur[j]);
AK_dV[j]=AK_dF[j]*(AK_Te[j]/365)*AK_Sp[j]*pow(10,5);
AK_Vp[j]=AK_Fur[j]*(AK_Te[j]/365);
AK_V_T[j]=AK_Vp[j]*AK_Sp[j]*pow(10,5);
AK_CH[j]=3.3*AK_koef*(AK_V_T[j]-AK_dV[j]);
AK_Con1[i][j]=AK_WR_1[j]*AK_CH[j]*exp(-0.015*AK_x[i]-0.6-0.3*z);
AK_Con2[i][j]=AK_WR_2[j]*AK_CH[j]*exp(-0.015*AK_x[i]-0.6-0.3*z);
AK_Con3[i][j]=AK_WR_3[j]*AK_CH[j]*exp(-0.015*AK_x[i]-0.6-0.3*z);
                        }
    AK_x[i+1]=AK_x[i]+25;
    }
    for(int i=0;i<m;i++) {
    cout<<setprecision(1)<<setiosflags(ios::fixed|ios::showpoint)<<AK_x[i]<<" \t| ";
   for(int j=0;j<n;j++){
    AK_Con[i][j]=AK_Con1[i][j]+AK_Con2[i][j]+AK_Con3[i][j];
       cout <<setprecision(3)<<setiosflags(ios::fixed|ios::showpoint)<<AK_Con[i][j]<<" \t| ";
                }
                cout<<endl;

    }
     float US_x[m];
float US_t[]={11.4,17.8,17.2,15.5,15,16.3}; //Температура воздуха (°C)
float US_p[]={1015.7,1015.2,1016.3,1017.1,1017.2,1016.4}; //  Атмосферное давление (гПа)
float US_u[]={4.3,3.1,3.3,3.9,4.5,4.9}; //Скорость ветра (м/с)
float US_Te[]={14.41,8.32,11.64,15.44,16.86,16.55}; // продолжительность энергоактивных скоростей ветра
float US_Sp[]={196.1,196.8,197.7,198.2,199.4,200}; // Динамика площади пустынь
float US_OPP[]={0.7,0.7,0.6,0.5,0.5,0.4}; //ОПП
 float US_WR_1[]={3,4.7,2.7,3,3.5,4.1}; // З
float US_WR_2[]={4.4,2.4,0.8,1.9,2.2,2.1}; // СЗ
float US_Vp[n];// Вынос пустынного аэрозоля
float US_V_T[n];// вынос пустынного аэрозоля со всей площади
float US_dV[n]; //уменьшение выноса пустынного аэрозоля с единицы площади растительным слоем с ОПП
float US_dF[n];// уменьшения мощности пылеиспускания
float US_ur[n]; // степени ослабления ветра растительным покровом
float US_ro[n];     //плотность воздуха (г/м3)
float US_uua[n],US_uur[n]; //скорость трения (м/с)
float US_wg[n]; //Скорость гравитационного осаждения примеси (м/с)
float US_ca[n],US_cr[n];  //Коэффициент Оуэна
float US_ukr[n]; //Критическая скорость трения (м/с)
float US_Fua[n],US_Fur[n]; //Мощность источника (г/м2с)
 float US_Qa[n],US_Qr[n]; //Расход примеси (г/м·с)
 float US_koef=2*pow(10,-6); //коэффициент соразмерности
float US_Con[m][n],US_Con1[m][n],US_Con2[m][n],US_CH[n];
 float US_myu[n]; //динамическая вязкость воздуха
float US_v[n];// кинематическая вязкость воздуха (м2/с)
   cout<<endl;
cout<<"                    Устюрт                    "<<endl;
```

```
 cout<<"  X  \t|  \t1  \t|  \t2 \t|  \tÇ \t|  \t4 \t|  \t5 \t|  \t6 \t|"<<endl;
US_x[0]=0;
US_Con[0][0]=0;
for(i=0;i<m;i++)
{
    for(j=0;j<n;j++){
                US_ro[j]=2900*US_p[j]/(8.314*(273+US_t[j]));
                US_myu[j]=1717*pow(10,-5)*pow(((273+US_t[j])/273),0.683);
                US_v[j]=US_myu[j]/US_ro[j];
US_wg[j]=2*9.8*d*d*(rod/US_ro[j]-1)/(9*US_v[j]);
US_ukr[j]=sqrt(0.0123*(rod*9.8*d/US_ro[j]+0.3/(US_ro[j]*d)));
US_ur[j]=0.83*OP*pow(CHh,(1./2))*US_u[j]+(1-OP)*US_u[j];
US_uua[j]=0.04*(US_u[j]-10)+US_ukr[j];
US_uur[j]=0.04*(US_ur[j]-10)+US_ukr[j];
US_ca[j]=0.25+0.33*US_wg[j]/US_uua[j];
US_cr[j]=0.25+0.33*US_wg[j]/US_uur[j];
US_Qa[j]=US_ca[j]*US_ro[j]*pow(US_uua[j],3)*abs(1-pow((US_ukr[j]/US_uua[j]),2))/9.8;
US_Qr[j]=US_cr[j]*US_ro[j]*pow(US_uur[j],3)*abs(1-pow((US_ukr[j]/US_uur[j]),2))/9.8;
US_Fua[j]=0.12*9.8*calfa*fd*pb*US_Qa[j]/pd;
US_Fur[j]=0.12*9.8*calfa*fd*pb*US_Qr[j]/pd;
US_dF[j]=abs(US_Fua[j]-US_Fur[j]);
US_dV[j]=US_dF[j]*(US_Te[j]/365)*US_Sp[j]*pow(10,5);
US_Vp[j]=US_Fur[j]*(US_Te[j]/365);
US_V_T[j]=US_Vp[j]*US_Sp[j]*pow(10,5);
US_CH[j]=3.3*US_koef*(US_V_T[j]-US_dV[j]);
US_Con1[i][j]=US_WR_1[j]*US_CH[j]*exp(-0.015*US_x[i]-0.6-0.3*z);
US_Con2[i][j]=US_WR_2[j]*US_CH[j]*exp(-0.015*US_x[i]-0.6-0.3*z);
                        }
    US_x[i+1]=US_x[i]+25;
    }
    for(int i=0;i<m;i++) {
                cout<<setprecision(1)<<setiosflags(ios::fixed|ios::showpoint)<<US_x[i]<<" \t| ";
   for(int j=0;j<n;j++){
    US_Con[i][j]=US_Con1[i][j]+US_Con2[i][j];
        cout <<setprecision(3)<<setiosflags(ios::fixed|ios::showpoint) <<US_Con[i][j]<<" \t| ";
                }
                cout<<endl;

    }
     float KZ_x[m];
     float KZ_t[]={17,15.5,15.2,14,14.3,16.1}; //Температура воздуха (°C)
 float KZ_p[]={1016,1020.8,1019.4,1016.8,1017.2,1017.4}; //  Атмосферное давление (гПа)
 float KZ_u[]={2.6,2.7,2.5,2.8,3.6,5.1}; //Скорость ветра (м/с)
 float KZ_Te[]={7.16,7.65,7.7,7.99,7.27,6.33}; // продолжительность энергоактивных скоростей ветра
 float KZ_Sp[]={295.9,296.7,297.5,298.3,299.1,300}; // Динамика площади пустынь
 float KZ_OPP[]={0.6,0.5,0.5,0.4,0.4,0.3}; //ОПП
  float KZ_WR_1[]={3.2,3.1,5.3,4,2.6,1.6}; // СВ
 float KZ_WR_2[]={5,4,5.9,3.9,4.5,7.3}; // В
 float KZ_WR_3[]={4.3,4.3,3.2,1.8,3.1,5.4}; // ЮВ
 float KZ_Vp[n];// Вынос пустынного аэрозоля
 float KZ_V_T[n];// вынос пустынного аэрозоля со всей площади
 float KZ_dV[n]; //уменьшение выноса пустынного аэрозоля с единицы площади растительным слоем с ОПП
 float KZ_dF[n];// уменьшения мощности пылеиспускания
 float KZ_ur[n]; // степени ослабления ветра растительным покровом
 float KZ_ro[n];     //плотность воздуха (г/м3)
 float KZ_uua[n],KZ_uur[n]; //скорость трения (м/с)
 float KZ_wg[n]; //Скорость гравитационного осаждения примеси (м/с)
 float KZ_ca[n],KZ_cr[n];  //Коэффициент Оуэна
 float KZ_ukr[n]; //Критическая скорость трения (м/с)
 float KZ_Fua[n],KZ_Fur[n]; //Мощность источника (г/м2с)
  float KZ_Qa[n],KZ_Qr[n]; //Расход примеси (г/м·с)
```

```
 float KZ_koef=7*pow(10,-6); //коэффициент соразмерности
 float KZ_Con[m][n],KZ_Con1[m][n],KZ_Con2[m][n],KZ_Con3[m][n],KZ_CH[n];
  float KZ_myu[n]; //динамическая вязкость воздуха
 float KZ_v[n];// кинематическая вязкость воздуха (м2/с)
 cout<<endl;
 cout<<"                    Кызылкум                    "<<endl;
 cout<<"  X  \t|  \t1  \t|  \t2 \t|  \tÇ \t|  \t4 \t|  \t5 \t|  \t6 \t|"<<endl;
KZ_x[0]=0;KZ_Con[0][0]=0;
for(i=0;i<m;i++)
{
    for(j=0;j<n;j++){
              KZ_ro[j]=2900*KZ_p[j]/(8.314*(273+KZ_t[j]));
              KZ_myu[j]=1717*pow(10,-5)*pow(((273+KZ_t[j])/273),0.683);
              KZ_v[j]=KZ_myu[j]/KZ_ro[j];
KZ_wg[j]=2*9.8*d*d*(rod/KZ_ro[j]-1)/(9*KZ_v[j]);
KZ_ukr[j]=sqrt(0.0123*(rod*9.8*d/KZ_ro[j]+0.3/(KZ_ro[j]*d)));
KZ_ur[j]=0.83*OP*pow(CHh,(1./2))*KZ_u[j]+(1-OP)*KZ_u[j];
KZ_uua[j]=0.04*(KZ_u[j]-10)+KZ_ukr[j];
KZ_uur[j]=0.04*(KZ_ur[j]-10)+KZ_ukr[j];
KZ_ca[j]=0.25+0.33*KZ_wg[j]/KZ_uua[j];
KZ_cr[j]=0.25+0.33*KZ_wg[j]/KZ_uur[j];
KZ_Qa[j]=KZ_ca[j]*KZ_ro[j]*pow(KZ_uua[j],3)*abs(1-pow((KZ_ukr[j]/KZ_uua[j]),2))/9.8;
KZ_Qr[j]=KZ_cr[j]*KZ_ro[j]*pow(KZ_uur[j],3)*abs(1-pow((KZ_ukr[j]/KZ_uur[j]),2))/9.8;
KZ_Fua[j]=0.12*9.8*calfa*fd*pb*KZ_Qa[j]/pd;
KZ_Fur[j]=0.12*9.8*calfa*fd*pb*KZ_Qr[j]/pd;
KZ_dF[j]=abs(KZ_Fua[j]-KZ_Fur[j]);
KZ_dV[j]=KZ_dF[j]*(KZ_Te[j]/365)*KZ_Sp[j]*pow(10,5);
KZ_Vp[j]=KZ_Fur[j]*(KZ_Te[j]/365);
KZ_V_T[j]=KZ_Vp[j]*KZ_Sp[j]*pow(10,5);
KZ_CH[j]=3.3*KZ_koef*(KZ_V_T[j]-KZ_dV[j]);
KZ_Con1[i][j]=KZ_WR_1[j]*KZ_CH[j]*exp(-0.015*KZ_x[i]-0.6-0.3*z);
KZ_Con2[i][j]=KZ_WR_2[j]*KZ_CH[j]*exp(-0.015*KZ_x[i]-0.6-0.3*z);
KZ_Con3[i][j]=KZ_WR_3[j]*KZ_CH[j]*exp(-0.015*KZ_x[i]-0.6-0.3*z);
                        }
    KZ_x[i+1]=KZ_x[i]+25;
    }
    for(int i=0;i<m;i++) {
    cout<<setprecision(1)<<setiosflags(ios::fixed|ios::showpoint)<<KZ_x[i]<<" \t| ";
   for(int j=0;j<n;j++){
    KZ_Con[i][j]=KZ_Con1[i][j]+KZ_Con2[i][j]+KZ_Con3[i][j];
       cout <<setprecision(3)<<setiosflags(ios::fixed|ios::showpoint)<<KZ_Con[i][j]<<" \t| ";
              }
              cout<<endl;

    }
     float KR_x[m];
     float KR_t[]={16.4,15.1,14.9,14.8,15.7,18.1}; //Температура воздуха (°C)
 float KR_p[]={1015.7,1020.2,1017.8,1016.5,1017,1016.7}; //  Атмосферное давление (гПа)
 float KR_u[]={3.6,4,3.1,2.9,3.2,3.3}; //Скорость ветра (м/с)
 float KR_Te[]={12.6,16.6,9.6,7.7,10.6,12.2}; // продолжительность энергоактивных скоростей ветра
 float KR_Sp[]={347.1,347.8,348.4,348.9,349.5,350}; // Динамика площади пустынь
 float KR_OPP[]={0.4,0.4,0.3,0.3,0.3,0.3}; //ОПП
  float KR_WR_1[]={5,2.2,1.8,1.4,2.9,4.9}; // Ю
 float KR_WR_2[]={2.1,0.4,0.1,0.7,1,1.7}; // ЮЗ
 float KR_Vp[n];// Вынос пустынного аэрозоля
 float KR_V_T[n];// вынос пустынного аэрозоля со всей площади
 float KR_dV[n]; //уменьшение выноса пустынного аэрозоля с единицы площади растительным слоем с ОПП
 float KR_dF[n];// уменьшения мощности пылеиспускания
 float KR_ur[n]; // степени ослабления ветра растительным покровом
 float KR_ro[n];     //плотность воздуха (г/м3)
 float KR_uua[n],KR_uur[n]; //скорость трения (м/с)
```

```
 float KR_wg[n]; //Скорость гравитационного осаждения примеси (м/с)
 float KR_ca[n],KR_cr[n];  //Коэффициент Оуэна
 float KR_ukr[n]; //Критическая скорость трения (м/с)
 float KR_Fua[n],KR_Fur[n]; //Мощность источника (г/м2с)
  float KR_Qa[n],KR_Qr[n]; //Расход примеси (г/м·с)
  float KR_koef=4*pow(10,-6); //коэффициент соразмерности
 float KR_Con[m][n],KR_Con1[m][n],KR_Con2[m][n],KR_CH[n];
  float KR_myu[n]; //динамическая вязкость воздуха
 float KR_v[n];// кинематическая вязкость воздуха (м2/с)
 cout<<endl;
 cout<<"                    Каракумы                    "<<endl;
 cout<<"  X  \t|  \t1  \t|  \t2 \t|  \tÇ \t|  \t4 \t|  \t5 \t|  \t6 \t|"<<endl;
KR_x[0]=0;KR_Con[0][0]=0;
for(i=0;i<m;i++)
{
    for(j=0;j<n;j++){
                KR_ro[j]=2900*KR_p[j]/(8.314*(273+KR_t[j]));
                KR_myu[j]=1717*pow(10,-5)*pow(((273+KR_t[j])/273),0.683);
                KR_v[j]=KR_myu[j]/KR_ro[j];
KR_wg[j]=2*9.8*d*d*(rod/KR_ro[j]-1)/(9*KR_v[j]);
KR_ukr[j]=sqrt(0.0123*(rod*9.8*d/KR_ro[j]+0.3/(KR_ro[j]*d)));
KR_ur[j]=0.83*OP*pow(CHh,(1./2))*KR_u[j]+(1-OP)*KR_u[j];
KR_uua[j]=0.04*(KR_u[j]-10)+KR_ukr[j];
KR_uur[j]=0.04*(KR_ur[j]-10)+KR_ukr[j];
KR_ca[j]=0.25+0.33*KR_wg[j]/KR_uua[j];
KR_cr[j]=0.25+0.33*KR_wg[j]/KR_uur[j];
KR_Qa[j]=KR_ca[j]*KR_ro[j]*pow(KR_uua[j],3)*abs(1-pow((KR_ukr[j]/KR_uua[j]),2))/9.8;
KR_Qr[j]=KR_cr[j]*KR_ro[j]*pow(KR_uur[j],3)*abs(1-pow((KR_ukr[j]/KR_uur[j]),2))/9.8;
KR_Fua[j]=0.12*9.8*calfa*fd*pb*KR_Qa[j]/pd;
KR_Fur[j]=0.12*9.8*calfa*fd*pb*KR_Qr[j]/pd;
KR_dF[j]=abs(KR_Fua[j]-KR_Fur[j]);
KR_dV[j]=KR_dF[j]*(KR_Te[j]/365)*KR_Sp[j]*pow(10,5);
KR_Vp[j]=KR_Fur[j]*(KR_Te[j]/365);
KR_V_T[j]=KR_Vp[j]*KR_Sp[j]*pow(10,5);
KR_CH[j]=3.3*KR_koef*(KR_V_T[j]-KR_dV[j]);
KR_Con1[i][j]=KR_WR_1[j]*KR_CH[j]*exp(-0.015*KR_x[i]-0.6-0.3*z);
KR_Con2[i][j]=KR_WR_2[j]*KR_CH[j]*exp(-0.015*KR_x[i]-0.6-0.3*z);
                    }
    KR_x[i+1]=KR_x[i]+25;
    }
    for(int i=0;i<m;i++) {
cout<<setprecision(1)<<setiosflags(ios::fixed|ios::showpoint)<<KR_x[i]<<" \t| ";
   for(int j=0;j<n;j++){
    KR_Con[i][j]=KR_Con1[i][j]+KR_Con2[i][j];
       cout <<setprecision(3)<<setiosflags(ios::fixed|ios::showpoint)<<KR_Con[i][j]<<" \t| ";
                }
                cout<<endl;
                    }
    float C_109[n],C_134[n],C_159[n],C_184[n],C_209[n];
    float C_110[n],C_135[n],C_160[n],C_185[n],C_210[n],C_235[n];
    float C_111[n],C_136[n],C_161[n],C_186[n],C_211[n];
    float C_137[n],C_162[n],C_187[n],C_212[n],C_237[n];
    float C_138[n],C_163[n],C_188[n],C_213[n],C_238[n],C_263[n];
    float C_139[n],C_164[n],C_189[n],C_214[n],C_239[n];
    float C_115[n],C_140[n],C_165[n],C_190[n],C_215[n];
    float C_116[n],C_141[n],C_166[n],C_191[n],C_216[n],C_241[n];
    float C_117[n],C_142[n],C_167[n],C_192[n],C_217[n],C_242[n];
    float C_143[n],C_168[n],C_193[n],C_218[n],C_243[n],C_268[n],C_293[n],C_318[n],C_343[n];
    float C_144[n],C_169[n],C_194[n],C_219[n],C_244[n],C_269[n],C_294[n],C_319[n];
    float C_245[n],C_270[n],C_295[n],C_320[n];
    for (j=0;j<n;j++)
```

```
{
C_109[j]=AK_Con[0][j]+US_Con[0][j]+KZ_Con[4][j]+KR_Con[11][j];
C_134[j]=AK_Con[0][j]+US_Con[1][j]+KZ_Con[3][j]+KR_Con[11][j];
C_159[j]=AK_Con[0][j]+US_Con[2][j]+KZ_Con[2][j]+KR_Con[11][j];
C_184[j]=AK_Con[0][j]+US_Con[3][j]+KZ_Con[1][j]+KR_Con[11][j];
C_209[j]=AK_Con[0][j]+US_Con[4][j]+KZ_Con[0][j]+KR_Con[11][j];
C_110[j]=AK_Con[1][j]+US_Con[0][j]+KZ_Con[5][j]+KR_Con[10][j];
C_135[j]=AK_Con[1][j]+US_Con[1][j]+KZ_Con[4][j]+KR_Con[10][j];
C_160[j]=AK_Con[1][j]+US_Con[2][j]+KZ_Con[3][j]+KR_Con[10][j];
C_185[j]=AK_Con[1][j]+US_Con[3][j]+KZ_Con[2][j]+KR_Con[10][j];
C_210[j]=AK_Con[1][j]+US_Con[4][j]+KZ_Con[1][j]+KR_Con[10][j];
C_235[j]=AK_Con[1][j]+US_Con[5][j]+KZ_Con[0][j]+KR_Con[10][j];
C_111[j]=AK_Con[2][j]+US_Con[0][j]+KZ_Con[4][j]+KR_Con[9][j];
C_136[j]=AK_Con[2][j]+US_Con[1][j]+KZ_Con[3][j]+KR_Con[9][j];
C_161[j]=AK_Con[2][j]+US_Con[2][j]+KZ_Con[2][j]+KR_Con[9][j];
C_186[j]=AK_Con[2][j]+US_Con[3][j]+KZ_Con[1][j]+KR_Con[9][j];
C_211[j]=AK_Con[2][j]+US_Con[4][j]+KZ_Con[0][j]+KR_Con[9][j];
C_137[j]=AK_Con[3][j]+US_Con[1][j]+KZ_Con[4][j]+KR_Con[8][j];
C_162[j]=AK_Con[3][j]+US_Con[2][j]+KZ_Con[3][j]+KR_Con[8][j];
C_187[j]=AK_Con[3][j]+US_Con[3][j]+KZ_Con[2][j]+KR_Con[8][j];
C_212[j]=AK_Con[3][j]+US_Con[4][j]+KZ_Con[1][j]+KR_Con[8][j];
C_237[j]=AK_Con[3][j]+US_Con[5][j]+KZ_Con[0][j]+KR_Con[8][j];
C_138[j]=AK_Con[4][j]+US_Con[1][j]+KZ_Con[5][j]+KR_Con[7][j];
C_163[j]=AK_Con[4][j]+US_Con[2][j]+KZ_Con[4][j]+KR_Con[7][j];
C_188[j]=AK_Con[4][j]+US_Con[3][j]+KZ_Con[3][j]+KR_Con[7][j];
C_213[j]=AK_Con[4][j]+US_Con[4][j]+KZ_Con[2][j]+KR_Con[7][j];
C_238[j]=AK_Con[4][j]+US_Con[5][j]+KZ_Con[1][j]+KR_Con[7][j];
C_263[j]=AK_Con[4][j]+US_Con[6][j]+KZ_Con[0][j]+KR_Con[7][j];
C_139[j]=AK_Con[5][j]+US_Con[1][j]+KZ_Con[4][j]+KR_Con[6][j];
C_164[j]=AK_Con[5][j]+US_Con[2][j]+KZ_Con[3][j]+KR_Con[6][j];
C_189[j]=AK_Con[5][j]+US_Con[3][j]+KZ_Con[2][j]+KR_Con[6][j];
C_214[j]=AK_Con[5][j]+US_Con[4][j]+KZ_Con[1][j]+KR_Con[6][j];
C_239[j]=AK_Con[5][j]+US_Con[5][j]+KZ_Con[0][j]+KR_Con[6][j];
C_115[j]=AK_Con[6][j]+US_Con[0][j]+KZ_Con[4][j]+KR_Con[5][j];
C_140[j]=AK_Con[6][j]+US_Con[1][j]+KZ_Con[3][j]+KR_Con[5][j];
C_165[j]=AK_Con[6][j]+US_Con[2][j]+KZ_Con[2][j]+KR_Con[5][j];
C_190[j]=AK_Con[6][j]+US_Con[3][j]+KZ_Con[1][j]+KR_Con[5][j];
C_215[j]=AK_Con[6][j]+US_Con[4][j]+KZ_Con[0][j]+KR_Con[5][j];
C_116[j]=AK_Con[7][j]+US_Con[0][j]+KZ_Con[5][j]+KR_Con[4][j];
C_141[j]=AK_Con[7][j]+US_Con[1][j]+KZ_Con[4][j]+KR_Con[4][j];
C_166[j]=AK_Con[7][j]+US_Con[2][j]+KZ_Con[3][j]+KR_Con[4][j];
C_191[j]=AK_Con[7][j]+US_Con[3][j]+KZ_Con[2][j]+KR_Con[4][j];
C_216[j]=AK_Con[7][j]+US_Con[4][j]+KZ_Con[1][j]+KR_Con[4][j];
C_241[j]=AK_Con[7][j]+US_Con[5][j]+KZ_Con[0][j]+KR_Con[4][j];
C_117[j]=AK_Con[8][j]+US_Con[0][j]+KZ_Con[5][j]+KR_Con[3][j];
C_142[j]=AK_Con[8][j]+US_Con[1][j]+KZ_Con[4][j]+KR_Con[3][j];
C_167[j]=AK_Con[8][j]+US_Con[2][j]+KZ_Con[3][j]+KR_Con[3][j];
C_192[j]=AK_Con[8][j]+US_Con[3][j]+KZ_Con[2][j]+KR_Con[3][j];
C_217[j]=AK_Con[8][j]+US_Con[4][j]+KZ_Con[1][j]+KR_Con[3][j];
C_242[j]=AK_Con[8][j]+US_Con[5][j]+KZ_Con[0][j]+KR_Con[3][j];
C_143[j]=AK_Con[9][j]+US_Con[1][j]+KZ_Con[8][j]+KR_Con[2][j];
C_168[j]=AK_Con[9][j]+US_Con[2][j]+KZ_Con[7][j]+KR_Con[2][j];
C_193[j]=AK_Con[9][j]+US_Con[3][j]+KZ_Con[6][j]+KR_Con[2][j];
C_218[j]=AK_Con[9][j]+US_Con[4][j]+KZ_Con[5][j]+KR_Con[2][j];
C_243[j]=AK_Con[9][j]+US_Con[5][j]+KZ_Con[4][j]+KR_Con[2][j];
C_268[j]=AK_Con[9][j]+US_Con[6][j]+KZ_Con[3][j]+KR_Con[2][j];
C_293[j]=AK_Con[9][j]+US_Con[7][j]+KZ_Con[2][j]+KR_Con[2][j];
C_318[j]=AK_Con[9][j]+US_Con[8][j]+KZ_Con[1][j]+KR_Con[2][j];
C_343[j]=AK_Con[9][j]+US_Con[9][j]+KZ_Con[0][j]+KR_Con[2][j];
C_144[j]=AK_Con[10][j]+US_Con[1][j]+KZ_Con[7][j]+KR_Con[1][j];
```

```
            C_169[j]=AK_Con[10][j]+US_Con[2][j]+KZ_Con[6][j]+KR_Con[1][j];
            C_194[j]=AK_Con[10][j]+US_Con[3][j]+KZ_Con[5][j]+KR_Con[1][j];
            C_219[j]=AK_Con[10][j]+US_Con[4][j]+KZ_Con[4][j]+KR_Con[1][j];
            C_244[j]=AK_Con[10][j]+US_Con[5][j]+KZ_Con[3][j]+KR_Con[1][j];
            C_269[j]=AK_Con[10][j]+US_Con[6][j]+KZ_Con[2][j]+KR_Con[1][j];
            C_294[j]=AK_Con[10][j]+US_Con[7][j]+KZ_Con[1][j]+KR_Con[1][j];
            C_319[j]=AK_Con[10][j]+US_Con[8][j]+KZ_Con[0][j]+KR_Con[1][j];
            C_245[j]=AK_Con[11][j]+US_Con[5][j]+KZ_Con[3][j]+KR_Con[0][j];
            C_270[j]=AK_Con[11][j]+US_Con[6][j]+KZ_Con[2][j]+KR_Con[0][j];
            C_295[j]=AK_Con[11][j]+US_Con[7][j]+KZ_Con[1][j]+KR_Con[0][j];
            C_320[j]=AK_Con[11][j]+US_Con[8][j]+KZ_Con[0][j]+KR_Con[0][j];
        cout<<endl;
            cout<<endl;
            cout<<setprecision(8)<<setiosflags(ios::fixed|ios::showpoint)<<"\t|| "<<" j= "<<j<<" \t|| "<<endl;
            cout<<"|------------\t|------------\t|------------\t|------------\t|------------\t|"<<endl;
            cout<<"| "<<C_109[j]<<" \t| "<<C_134[j]<<" \t| "<<C_159[j]<<" \t| "<<C_184[j]<<" \t| "<<C_209[j]<<" \t| "<<endl;
            cout<<"|------------\t|------------\t|------------\t|------------\t|------------\t|------------\t|"<<endl;
            cout<<"|  "<<C_110[j]<<"  \t|  "<<C_135[j]<<"  \t|  "<<C_160[j]<<"  \t|  "<<C_185[j]<<"  \t|  "<<C_210[j]<<"  \t|
"<<C_235[j]<<" \t| "<<endl;
            cout<<"|------------\t|------------\t|------------\t|------------\t|------------\t|------------\t|"<<endl;
            cout<<"| "<<C_111[j]<<" \t| "<<C_136[j]<<" \t| "<<C_161[j]<<" \t| "<<C_186[j]<<" \t| "<<C_211[j]<<" \t| "<<endl;
            cout<<"|------------\t|------------\t|------------\t|------------\t|------------\t|------------\t|"<<endl;
            cout<<"|     "<<"      \t| "<<C_137[j]<<" \t| "<<C_162[j]<<" \t| "<<C_187[j]<<" \t| "<<C_212[j]<<" \t| "<<C_237[j]<<"
\t| "<<endl;
            cout<<"|------------\t|------------\t|------------\t|------------\t|------------\t|------------\t|"<<endl;
            cout<<"|     "<<"      \t| "<<C_138[j]<<" \t| "<<C_163[j]<<" \t| "<<C_188[j]<<" \t| "<<C_213[j]<<" \t| "<<C_238[j]<<"
\t| "<<C_263[j]<<" \t| "<<endl;
            cout<<"|------------\t|------------\t|------------\t|------------\t|------------\t|------------\t|"<<endl;
            cout<<"|     "<<"      \t| "<<C_139[j]<<" \t| "<<C_164[j]<<" \t| "<<C_189[j]<<" \t| "<<C_214[j]<<" \t| "<<C_239[j]<<"
\t| "<<endl;
            cout<<"|------------\t|------------\t|------------\t|------------\t|------------\t|------------\t|"<<endl;
            cout<<"| "<<C_115[j]<<" \t| "<<C_140[j]<<" \t| "<<C_165[j]<<" \t| "<<C_190[j]<<" \t| "<<C_215[j]<<" \t| "<<endl;
            cout<<"|------------\t|------------\t|------------\t|------------\t|------------\t|------------\t|"<<endl;
            cout<<"|  "<<C_116[j]<<"  \t|  "<<C_141[j]<<"  \t|  "<<C_166[j]<<"  \t|  "<<C_191[j]<<"  \t|  "<<C_216[j]<<"  \t|
"<<C_241[j]<<" \t| "<<endl;
            cout<<"|------------\t|------------\t|------------\t|------------\t|------------\t|------------\t|"<<endl;
            cout<<"|  "<<C_117[j]<<"  \t|  "<<C_142[j]<<"  \t|  "<<C_167[j]<<"  \t|  "<<C_192[j]<<"  \t|  "<<C_217[j]<<"  \t|
"<<C_242[j]<<" \t| "<<endl;
            cout<<"|------------\t|------------\t|------------\t|------------\t|------------\t|------------\t|------------\t|----
----------\t|------------\t|"<<endl;
            cout<<"|     "<<"      \t| "<<C_143[j]<<" \t| "<<C_168[j]<<" \t| "<<C_193[j]<<" \t| "<<C_218[j]<<" \t| "<<C_243[j]<<"
\t| "<<C_268[j]<<" \t| "<<C_293[j]<<" \t| "<<C_318[j]<<" \t| "<<C_343[j]<<" \t| "<<endl;
            cout<<"|------------\t|------------\t|------------\t|------------\t|------------\t|------------\t|------------\t|----
----------\t|------------\t|"<<endl;
            cout<<"|     "<<"      \t| "<<C_144[j]<<" \t| "<<C_169[j]<<" \t| "<<C_194[j]<<" \t| "<<C_219[j]<<" \t| "<<C_244[j]<<"
\t| "<<C_269[j]<<" \t| "<<C_294[j]<<" \t| "<<C_319[j]<<" \t| "<<endl;
            cout<<"|------------\t|------------\t|------------\t|------------\t|------------\t|------------\t|------------\t|----
----------\t|"<<endl;
            cout<<"|     "<<"      \t| "<<"          \t| "<<"          \t|    "<<"      \t|    "<<"      \t| "<<C_245[j]<<" \t| "<<C_270[j]<<"
\t| "<<C_295[j]<<" \t| "<<C_320[j]<<" \t| "<<endl;
            cout<<"|------------\t|------------\t|------------\t|------------\t|------------\t|------------\t|------------\t|----
----------\t|"<<endl;
                    }
    return 0;
    }
```

Appendix 4: Computer Model for Effectiveness Evaluation

This appendix presents the source code for the implementation of the MYADL (Multi-Year Atmospheric Dust Load) model. The program calculates the annual dust load (ADL) based on long-term meteorological and environmental input data such as wind speed, surface salinity, and vegetation cover. The code is written in C++ and intended for research and educational purposes. Users should input the necessary parameters as prompted in the console interface to simulate ADL dynamics for specific years and regions.

```
unit Unit1;

interface

uses
  Windows, Messages, SysUtils, Variants, Classes, Graphics, Controls, Forms,
  Dialogs, StdCtrls;

type
  TForm1 = class(TForm)
    lbl1: TLabel;
    btn1: TButton;
    edt1: TEdit;
    edt2: TEdit;
    lbl2: TLabel;
    lbl3: TLabel;
    edt3: TEdit;
    edt4: TEdit;
    lbl4: TLabel;
    edt5: TEdit;
    lbl5: TLabel;
    edt6: TEdit;
    edt7: TEdit;
    edt8: TEdit;
    lbl6: TLabel;
    lbl7: TLabel;
    lbl8: TLabel;
    lbl9: TLabel;
    edt9: TEdit;
    edt10: TEdit;
    lbl10: TLabel;
    lbl11: TLabel;
    lbl12: TLabel;
    Label1: TLabel;
    lbl13: TLabel;
    lbl14: TLabel;
    lbl15: TLabel;
    lbl16: TLabel;
    lbl17: TLabel;
    lbl18: TLabel;
    btn2: TButton;
    edt11: TEdit;
    lbl19: TLabel;
    lbl20: TLabel;
    lbl21: TLabel;
    edt12: TEdit;
    edt13: TEdit;
    lbl22: TLabel;
    lbl23: TLabel;
    edt14: TEdit;
    edt15: TEdit;
    lbl24: TLabel;
    edt16: TEdit;
```

```
    lbl25: TLabel;
    edt17: TEdit;
    lbl26: TLabel;
    edt18: TEdit;
    lbl27: TLabel;
    edt19: TEdit;
    lbl28: TLabel;
    edt20: TEdit;
    lbl29: TLabel;
    edt21: TEdit;
    lbl30: TLabel;
    edt22: TEdit;
    lbl31: TLabel;
    edt23: TEdit;
    lbl32: TLabel;
    edt24: TEdit;
    lbl33: TLabel;
    edt25: TEdit;
    lbl34: TLabel;
    edt26: TEdit;
    lbl35: TLabel;
    edt27: TEdit;
    lbl36: TLabel;
    edt28: TEdit;
    lbl37: TLabel;
    edt29: TEdit;
    lbl38: TLabel;
    lbl39: TLabel;
    lbl40: TLabel;
    lbl41: TLabel;
    lbl42: TLabel;
    lbl43: TLabel;
    procedure btn1Click(Sender: TObject);
    procedure btn2Click(Sender: TObject);
  private
    { Private declarations }
  public
    { Public declarations }
  end;

var
  Form1: TForm1;
B , B B , B B B , B B B B , B B B B B , B B B B B B , N , N N , N N N , N N N N , N N N N N , N N N N N N ,
Q,QQ,QQQ,QQQQ,QQQQQ,QQQQQQ,J,K,KK,KKK,KKKK,KKKKK,KKKKKK,KKKKKKK,  s,ss,  v,vv,vvv,vvvv,vvvvv,v-
vvvvv,vvvvvvv, p,pp,ppp,pppp,ppppp,pppppp, sol,god,des,t,tt,ttt,tttt,ttttt, tttttt,akv,osush,vs:real;
implementation

{$R *.dfm}

procedure TForm1.btn1Click(Sender: TObject);
begin
  god:=StrToFloat(Edt1.Text);
     t:=(god-1960);
     tt:=(god-1970);
      ttt:=(god-1980);
       tttt:=(god-1990);
        ttttt:=(god-2000);
         tttttt:=(god-2010);
 if t<=0 then akv:=0 else akv:=0.0003*t*t*t-0.0268*t*t-0.4531*t+66.799 ;
 if t<=0 then osush:=0 else osush:=68.9-akv;
 if t<=0 then sol:=0 else sol:=-0.0007*t*t+0.3394*t+1.12;
```

```
 if t<=0 then vs:=0 else vs:=0.0006*t*t*t-0.004*t*t+0.1481*t+0.1143;
  if sol<=0 then  Edt4.Text:=FloatToStr(0)  else  Edt4.Text:=FloatToStr(sol);
  if vs<=0 then Edt5.Text:=FloatToStr(0) else Edt5.Text:=FloatToStr(vs);
  if tt<=0 then Edt22.Text:=FloatToStr(0) else Edt22.Text:=FloatToStr(tt);
  if ttt<=0 then Edt23.Text:=FloatToStr(0) else Edt23.Text:=FloatToStr(ttt);
  if tttt<=0 then Edt16.Text:=FloatToStr(0) else Edt16.Text:=FloatToStr(tttt);
  if ttttt<=0 then Edt24.Text:=FloatToStr(0) else Edt24.Text:=FloatToStr(ttttt);
  if tttttt<=0 then Edt27.Text:=FloatToStr(0) else Edt27.Text:=FloatToStr(tttttt);
  Edt3.Text:=FloatToStr(osush);
  Edt2.Text:=FloatToStr(akv);
  Edt11.Text:=FloatToStr(t);

end;

procedure TForm1.btn2Click(Sender: TObject);
begin
   v:=StrToFloat(Edt6.Text);
  s:=StrToFloat(Edt7.Text);
  ss:=StrToFloat(Edt8.Text);
  if  Edt6.Text=' ' then Close;
  if  Edt7.Text=' ' then Close;
  if  Edt8.Text= ' ' then Close;
  if t<=0 then p:=0 else p:=0.00004*t*t*t - 0.005*t*t + 0.271*t + 64.819;
  if tt<=0 then pp:=0 else pp:=0.0002*tt*tt*tt - 0.0204*tt*tt + 0.7314*tt + 48.402;
  if ttt<=0 then ppp:=0 else ppp:=0.0002*ttt*ttt*ttt - 0.0196*ttt*ttt + 0.5731*ttt + 42.125;
  if tttt<=0 then pppp:=0 else pppp:=0.0021*tttt*tttt*tttt - 0.1309*tttt*tttt + 2.882*tttt + 1.6838;
  if ttttt<=0 then ppppp:=0 else ppppp:=0.0001*ttttt*ttttt*ttttt - 0.0042*ttttt*ttttt   + 0.1048*ttttt + 0.115;
 if tttttt<=0 then pppppp:=0 else pppppp:=0.000005*tttttt*tttttt*tttttt - 0.0021*tttttt*tttttt   + 0.0353*tttttt + 0.0321;
  if p<=0 then  Edt29.Text:=FloatToStr(0)  else  Edt29.Text:=FloatToStr(p);
  vv:=0.83*p*sqrt(0.023)*v+(1-p)*v;
  vvv:=0.83*pp*sqrt(0.023)*v+(1-pp)*v;
  vvvv:=0.83*ppp*sqrt(0.023)*v+(1-ppp)*v;
  vvvvv:=0.83*pppp*sqrt(0.023)*v+(1-pppp)*v;
  vvvvvv:=0.83*ppppp*sqrt(0.023)*v+(1-ppppp)*v;
  vvvvvvv:=0.83*pppppp*sqrt(0.023)*v+(1-pppppp)*v;
 J:=((0.258*34670*v*v*v)/9.8)*(1-(0.45/v)*(0.45/v));
 Q:=((0.258*34670*vv*vv*vv)/9.8)*(1-(0.45/vv)*(0.45/vv));
 QQ:=((0.258*34670*vvv*vvv*vvv)/9.8)*(1-(0.45/vvv)*(0.45/vvv));
 QQQ:=((0.258*34670*vvvv*vvvv*vvvv)/9.8)*(1-(0.45/vvvv)*(0.45/vvvv));
 QQQQ:=((0.258*34670*vvvvv*vvvvv*vvvvv)/9.8)*(1-(0.45/vvvvv)*(0.45/vvvvv));
 QQQQQ:=((0.258*34670*vvvvvv*vvvvvv*vvvvvv)/9.8)*(1-(0.45/vvvvvv)*(0.45/vvvvvv));
 QQQQQQ:=((0.258*34670*vvvvvvv*vvvvvvv*vvvvvvv)/9.8)*(1-(0.45/vvvvvvv)*(0.45/vvvvvvv));
 K:=((0.12*3.4*9.8)/(1800*1.2041))*J;
 KK:=((0.12*3.4*9.8)/(1800*1.2041))*Q;
 KKK:=((0.12*3.4*9.8)/(1800*1.2041))*QQ;
 KKKK:=((0.12*3.4*9.8)/(1800*1.2041))*QQQ;
 KKKKK:=((0.12*3.4*9.8)/(1800*1.2041))*QQQQ;
 KKKKKK:=((0.12*3.4*9.8)/(1800*1.2041))*QQQQQ;
 KKKKKKK:=((0.12*3.4*9.8)/(1800*1.2041))*QQQQQQ;
 B:=K*v*s*ss*sol;

end;

end.
```

Research Team:

Principal Investigator:

- **Dr. B.S. Tleumuratova**

Head of Research, Ecologist

Doctor of Physical-Mathematical Sciences (D.Sc.)

Core Researchers:

- **Dr. E.P. Urazymbetova**

GIS Specialist, Ecologist

Doctor of Philosophy in Technical Sciences (PhD)

- **Dr. Zh.Zh. Kublanov**

Ecologist

Doctor of Philosophy in Biological Sciences (PhD)

- **Dr. B.Zh. Narymbetov**

Physicist

Senior Research Associate (S.N.S.)

- **R.G. Sultashov**

Meteorologist

Base Doctoral Candidate

- **A.E. Urumbaev**

Ecologist

Base Doctoral Candidate

Affiliation:

All researchers are members of the *Laboratory for Ecological Process Modeling*, Karakalpak Branch of the Academy of Sciences of the Republic of Uzbekistan.